DEVELOPMENT AND EXPERIMENTAL VALIDATION OF DEFORMABLE CONNECTION FOR EARTHQUAKE-RESISTANT BUILDING SYSTEMS WITH REDUCED FLOOR ACCELERATIONS

By

Georgios Tsampras

Richard Sause

Technical Report

March 2015

ATLSS is a National Center for Engineering Research on Advanced Technology for Large Structural Systems

117 ATLSS Drive
Bethlehem, PA 18015-4729

Phone: (610)758-3525
Fax: (610)758-5902

www.atlss.lehigh.edu
Email:inatl@lehigh.edu

CONTENTS

ABSTRACT

This report briefly presents the development of the deformable connection of an earthquake-resistant building structural system in which the lateral force resisting system (LFRS) is connected to the gravity load resisting system (GLRS) using this type of connection instead of a rigid connection. The GLRS and LFRS are able to move relative to each other, and depending on the characteristics of the connection it is possible to limit the floor accelerations and the overall response of the structure. The deformable connection is accessible for inspection and replacement. It consists of a buckling restrained brace (BRB) or a friction device (FD) which acts as a limited-strength load-carrying hysteretic component, in parallel with low damping rubber bearings (RB). The RB provide the required out-of plane stability to the LFRS, post-elastic in-plane stiffness, and help with partial re-centering.

The main objective of this report is to present the experimental results for the nonlinear hysteretic response of two configurations of the full-scale deformable connection tested using the NEES@Lehigh Real-Time Multi-Directional earthquake simulation facility at the Advanced Technology for Large Structural Systems (ATLSS) Engineering Research Center.

ACKNOWLEDGEMENTS

This report is based upon work supported by grants from National Science Foundation, Award No. CMMI-1135033 in the George E. Brown, Jr. Network for Earthquake Engineering Simulation Research (NEESR) program, and Award No. CMMI-0402490 for the George E. Brown, Jr. Network for Earthquake Engineering Simulation (NEES) consortium operations. The authors are grateful for additional financial support provided by the Gerondelis Foundation, Yen Fellowship, and Lehigh University. The contributions of the P.I. Prof. Robert Fleischman, the Co-P.I. Prof. Jose Restrepo, Prof. Dichuan Zhang, the practicing engineers Dr. Joe Maffei, David Mar, other members of the research team, and the NEES@Lehigh Real-Time Multi-Directional (RTMD) earthquake simulation facility staff and the ATLSS Center staff are acknowledged. The authors appreciate the contribution of the companies DYMAT™, Star Seismic®, and ScanPac MFG., INC. Any opinions, findings, and conclusions expressed in this report are those of the authors and do not necessarily reflect the views of the National Science Foundation or others acknowledged here.

FIGURES

TABLES

ABBREVIATIONS

ATLSS	Advanced Technology for Large Structural Systems
ATS	Adaptive Time Series (compensation technique)
BRB	Buckling Restrained Brace
FD	Friction Device
GLRS	Gravity Load Resisting System
LFRS	Lateral Force Resisting System
LHPOST	Large High Performance Outdoor Shake Table
LVDT	Linear Variable Differential Transformer
NEES	Network of Earthquake Engineering Simulation
RB	Low Damping Rubber Bearings

SYMBOLS

A_{yz} Area of yielding zone of buckling restrained brace, $b_{yz} t_{yz}$

b_{kp} Width of knife plates of buckling restrained brace

b_{tz} Width of transition zone of buckling restrained brace

b_{yz} Width of yielding zone of buckling restrained brace

$C_{b,max}$ Maximum compressive force of buckling restrained brace, T_{max}/P_{yn}

D_{aE} East actuator stroke

D_{aW} West actuator stroke

d_b Diameter of the ASTM A325 bolts used at the slip interfaces of the friciton device

D_b Deformation of the strength-limited load carrying hysteretic component of the deformable connection

D_{by} Experimental yielding deformation of the limited-strength load-carrying hysteretic component of the deformable connection

$D_{by,a}$ Analytical estimate of the yielding deformation of the limited-strength load-carrying hysteretic component of the deformable connection

D_{cE} Command displacement for East actuator

D_{cW} Command displacement for West actuator

D_{cc} Collar to collar deformation of buckling restrained brace

D_{mE} Combination of measurements to control East actuator stroke

D_{mW} Combination of measurements to control West actuator stroke

D_{RB} Average deformation of the four low damping rubber bearings

D_t Target displacement (target deformation for deformable conneciton)

f Frequency of sinusoidal target displacement

F_i Inertial force generated by the acceleration of the mass of the floor system

F_s Static friction force of the friction device based on Coulomb theory

F_{ya} Actual material yielding strength of the yielding zone of buckling restrained brace

F_{yn} Nominal material yielding strength of the yielding zone of buckling restrained brace

G Nominal shear modulus of the rubber material of the low damping rubber bearings

L_{kp} Length of knife plates of buckling restrained brace

L_{tz} Length of transition zone of buckling restrained brace

L_{yz} Length of yielding zone of buckling restrained brace

n_b Number of ASTM A325 bolts used at the slip connection of the friction device

N_b Normal force applied by each bolt at the slip connection

n_s Number of slip interfaces at the slip connection of the friction device

P_b Force developed by the limited-strength load-carrying hystesetic component of the deformable connection

$P_{by,a}$	Actual yielding strength of the buckling restrained brace, $F_{ya}\ A_{yz}$
$P_{by,n}$	Nominal yielding strength of the buckling restrained brace, $F_{yn}\ A_{yz}$
P_{tot}	Total force calculated as the sum of the forces of the two actuators
R_y	Material overstrength of yielding zone of buckling restrained brace, $F_{ya}/\ F_{yn}$
$T_{b,max}$	Maximum tensile force of buckling restrained brace, T_{max}/P_{yn}
t_{fp}	Thickness of the friction plates used for the friction device
t_{kp}	Thickness of knife plates of buckling restrained brace
t_{tz}	Thickness of transition zone of buckling restrained brace
t_{yz}	Thickness of yielding zone of buckling restrained brace
V_t	Target velocity
V_{RB}	Approximation of the shear force generated by the four low damping rubber bearings
β	Compression strength adjustment factor of buckling restrained brace, C_{max}/T_{max}
μ_s	Static coefficient of friction provided by the manufacturer of the friction plate material
ω	Tension strength adjustment factor of buckling restrained brace, T_{max}/P_{yn}

1 INTRODUCTION

The inertial forces generated in building systems during an earthquake ground motion are directly related to the floor system acceleration and the seismic mass (associated with the floor system). In conventional earthquake-resistant building systems the gravity load resisting system (GLRS), in particular, the floor system, where most of the seismic mass is located, is rigidly attached to the lateral force resisting system (LFRS), which resists the seismic inertial force. The inertial force is transferred from the GLRS to the LFRS assuming a rigid connection between the floor system and the LFRS.

It has been shown that the seismic inertial forces generated in the floor system can be large relative to the floor diaphragm strength, and can lead to inelastic non-ductile response of the diaphragm [1]. The development of excessive inertial forces due to high floor accelerations can produce nonlinear response and severe damage of the LFRS that may lead to unsatisfactory seismic response [2] [3]. The nonlinear response of the LFRS can act as a “cut–off” mechanism that may limit the floor acceleration [4] [5]. However, even when ductile nonlinear response of the LFRS occurs, high floor accelerations may be observed, due to significant contributions to the response from second and higher modes [5] [6]. Studies of LFRS with flexural response controlled by inelastic rotation at the base show that high floor accelerations due to the higher-mode contributions to the response can be expected [7] [8] [9] [10] [11].

Skinner et al. (1975) sketched a building system with a “separated tower and frame” where the tower represents a stiff LFRS and the frame represents a flexible GLRS [12]. The system concept allowed relative deformation between the LFRS and GLRS using a deformable link element. Since the LFRS and GLRS have different dynamic characteristics (the LFRS is stiff with a small mass, the GLRS is flexible with a large mass) this system concept enables energy to be dissipated by the link element when significant relative deformation occurs [12]. Key (1984) performed a parametric numerical study to assess the effect of using an energy dissipation device to link the LFRS with the GLRS and showed that using the link element can reduce effectively the base shear of the GLRS and the LFRS [13]. Luco and De Barros (1998) studied the ability to control the seismic response of a composite tall building modelled by two shear beams interconnected with stiff or flexible link elements [14]. Mar and Tipping (2000) presented schematic structural details for a story isolation system [15]. They compared time history numerical analysis results for a conventional system (with a rigid link between the LFRS and GLRS) and the system with floor connected to the LFRS with viscous dampers and linear springs as link elements. The results showed reduced base shear and roof acceleration [15]. Crane (2004) conducted shake table tests on two small-scale 6 story buildings that had energy dissipative connections between the floors and the LFRS. Triangular-plate added damping and stiffness devices were used as the link elements. Reduced floor accelerations and base overturning moment were observed [16].

Based on this previous research, it appears that a deformable connection can be developed to allow relative motion between the LFRS and GLRS. In the present research, the objective of using such a deformable connection is to limit the force transferred from the GLRS to the LFRS at each floor level, and to reduce the floor accelerations. The use of the deformable connection makes it possible to mitigate the higher mode seismic response, and to reduce the LFRS story shear forces. The energy dissipation from the nonlinear response of the deformable connection is a potential further benefit of using the deformable connection but it is not the main objective, as in some of the previous studies. The deformable connection needs to be constructable, accesible for inspection, and repairable.

2 CONCEPTUAL DESIGN

To allow relative motion between the LFRS and the GLRS, an opening is needed at each floor around the LFRS (e.g. shear walls), as shown in Figure 2.1. The close up in Figure 2.1(b) demonstrates how the deformable connection can be used to connect the LFRS with the GLRS.

The concept studied in this research uses two different types of components in the deformable connection.

The first component is a limited-strength, load-carrying hysteretic component, which is required to transfer the inertial force from the floor to the LFRS and to ensure the stability of the GLRS. During an earthquake excitation, the limited-strength load-carrying hysteretic component will deform axially due to the relative horizontal motion in the plane of the LFRS. The characteristics of the limited-strength load-carrying hysteretic components determine the magnitude of force that can be transferred from each floor to the LFRS, which determines the magnitude of the floor accelerations that can develop.

The second component of the deformable connection is a set of bearings, which is needed to provide out-of-plane stability to the LFRS. This component braces the LFRS against the floor system, which is then braced by an orthogonal LFRS. The bearings must have significant compressive stiffness and strength to transfer the out-of-plane bracing force without significant deformation. The bearings need to have low shear stiffness compared to their compressive stiffness. Their response under shear deformation due to the relative horizontal motion in the plane of the LFRS provides additional stiffness to the deformable connection.

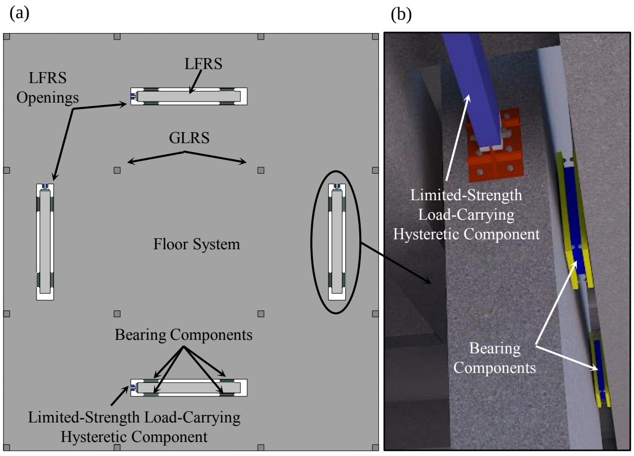

Figure 2.1: Conceptual design of proposed building system with deformable connections

3 IMPLEMENTATION

Extensive research on devices that might be used as components of the deformable connection was carried out and led to two different configurations. The first configuration consists of a buckling restrained brace (BRB) which is used as the limited-strength load-carrying hysteretic component and low damping rubber bearings (RB). BRBs are commonly used in seismic design practice and are commercially available. Individual BRB response has been extensively studied and it has been shown that they provide stable nonlinear hysteretic response. The strength and stiffness of a BRB are closely related, but it is possible to design a BRB to have the appropriate nonlinear characteristics for the deformable connection. RB are an appropriate choice for the bearings of the deformable connection. Their compressive stiffness is significantly higher than their shear stiffness. Low damping rubber bearings have large shear deformation capacity, and their response is approximately linear elastic [17].

The second configuration uses a friction device (FD) as the limited-strength load-carrying hysteretic component. RB are also included. For the FD, the strength and stiffness are not as closely related as for the BRB. Thus, a wider range of combinations of strength and stiffness can be considered for the deformable connection. However, FDs are not commonly used in seismic design practice. Thus, a FD that can accommodate the expected kinematics of the deformable connection was developed and validated experimentally. Therefore, one of the objectives of the present research is to study the deformable connection using FDs.

Figure 3.1 shows an installed deformable connection on a half-scale rocking shear wall structure built and tested at the NEES@UCSD Large High Performance Outdoor Shake Table (LHPOST) [18]. The objective of this work was to validate the structural response of a building with and without deformable connections between the LFRS and GLRS. In Figure 3.1(a) shows the elevation of the main rocking wall with deformable connections. The accessibility and minimum architectural impact can be observed. Figure 3.1(b) shows a close up view of the FD of the deformable connection. The attachment of the FD to the floor system and the shear wall (Figure 3.1(b)) were designed using standard details. RB are shown in Figure 3.1(c). The FD and RB are positioned so they can be inspected after an earthquake.

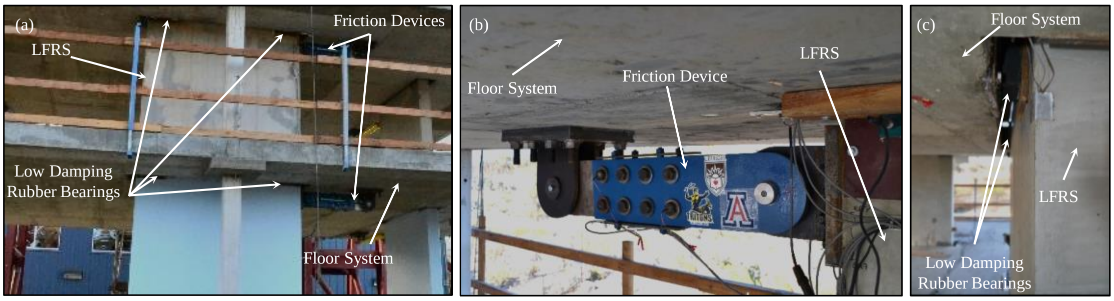

Figure 3.1: Implementation of the deformable connection on a rocking precast concrete shear wall structure at NEES@UCSD equipment site

4 FULL-SCALE COMPONENTS TESTS

To validate the response of the two configurations of the deformable connection, an experimental program was conducted using the NEES@Lehigh Real-Time Multi-Directional earthquake simulation facility at the Advanced Technology for Large Structural Systems (ATLSS) Engineering Research Center. The experimental set up includes a portion of the reinforced concrete shear wall structure for a twelve story building. As shown in Figure 4.1(a) part of the floor and part of the reinforced concrete shear wall were built in the laboratory. The components of the deformable connection were attached to these parts of the wall and floor. Figure 4.1(b) shows the test setup and specimen for the first configuration, including the wall and floor (without the concrete), the BRB (provided by Star Seismic®), and the steel reinforced RB. Figure 4.1(c) shows the second configuration of the deformable connection that consists of a FD (developed at Lehigh University) and carbon fiber reinforced RB (provide by DYMAT™). In the test set up, relative horizontal motion of the floor with respect to the shear wall is applied resulting in cyclic axial deformation of the limited-strength load-carrying hysteretic components and shear deformation of the bearings.

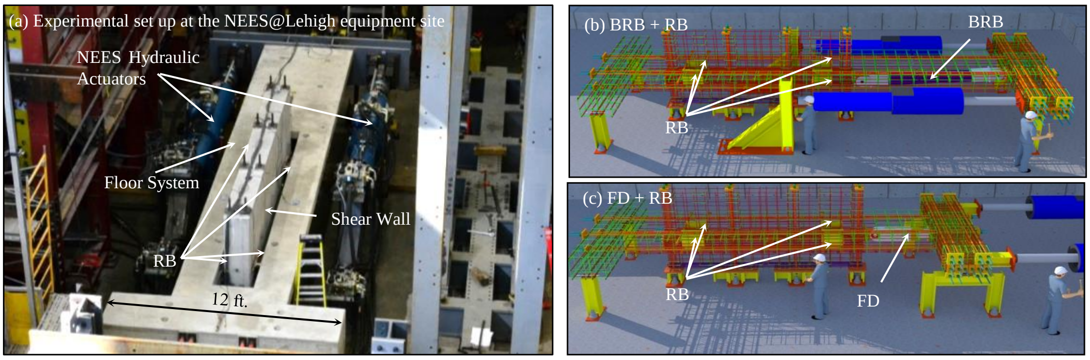

Figure 4.1: Experimental set up at NEES@Lehigh equipment site and the limited strength load carrying hysteretic components of the deformable connection

The summary of the experimental program is shown in Table 4.1. Phase I and II involve tests on the first and second configuration of the deformable connection respectively.

Table 4.1: Summary of experimental program

Testing Period	Phase I.D.	RB	[a]BRB	[b]FD
03/27 – 05/1 2014	I-1	Steel Reinforced	-	-
05/19 – 05/21 & 05/30/2014	I-2	Steel Reinforced	$P_{by,a}$=224 kips	-
05/27 – 05/30 2014	I-3	Steel Reinforced	$P_{by,a}$=224 kips	-
08/08 – 08/11 2014	II-1	Carbon Fiber Reinforced	-	AFT200
08/12 – 08/13 2014	II-2	Carbon Fiber Reinforced	-	RF42
09/26/2014	II-3	Carbon Fiber Reinforced	-	RF42
09/30/2014	II-4	Carbon Fiber Reinforced	-	Gatke 398

[a]Refers to the axial yielding strength of the BRB (if any)
[b]Refers to the material that has been used at the frictional interface (if any)

4.1 Objectives

The objectives of the experimental program are the following:

1. Demonstrate the feasibility of designing and constructing the deformable connection for full-scale seismic demands from a twelve story building structure
2. Assess the process for installing the components of the deformable connection
3. Validate the performance of the deformable connection under sinusoidal displacement histories at various frequencies and amplitudes, and also under displacement histories that represent expected seismic deformation demands.

4.2 Experimental Set Up

4.2.1 Floor System

The floor system consisted of two segments of a double T-shaped reinforced concrete member as shown in Figure 4.2 and Figure 4.3. The two segments were connected using unbonded post-tensioning bars. The BRB used in phase I was longer than the FD used in phase II. Thus, the length of the floor system was shortened from phase I to phase II. The shortening of the floor system was accomplished by removing one of the two segments.

Flexural and shear strength checks for the maximum expected forces during the test were performed based on the ACI 318-11 building code. ASTM A615 grade 60 reinforcing bars were used for both the longitudinal and confinement reinforcement. The 7-days compressive strength of the concrete was 6.2 ksi. The diameter of the post-tensioning bars was 1 ¼ inches and the pretension force of each bar was 112.5 kips. Table 4.2 shows the properties of the post-tensioning bars. PVC Schedule 40 pipes with diameter of 1 ½ inches were used to create the unbonded condition of the post-tensioning bars.

In order to cast the reinforced concrete members, plywood forms were used externally and styrofoam was used internally to create the shape. The construction process using the styrofoam was fast and easy since the blocks were produced in predefined shapes. However, the process to remove the styrofoam from the concrete was time consuming. The forms were removed 10 days after the concrete was poured.

Table 4.2: Post-tensioning bars nominal properties (from DSI)

Nominal Bar Diameter	Ultimate Stress (f_{pu})	Cross Section Area	Ultimate Strength ($f_{pu}A_{ps}$)	Prestressing Force 0.8 $f_{pu}A_{ps}$	0.7 $f_{pu}A_{ps}$	0.6 $f_{pu}A_{ps}$	Weight	Maximum Bar Diameter
[in]	[ksi]	[in^2]	[kips]	[kips]	[kips]	[kips]	[lbs/ft]	[in]
1	150	0.85	127.5	102.0	89.3	76.5	3.01	1.20
1-1/4	150	1.25	187.5	150.0	131.3	112.5	4.39	1.46
1-3/8	150	1.58	237.0	189.6	165.9	142.2	5.56	1.63
1-3/4	150	2.62	400.0	320.0	280.0	240.0	9.22	2.00
2-1/2	150	5.20	780.0	624.0	546.0	468.0	17.71	2.71

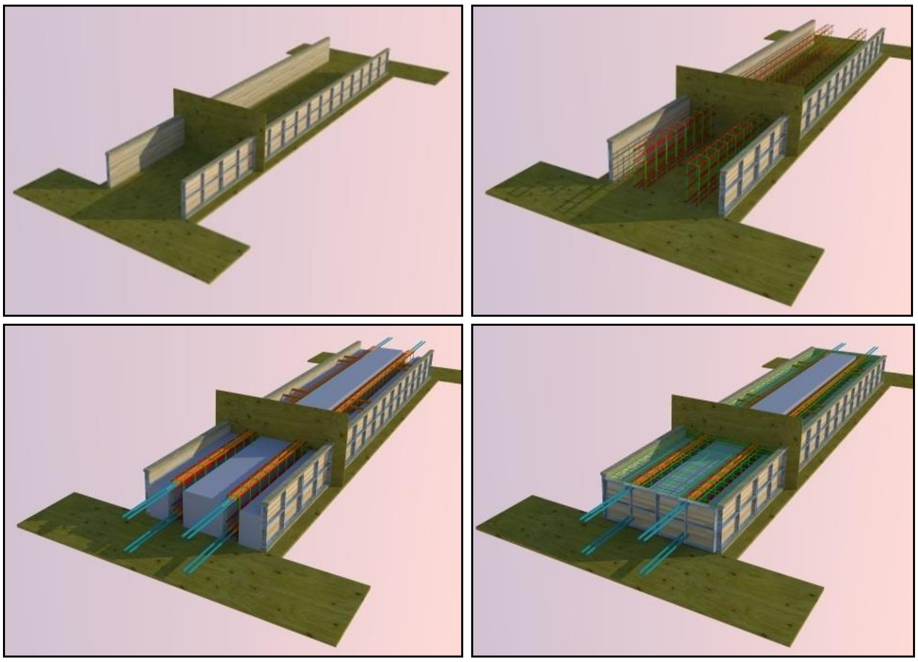

Figure 4.2: Visual representation of the construction process of the floor system members

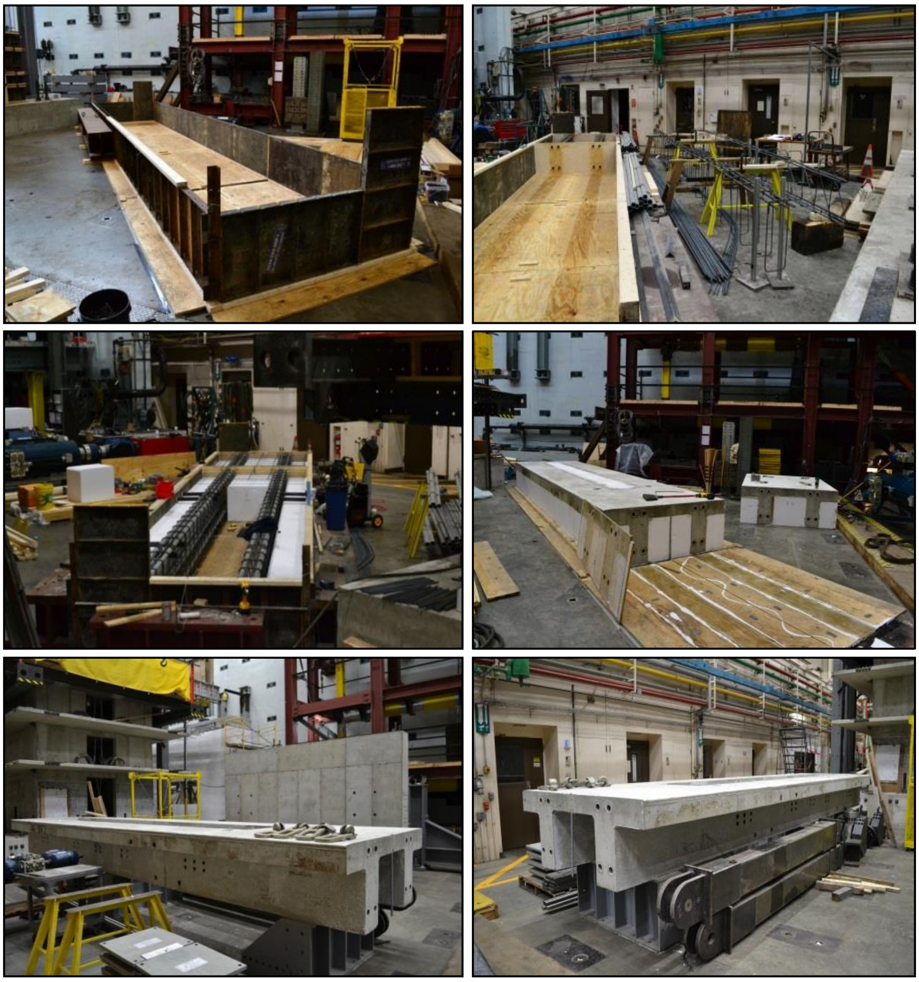

Figure 4.3: Construction process of floor system members

4.2.2 LFRS

A reinforced concrete shear wall was used as the LFRS. The wall was designed to react the forces developed by the deformable connection. The shear wall was post-tensioned with vertical bars in order to increase the base moment capacity.

The reinforcement was designed for the shear and moment demands on the shear wall using the ACI 318-11 building code. The ASTM A615 grade 60 reinforcing bars were used. The concrete compression strength test at 14 days was 7.0 ksi. Shear studs were used to transfer the base shear from the wall to the steel base. Additional transverse reinforcement was used at the base of the wall to avoid crack propagation due to the stress concentration around the studs. Plywood forms were used to cast the reinforced concrete shear wall. The forms were removed two weeks after the concrete was poured.

Figure 4.4 shows the construction process of the shear wall. The vertical PVC schedule 40 pipes were used to create the unbonded condition of the post-tensioning bars. Longitudinal PVC pipes were used to create the unbonded condition for the ASTM A163 B7 1 ¼ inch diameter threaded rods that were used to attach the clevis connection of the limited-strength load-carrying device to the shear wall. PVC pipes, placed through the thickness of the wall, were used to create the unbonded condition for the ASTM A163 B7 1 inch diameter threaded rods that were used to attach the bearings to the shear wall.

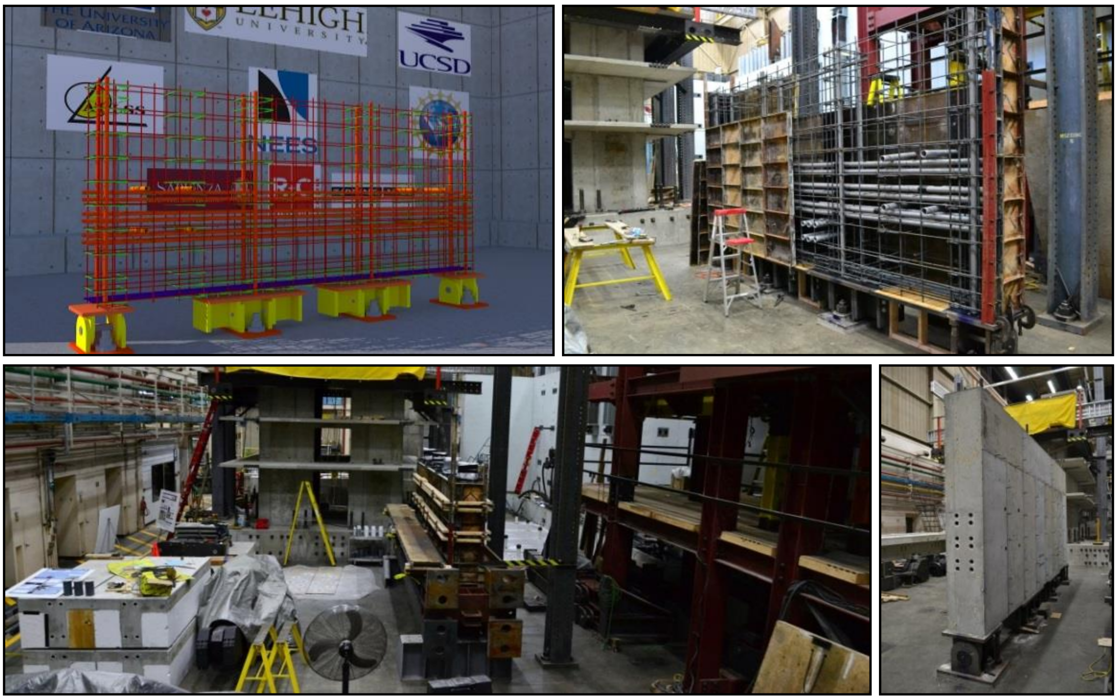

Figure 4.4: Photos during construction process of reinforced concrete shear wall

4.2.3 Loading block and gravity columns

The floor system was connected to the hydraulic actuators using a steel loading block as shown in Figure 4.5. The steel loading block consisted of two W14 x 398 sections. Gravity columns supported the floor system as shown in Figure 4.5 and in Figure 4.6. Contact interfaces of Teflon and steel reduced the friction. Guides restrained the out-of-plane motion of the floor system.

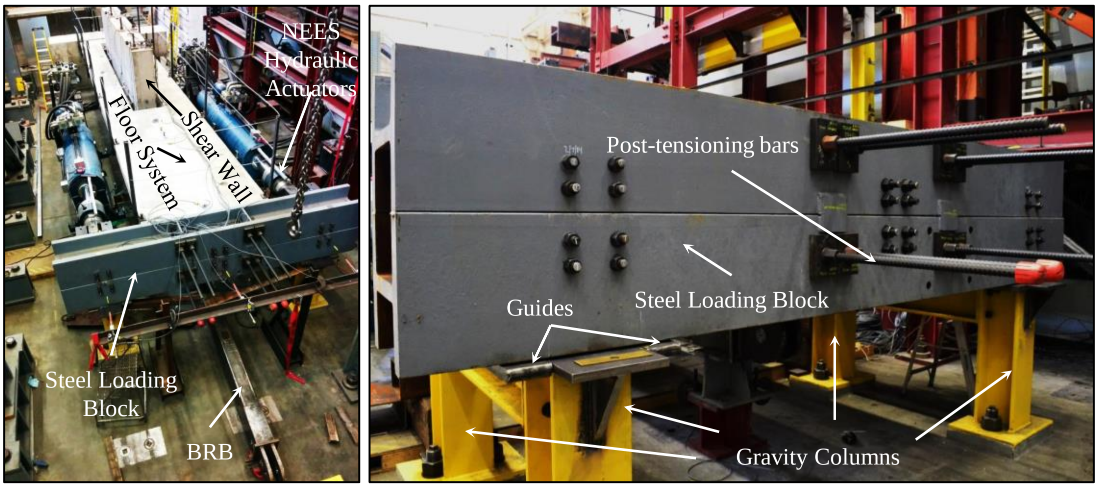

Figure 4.5: Steel actuator's block and gravity columns

Figure 4.6: Gravity columns and lateral guides

4.2.4 NEES@Lehigh Equipment

Two hydraulic actuators from the NEES@Lehigh facility with a force capacity 382 kips at 3000 psi of hydraulic pressure and approximate rate of applied deformation of 33 in./sec. were used to apply the displacement histories. Two servo–valves were mounted on each actuator. More information regarding the NEES equipment site at Lehigh University can be found at the following reference [19].

4.3 Phase I

Phase I assessed the response of the first configuration of the deformable connection. There were three subphases of tests in phase I. One set of steel reinforced RB was used in phase I. Two BRBs with the same characteristics were used in phase I-2 and phase I-3.

Phase I-1 assessed the response of the deformable connection with only the steel reinforced RB without the BRB. This allowed to run preliminary tests to ensure the functionality of the NEES equipment, the sensors and the fixture under of small force and deformation.

Phase I-2 assessed the response of the deformable connection consisted of the steel reinforced RB and the first BRB. This group of tests provided information about the response of the deformable connection, its individual components, and their attachments to the shear wall and the floor system. Sinusoidal cyclic displacement histories at different amplitudes and frequencies, and simulated seismic induced floor displacement histories were used.

Phase I-3 assessed the response of the deformable connection with the steel reinforced RB and the second BRB. The reliability of the results was increased by testing the same configuration of the deformable connection with different BRB.

4.3.1 Buckling Restrained Brace

Figure 4.7 shows the components of a buckling restrained brace (BRB), the two BRBs provided by Star Seismic®, and an installed BRB in the test specimen. Figure 4.8 shows a drawing of the BRB, and Table 4.3 gives important dimensions. The BRB used in phase I-2 and phase I-3 have the same characteristics. The symbols t, b, and L denote the thickness, width, and length respectively. Table 4.4 gives information about the yielding zone. The material, the actual material yielding strength F_{ya}, the area A_{yz}, the nominal yielding strength $P_{by,n}$, the actual yielding strength $P_{by,a}$, the material overstrength factor R_y, and the analytical estimate of the yielding deformation $D_{by,a}$ based on the actual yielding strength are given. The normalized deformation D_b/L_{yz}, the compression strength adjustment factor $\beta\omega$ [20] [21], the tension strength adjustment factor ω [20] [21], the expected maximum BRB compression force $P_{b,max}$, and the maximum tensile force $T_{b,max}$ at two BRB deformations D_b are given in Table 4.5.

Table 4.3: BRB components dimensions

Yielding Zone				Transition Zone			Knife Plates			Clevis		
No. Plates	t_{yz} [in]	b_{yz} [in]	L_{yz} [in]	t_{tz} [in]	b_{tz} [in]	L_{tz} [in]	t_{kp} [in]	b_{kp} [in]	L_{kp} [in]	t_c [in]	b_c [in]	L_c [in]
1	1.00	5.48	90.60	1.00	10.00	15.70	1.5	13.00	14.50	2.50	13.00	14.75

Table 4.4: Material properties and strength of BRB yielding zone

Material	F_{ya}[1] **[ksi]**	A_{yz} **[in²]**	$P_{by,n}$ **[kips]**	$P_{by,a}$ **[kips]**	R_y **[-]**	$D_{by,a}$ **[in]**
ASTM A36	40.90	5.48	197	224	1.14	0.185

[1]Actual material yield strength provided by Star Seismic®

Table 4.5: BRB expected response quantities at two deformation levels

D_b **[in]**	D_b/L_{yz} **[%]**	$\beta\omega$ **[-]**	ω **[-]**	$P_{b,max}$ **[kips]**	$T_{b,max}$ **[kips]**
2.00	2.20	1.70	1.52	380	340
3.50	3.86	1.88	1.68	421	376

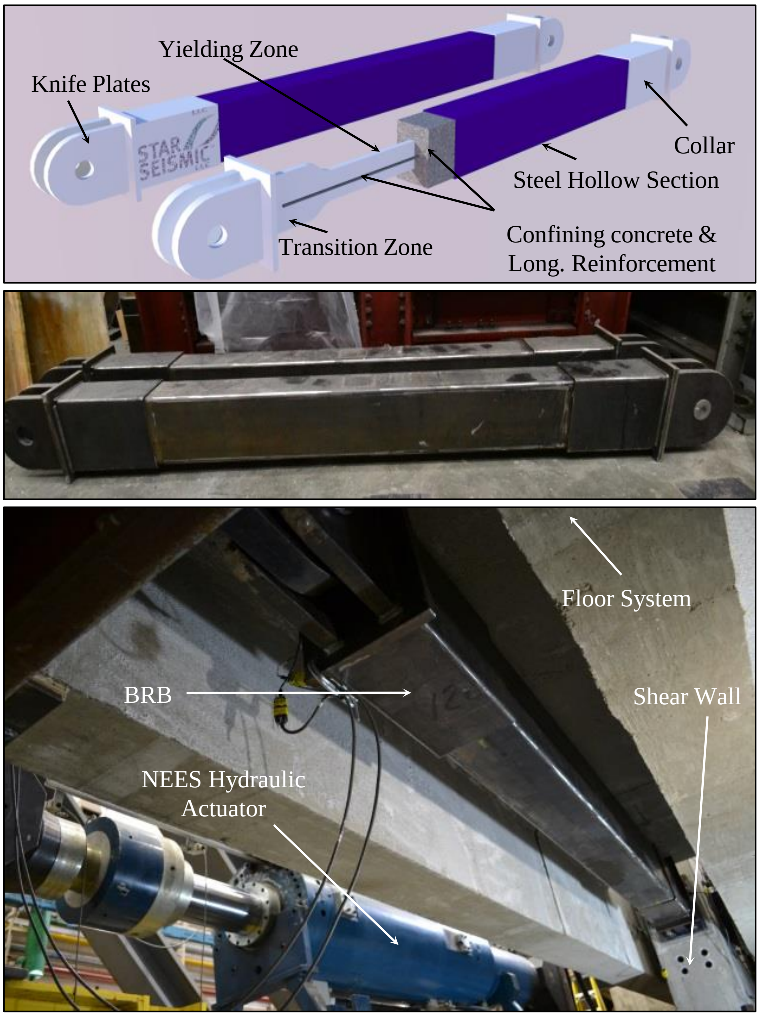

Figure 4.7: BRB used in phase I

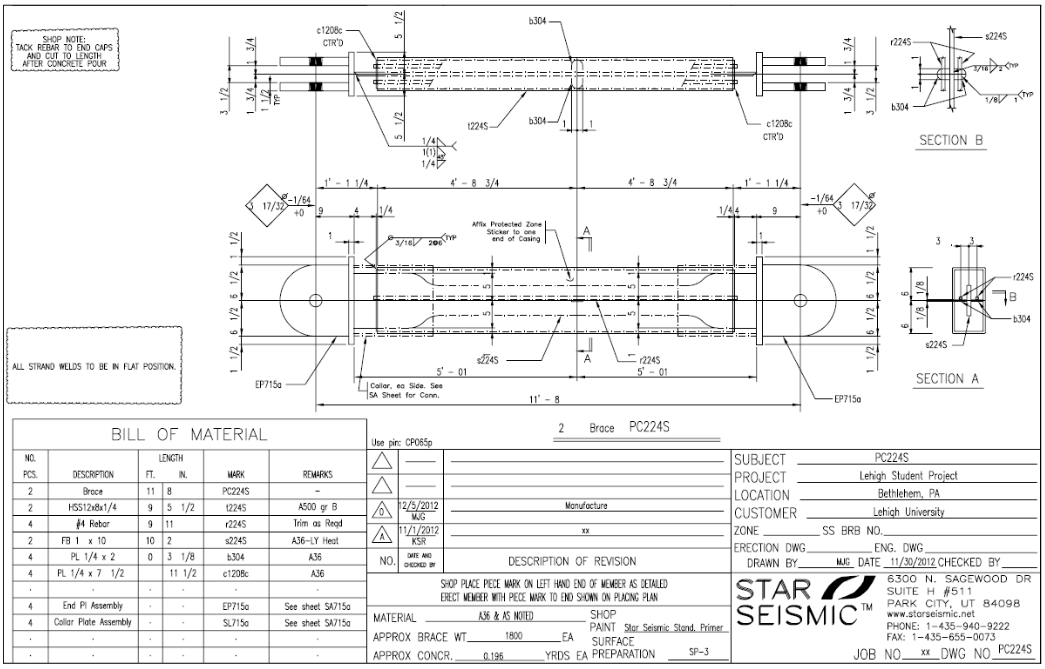

Figure 4.8: Drawing of BRB by Star Seismic®

4.3.2 Steel Reinforced Low Damping Rubber Bearings

The steel reinforced RB are identical with those used in bridge applications. Layers of reinforced rubber pads and steel shims are bonded between two external steel plates to make a steel reinforced RB. In phase I, steel reinforced RB provided by DS Brown were used. Each RB consisted of 4 layers of steel reinforced neoprene 50+/-5 Duro Gr. 3 rubber pads with a nominal shear modulus *G*=0.12 ksi. The steel reinforced RB were designed for the maximum expected horizontal and vertical shear deformation combined with the out-of-plane rotation expected at the twelfth floor of a building structure with the deformable connection subjected to a design level earthquake ground motion. The AASHTO specifications [22] [23] and references [24] [25] were used for the design. Only horizontal deformation was applied in the test. Figure 4.9 shows the installed steel reinforced RB and a close up view of the North East RB of the test specimen. The dimensions of the steel reinforced RB are shown in Figure 4.10.

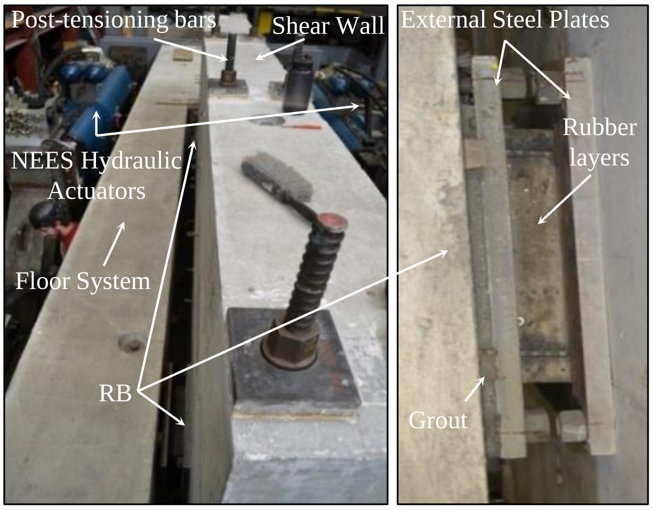

Figure 4.9: Steel reinforced low damping rubber bearings in phase I

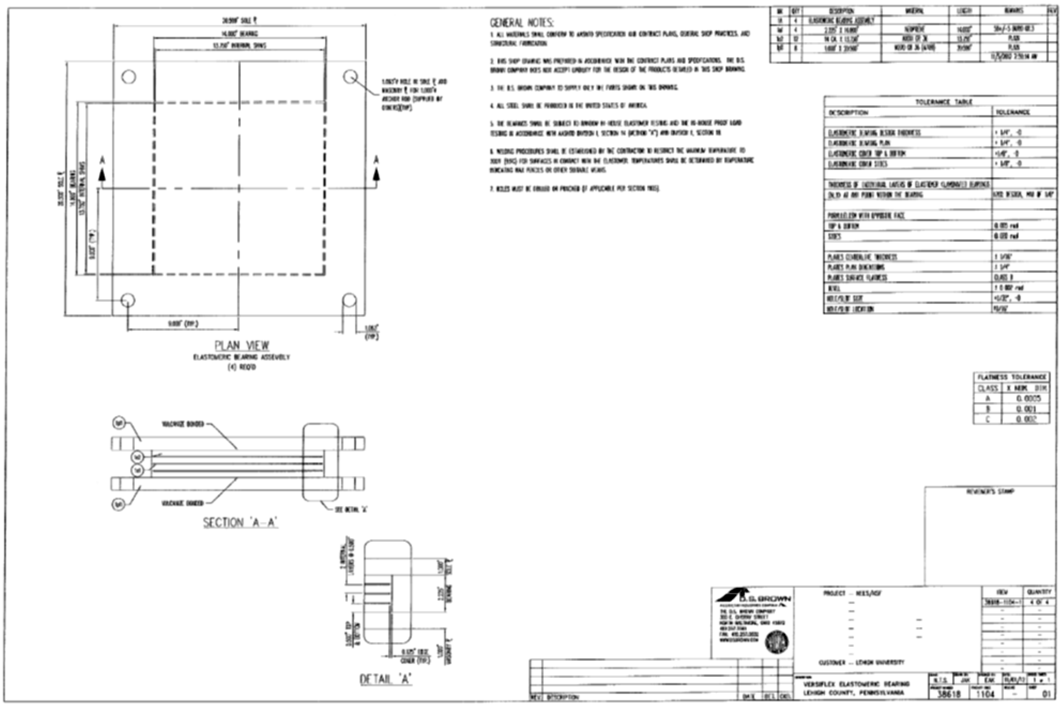

Figure 4.10: Drawing of the steel reinforced RB provided by DS Brown

4.3.3 Instrumentation

The instrumentation plan is shown in Figure 4.11. The list of the instruments is given in Table 4.6. LVDTs were used for the deformation and displacement measurements as shown in Figure 4.12. Plastic slides were used to measure slip of the external steel plates of the RB with respect to the wall and the slab. Accelerometers at various locations were used to measure the accelerations. LVDTs used to record the deformation of the RB, a representative plastic slide, and accelerometers are shown in Figure 4.13. An instrumented pin was used to measure the axial force in the BRB and the FD. The instrumented pin is shown in Figure 4.14. The forces in the actuators was measured using load cells.

Table 4.6: Phase I - Instruments list

Serial	**Type Of Instrument**	**Stroke/ Magnitude**	**Direction**	**Location**	**Mounted from**	**Mounted to**
LV11	LVDT	+/- 4"	N -S	NE	Loading Block (Centered to actuator)	Strong floor
LV12	LVDT	+/- 4"	N -S	NW	Loading Block (Centered to actuator)	Strong floor
LV13	LVDT	+/- 4"	N -S	N	Loading Block (centered to section)	Strong floor
LV21	LVDT	+/- 4"	N -S	N	South Collar of BRB	North Collar of BRB
LV22	LVDT	+/-1/8"	N -S	N	Loading Block	Clevis plates of BRB
LV23	LVDT	+/-1/8"	N -S	N	Shear Wall	Clevis plates of BRB
LV31	LVDT	+/- 4"	N -S	N	Shear Wall	Centered on the wall on the top surface of the slab. Far in order to minimize angle effects
LV32	LVDT	+/- 4"	N -S	S	Shear Wall	Centered on the wall on the top surface of the concrete block. Far in order to minimize angle effects
LV41	LVDT	+/-1/8"	N -S	N	Top steel plate of the base of the wall	Strong floor
LV51	LVDT	+/-1/8"	Vertical	N	Top steel plate of the base of the wall	Strong floor
LV52	LVDT	+/-1/8"	Vertical	S	Top steel plate of the base of the wall	Strong floor
LV61	LVDT	+/- 4"	N -S	S	Floor system	Wall
LV62	LVDT	+/- 4"	N -S	S	Floor System	Wall

Serial	Type Of Instrument	Stroke/ Magnitude	Direction	Location	Mounted from	Mounted to
LP63	Linear Potentiometer (Plastic Slide)	+/-1/2"	N -S	S	Steel Plate of bearing	Wall
LP64	Linear Potentiometer (Plastic Slide)	+/-1/2"	N -S	S	Steel Plate of rubber bearing	Wall
LP65	Linear Potentiometer (Plastic Slide)	+/-1/2"	N -S	S	Steel Plate of rubber bearing	Floor system
LP66	Linear Potentiometer (Plastic Slide)	+/-1/2"	N -S	S	Steel Plate of rubber bearing	Floor system
LV71	LVDT	+/- 4"	N -S	N	Floor system	Wall
LV72	LVDT	+/- 4"	N -S	N	Floor system	Wall
LP73	Linear Potentiometer (Plastic Slide)	+/-1/2"	N -S	N	Steel Plate of rubber bearing	Wall
LP74	Linear Potentiometer (Plastic Slide)	+/-1/2"	N -S	N	Steel Plate of rubber bearing	Wall
LP75	Linear Potentiometer (Plastic Slide)	+/-1/2"	N -S	N	Steel Plate of rubber bearing	Floor system
LP76	Linear Potentiometer (Plastic Slide)	+/-1/2"	N -S	N	Steel Plate of rubber bearing	Floor system
LV81	LVDT	+/-1/2"	Vertical	Middle	Loading block	Strong floor
ACC11	Accelerometer	-	N -S	NE	-	Top of actuator’s adapter plate
ACC12	Accelerometer	-	N -S	NW	-	Top of actuator’s adapter plate
ACC21	Accelerometer	-	N -S	N	-	Floor system. Centered to wall
ACC22	Accelerometer	-	N -S	N	-	Floor system. Centered to wall
ACC23	Accelerometer	-	N -S	S	-	Floor system. Centered to wall
ACC31	Accelerometer	-	N -S	N	-	Top of wall
ACC41	Accelerometer	-	N -S	Middle	-	Top of floor system middle of wall

Serial	Type Of Instrument	Stroke/ Magnitude	Direction	Location	Mounted from	Mounted to
ACC42	Accelerometer	-	N -S	Middle	-	Top of floor system middle of wall
LC11	Load Cell	N/A	N-S	East	-	East Actuator
LC12	Load Cell	N/A	N-S	West	-	West Actuator
PN11	Load Pin	450 kips	N-S	Middle	-	Clevis at wall's end

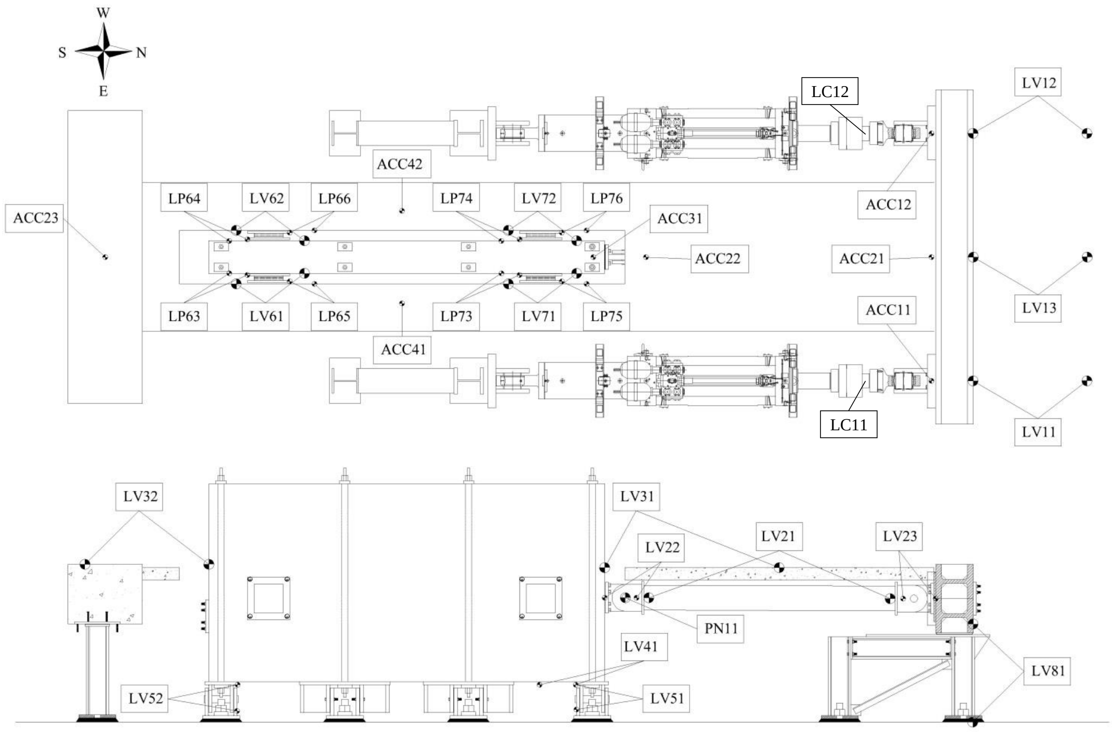

Figure 4.11: Instrumentation in phase I

LV11 – LV12 – LV13

LV22 – LV21 – LV23

LV41 – LV51 – LV52

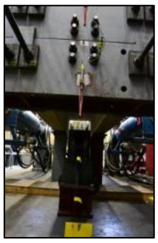

LV32 – LV31

LV81

Figure 4.12: LVDTs

LVDT: LV6# or LV7# (Typ.)

Plastic Slides: LP## (Typ.)

Accelerometers (Typ.)

Figure 4.13: LVDT, plastic slides and accelerometers

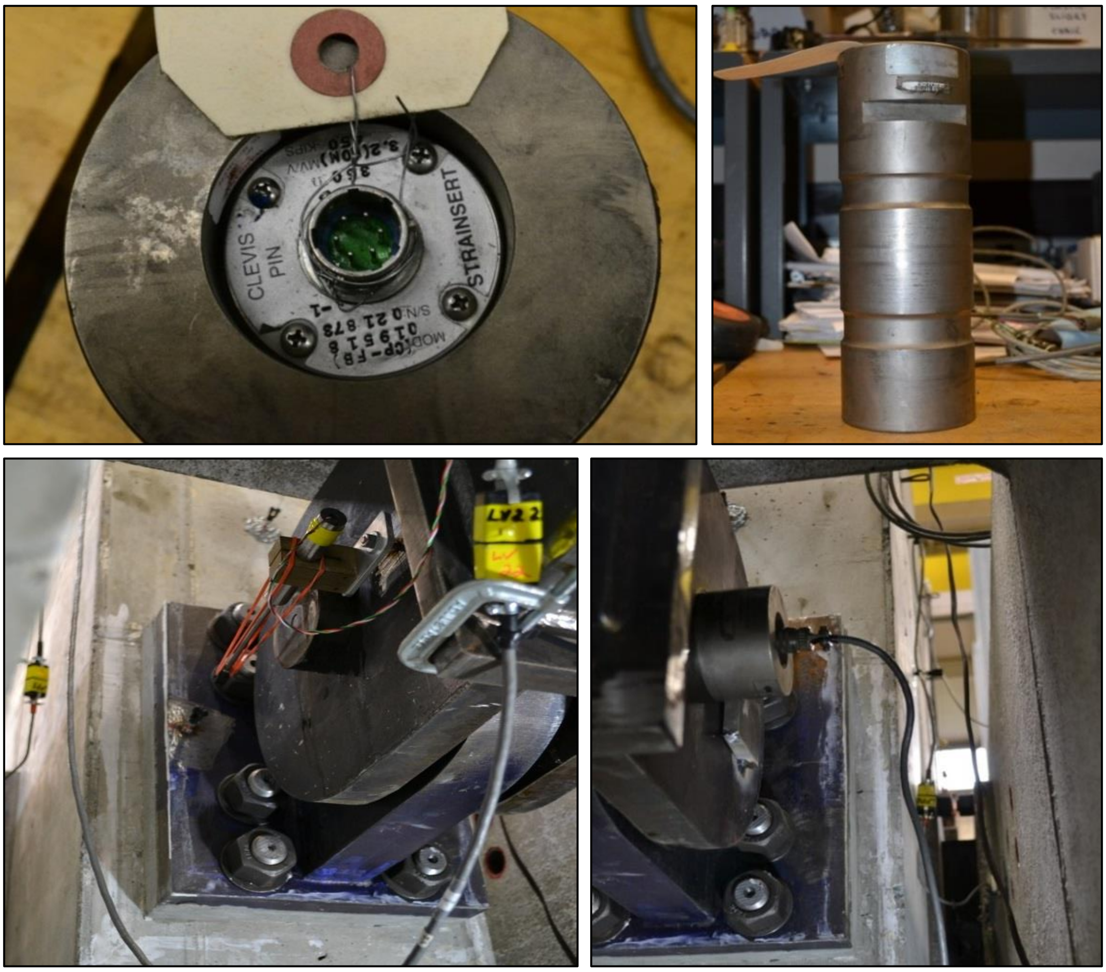

Figure 4.14: Instrumented pin by Strainsert

4.3.4 Notation

Total Force, P_{tot} is the sum of the forces measured by the actuator load cells LC11 and LC12. The total force includes the force in the BRB, the force in the steel reinforced RB, any friction force generated at the contact interface between the Teflon and steel at the top of the gravity columns, and the inertial force F_i. The inertial force was estimated by multiplying the total mass of the floor system by the acceleration measured by accelerometers ACC21, ACC22, ACC23, ACC41, and ACC42.

The *BRB Force*, P_b is the axial force in the BRB and was directly measured using the instrumented pin PN11.

The *RB Force*, V_{RB} is the estimated shear force generated by the RB. It is approximated by calculating the difference between the P_{tot} and the P_b ($V_{RB} \approx P_{tot} - P_b$). This approximation is valid for the low frequency tests were the inertial force, F_i, was not significant and any friction force at the top of the gravity columns was small. For the high frequency tests the inertial force was significant compared to the force developed by the RB making the approximation inaccurate.

The *Average Bearing Deformation*, D_{RB} is the average of the measurements of the four LVDTs LV61, LV62, LV71, and LV72.

The *BRB Deformation*, D_b is the sum of the measurements of LVDTs LV21, LV22, and LV23.

The *Collar to Collar Deformation*, $D_{cc} = LV21_m$ is the deformation measured by LVDT LV21.

The *Target Displacement, D_t* represents the histories shown in Figure 4.16 for phase I-1, in Figure 4.19, Figure 4.20, and Figure 4.21 for phase I-2 and in Figure 4.37, Figure 4.38, Figure 4.39, Figure 4.40, and in Figure 4.41 for phase I-3.

Figure 4.15 shows the control scheme used in the testing program. Each actuator was servo-controlled with an inner loop using the actuator stroke as the feedback signal and PID control. For the tests, however, the target displacement histories were intended to be the target displacement, so outer control loops were added as shown in Figure 4.15. For these outer control loops, the target displacement was the feedback signal and the target displacement histories were the input. For the low frequency sinusoidal loading tests and the seismic response input, PID control was used for the outer loops. For the high frequency sinusoidal loading tests, the adaptive time series (ATS) [26] compensator was used for the outer loops to compensate for the dynamic characteristics of the servo-hydraulic controllers, actuators, test fixtures, and test specimen.

D_{cE} and D_{cW} are the East and West actuator command displacements, and D_{aE} and D_{aW} are the East and West actuator strokes.

Table 4.7 gives the expressions of the displacements D_{mE} and D_{mW} that were functions of the LVDT measurements. D_{mE} and D_{mW} were feedback to the PID control or ATS compensation. The subscript $_m$ next to the name of each LVDT is referring to the measurement by the LVDT.

Table 4.7: Phase I, Displacements as function of LVDT measurements

Test	D_{mE}	D_{mW}
1 through 20	$LV13_m$	$LV13_m$
21 through 32	$\frac{LV11_m - LV12_m}{2} + LV13_m - LV41_m$	$\frac{LV12_m - LV11_m}{2} + LV13_m - LV41_m$

Note: The subscript *m* is a reference to the measurement of the LVDT

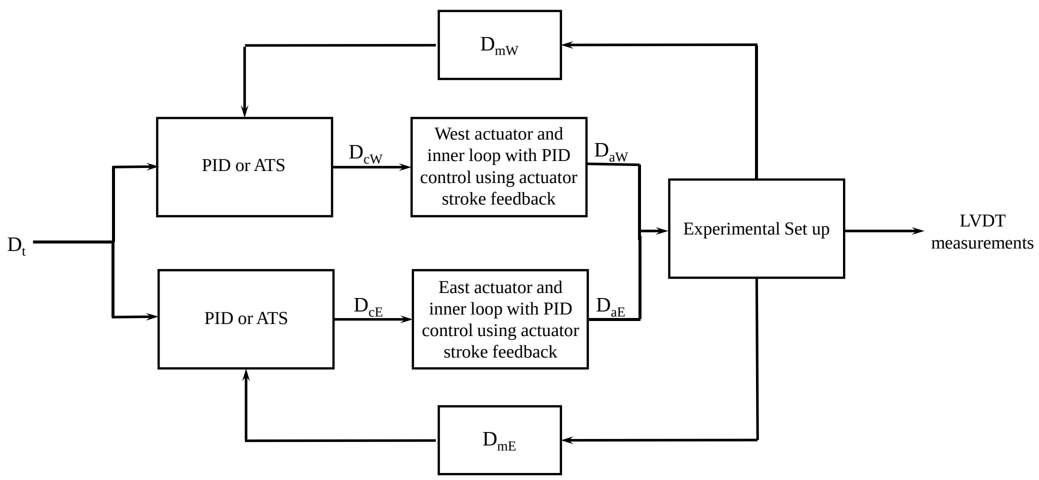

Figure 4.15: Control scheme of testing program

4.3.5 Filtering

The force-deformation plots presented in this section were filtered using a bi-directional 3rd order Butterworth digital filter with zero-phase distortion. 15 Hz and 80Hz were the cut off frequencies for the low and higher frequency tests respectively.

4.3.6 Sign Convention

A positive target displacement corresponds to movement of the floor system towards the North direction, compressing the BRB. Thus, to keep the sign of the response quantities for the deformable connection consistent with the sign of the displacement, the raw data of the LVDTs, the force measurements from the instrumented pin PN11, and the actuator load cells were multiplied by -1.

4.3.7 Phase I-1

The displacement histories that were used in phase I are sinusoidal waves with a ramp up, a ramp down and constant amplitude cycles as described in Table 4.8 and shown in Figure 4.16. The frequencies of the sine waves ramped from 0.12 Hz to 6.05 Hz.

All the instruments worked as expected.

Under a low amplitude and low frequency displacement history, the steel reinforced RB performed as expected without loss of shear stiffness. Under a low amplitude and high frequency displacement history, the response of the steel reinforced RB could not be evaluated due to the significant inertial forces compared to the force in the steel reinforced RB.

Table 4.8: Phase I-1 testing sequence

Day	Test	Name	$D_{t,max}$ [in]	$V_{t,max}$ [in/sec]	f [Hz]	# Ramp up cycles	# Ramp down cycles	# Max. amplitude cycles
03-27-2014	1	S0	0.13	0.10	0.12	1	1	1
	2	S1	0.5	1.00	0.32	3	3	6
	3i	S2	0.5	10.00	3.18	3	3	6
	3ii	S2	0.5	10.00	3.18	3	3	6
	3	S2	0.5	10.00	3.18	3	3	6
03-28-2014	4	S1	0.5	1.00	0.32	3	3	6
	5	S2	0.5	10.00	3.18	3	3	6
	6	S1.5	0.5	5.00	1.59	3	3	6
04-29-2014	4b	S1	0.5	1.00	0.32	3	3	6
	5b	S2	0.5	10.00	3.18	3	3	6
	6b	S1.5	0.5	5.00	1.59	3	3	6
05-07-2014	4c	S1	0.5	1.00	0.32	3	3	6
	5c	S2	0.5	10.00	3.18	3	3	6
	6c	S1.5	0.5	5.00	1.59	3	3	6
05-13-2014	7	S3	0.5	13.00	4.14	3	3	6
	8	S4	0.5	19.00	6.05	3	3	6

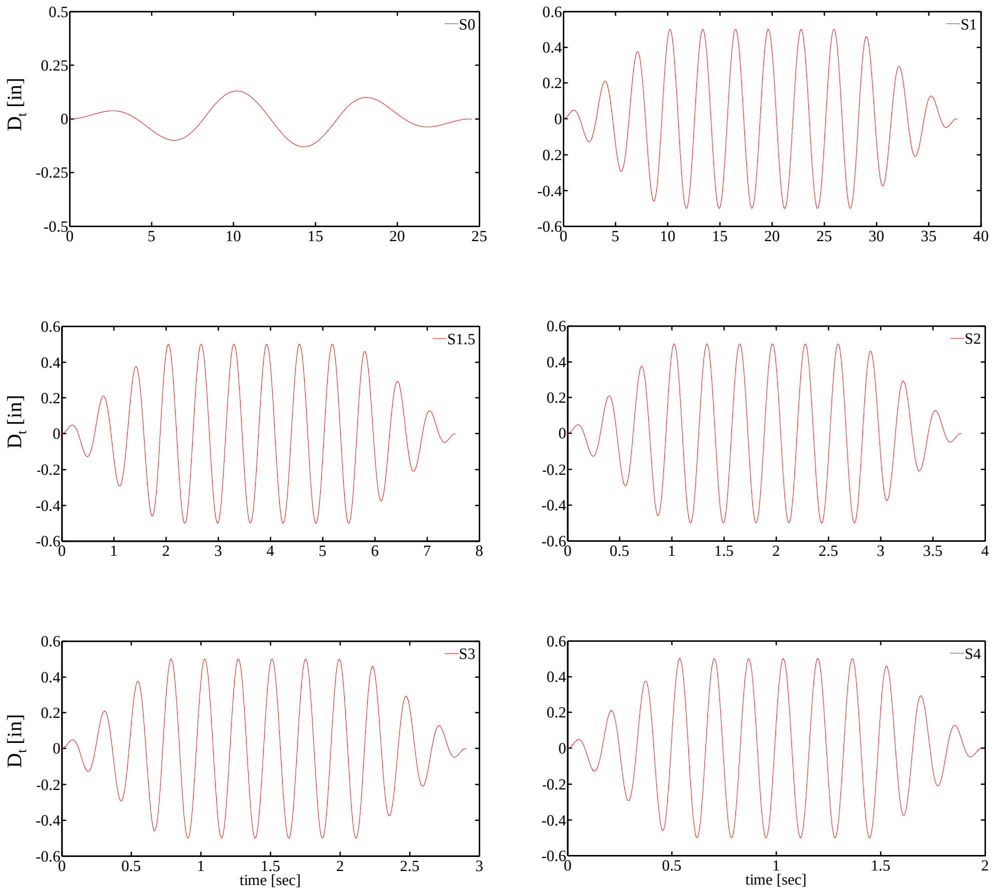

Figure 4.16: Phase I–1 target displacement histories

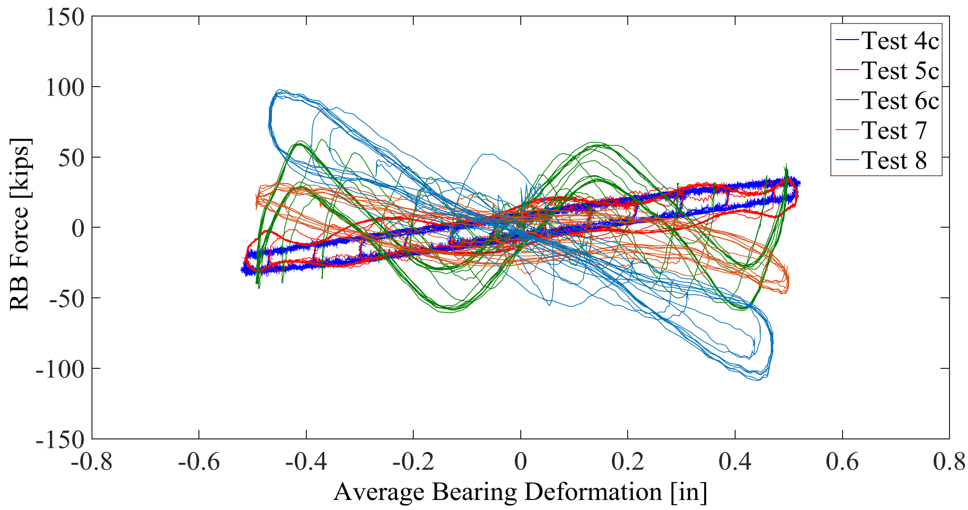

Figure 4.17: Force-deformation plots from tests 4c - 8

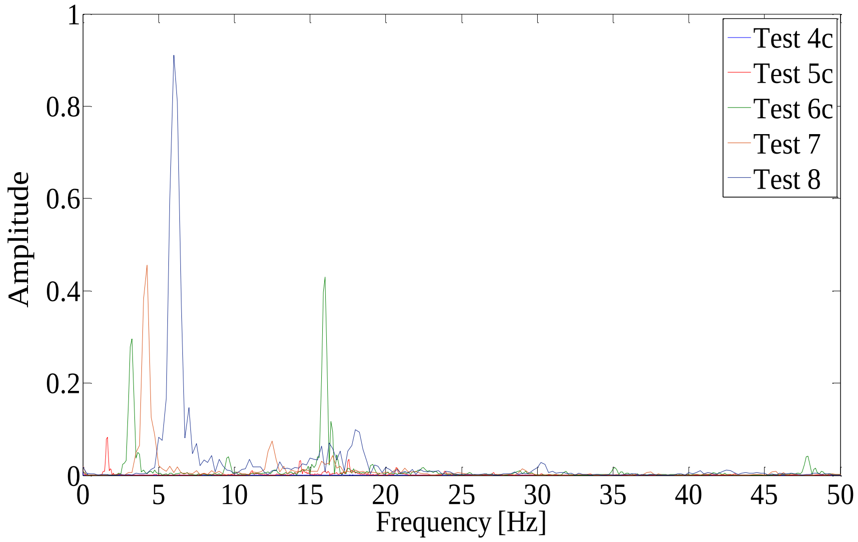

Figure 4.18: Fourier amplitude spectra of mean accelerations

4.3.8 Phase I-2

The testing sequence of phase I-2 is shown in Table 4.9

4.3.8.1 Test 9 through 13

Test 9 used sine wave S0BRB1 (Figure 4.19). The test was not completed since a load limit stopped it. The force-deformation plots of the deformable connection and its individual components (BRB and steel reinforced RB) are shown in Figure 4.22 for the completed cycles.

Test 10 used sine wave S0BRB1 (Figure 4.19). It was completed successfully but yielding did not occur. The flexibilities of the fixture and the gap between the pins and the clevis holes of the BRB connection had to be considered to increase the target displacement and achieve yielding of the BRB. The force-deformation plots of the deformable connection are shown in Figure 4.23.

Test 11 and12 used S02BRB1 (Figure 4.19). Yielding did not occur. The force-deformation plots are shown in Figure 4.24 and Figure 4.25.

Test 13[y] was completed successfully. Sine wave S03BRB1 (Figure 4.19) was used. Yielding during compression of the BRB. The experimental yielding force of the BRB was P_{by} = -217 kips and the elastic stiffness was K_b = 1100 kips/in which leads to a yielding deformation D_{by} =-0.20 inches (Figure 4.26). The force and deformation data at the target displacement peaks are shown in Table 4.10.

4.3.8.2 Test 14: EQ1BRB1

Test 14 was completed successfully. The displacement target is shown in Figure 4.21. Force-deformation plots of the deformable connection and its individual components are shown in Figure 4.27.

4.3.8.3 Test 15: S1BRB1 (ValveProblem)

Test 15 stopped at the 4th cycle because of a problem with one of the servo valves of the actuators. The complete displacement target is shown in Figure 4.20. Force-deformation plots of the completed cycles are presented in Figure 4.28. Due to the valve problem, spikes can be observed in the force-deformation plots. However, this did not affect the quality of the collected data. The force and deformation data collected at the target displacement peaks are shown in Table 4.11.

4.3.8.4 Test 16: S1BRB1 (ATS)

Test 16 was completed successfully. The displacement target is shown in Figure 4.20. The plots related to the performance of the deformable connection are shown in Figure 4.29. In Table 4.12 force and deformation quantities are presented at the displacement peak.

4.3.8.5 Test 17: S2BRB1 (ATS)

Test 17 assessed the performance of the deformable connection at higher frequency. The test was completed successfully using ATS compensation [26]. The displacement target is shown in Figure 4.20. The displacement target is shown in Figure 4.20. The plots of the response of the deformable connection are shown in Figure 4.30. In Table 4.13 the force and deformation data measured at the target displacement peaks are presented.

4.3.8.6 Test 18: S1BRB1 (NoComp)

Test 18 used sine wave S1BRB1 without any compensation. The displacement target is shown in Figure 4.20. The results related to the response of the deformable connection are shown in Figure 4.31. In Table 4.14 force and deformation information are presented at the target displacement peaks.

4.3.8.7 Test 19: S1BRB1 (PID)

Test 19 used sine wave S1BRB1 applying PID control. It was completed successfully. The displacement target is shown in Figure 4.20. The results from the response of the deformable connection are shown in Figure 4.32. In Table 4.15 force and deformation information are presented at the target displacement peaks.

4.3.8.8 Test 20: S3BRB1 (PID LoadLimit)

Test 20 stopped due to triggering of a load limit. The displacement target is shown in Figure 4.20. The results from the response of the deformable connection are shown in Figure 4.33. In Table 4.16 force and deformation information are presented at the target displacement peaks. The North West RB slipped during the last cycle. The rods connecting the RB to the wall were re-tightened and slip did not occur in the following tests.

4.3.8.9 Test 21: S3BRB1

Test 21 was completed successfully using sine wave S3BRB1. The displacement target is shown in Figure 4.20. Fracture of the BRB occurred. The plots related to the response of the deformable connection are shown in Figure 4.34. In Figure 4.35, the force-deformation results for the deformable connection are shown up to the fracture point. The notation *Test* 21^{fr} refers to the data of the Test 21 up to the fracture point. In Table 4.17, force and deformation information are presented at the target displacement peaks. In Figure 4.36 the steel reinforced RB are shown at the peak deformation.

Table 4.9: Phase I-2 testing sequence

Day	Test	Name	$D_{t,max}$ [in]	$V_{t,max}$ [in/sec]	f [Hz]	# Ramp up cycles	# Ramp down cycles	# Max. amplitude cycles
05-19-2014	9	S0BRB1 (LoadLimit)	0.2	0.10	0.06	1	1	0
	10	S0BRB1	0.2	0.10	0.06	1	1	0
	11	S02BRB1	0.3	0.10	0.04	1	1	0
05-20-2014	12	S02BRB1	0.3	0.10	0.04	1	1	0
	13[y]	S03BRB1	0.4	0.10	0.03	1	1	0
	14	EQ1BRB1	2.66	0.45	-	-	-	-
	15	S1BRB1 (ValveProblem)	1.0	0.20	0.03	3	3	3
05-21-2014	16	S1BRB1 (ATS)	1.0	0.20	0.03	3	3	3
	17	S2BRB1 (ATS)	1.0	10.00	1.59	3	3	3
	18	S1BRB1 (NoComp)	1.0	0.20	0.03	3	3	3
	19	S1BRB1 (PID)	1.0	0.20	0.03	3	3	3
	20	S3BRB1(PID LoadLimit)	3.5	0.70	0.03	3	3	3
05-30-2014	21	S3BRB1	3.5	0.70	0.03	3	3	3

Table 4.10: Test 13[y], Response data at target displacement peaks

Cycle #	Peak #	D_t [in]	D_{mE} [in]	D_{mW} [in]	D_b [in]	$\|D_b/D_{by}\|$ [in/in]	D_{cc} [in]	D_{RB} [in]	P_{tot} [kips]	P_b [kips]	V_{RB} [kips]
1	1	-0.15	0.15	0.15	0.13	0.63	0.07	0.13	95	90	5
	2	0.40	-0.40	-0.40	-0.30	1.50	-0.27	-0.30	-223	-205	-18
2	3	-0.40	0.40	0.40	0.33	1.63	0.24	0.33	222	211	11
	4	0.15	-0.15	-0.15	-0.08	0.38	-0.05	-0.09	-151	-142	-9

Table 4.11: Test 15, Response data at target displacement peaks

Cycle #	Peak #	D_t [in]	D_{mE} [in]	D_{mW} [in]	D_b [in]	$\|D_b/D_{by}\|$ [in/in]	D_{cc} [in]	D_{RB} [in]	P_{tot} [kips]	P_b [kips]	V_{RB} [kips]
1	1	0.10	-0.09	-0.09	-0.08	0.40	-0.06	-0.08	5	16	-11
	2	-0.26	0.26	0.26	0.18	0.91	0.16	0.18	197	195	2
2	3	0.42	-0.41	-0.41	-0.29	1.44	-0.16	-0.30	-218	-201	-18
	4	-0.59	0.59	0.59	0.49	2.45	0.45	0.50	260	244	15
3	5	0.75	-0.75	-0.75	-0.60	2.98	-0.45	-0.62	-300	-270	-30
	6	-0.92	0.92	0.92	0.81	4.05	0.77	0.82	292	264	27
4	7	1.00	-1.00	-1.00	-0.83	4.16	-0.69	-0.86	-310	-275	-34
	8	-1.00	1.00	1.00	0.89	4.43	0.84	0.90	297	268	28

Table 4.12: Test 16, Response data at target displacement peaks

Cycle #	Peak #	D_t [in]	D_{mE} [in]	D_{mW} [in]	D_b [in]	$\|D_b/D_{by}\|$ [in/in]	D_{cc} [in]	D_{RB} [in]	P_{tot} [kips]	P_b [kips]	V_{RB} [kips]
1	1	0.10	-0.10	-0.10	-0.08	0.39	-0.03	-0.09	-4	0	-4
	2	-0.26	0.26	0.26	0.15	0.74	0.12	0.15	193	187	6
2	3	0.42	-0.42	-0.42	-0.31	1.55	-0.19	-0.33	-246	-233	-13
	4	-0.59	0.59	0.59	0.46	2.29	0.41	0.46	261	241	20
3	5	0.75	-0.75	-0.75	-0.63	3.17	-0.50	-0.65	-286	-266	-20
	6	-0.92	0.92	0.92	0.77	3.86	0.72	0.78	297	265	32
4	7	1.00	-1.00	-1.00	-0.87	4.33	-0.73	-0.89	-311	-277	-34
	8	-1.00	1.00	1.00	0.85	4.26	0.80	0.86	304	269	35
5	9	1.00	-1.00	-1.00	-0.87	4.34	-0.74	-0.89	-310	-277	-34
	10	-1.00	1.00	1.00	0.85	4.25	0.80	0.86	303	268	35
6	11	1.00	-1.00	-1.00	-0.87	4.33	-0.73	-0.89	-309	-275	-34
	12	-1.00	1.00	1.00	0.85	4.26	0.80	0.86	302	267	34
7	13	0.92	-0.92	-0.92	-0.79	3.96	-0.66	-0.81	-299	-270	-28
	14	-0.75	0.75	0.75	0.61	3.06	0.56	0.62	283	258	25
8	15	0.59	-0.59	-0.59	-0.47	2.33	-0.34	-0.49	-264	-246	-18
	16	-0.42	0.42	0.42	0.30	1.48	0.25	0.30	238	225	12
9	17	0.26	-0.25	-0.25	-0.17	0.85	-0.06	-0.19	-158	-153	-6
	18	-0.10	0.10	0.10	0.09	0.45	0.09	0.09	72	64	8

Table 4.13: Test 17, Response data at target displacement peaks

Cycle #	Peak #	D_t [in]	D_{mE} [in]	D_{mW} [in]	D_b [in]	$\|D_b/D_{by}\|$ [in/in]	D_{cc} [in]	D_{RB} [in]	P_{tot} [kips]	P_b [kips]
1	1	0.10	-0.08	-0.08	-0.08	0.38	-0.01	-0.08	-13	-12
	2	-0.26	0.19	0.19	0.12	0.59	0.09	0.12	140	130
2	3	0.42	-0.41	-0.41	-0.31	1.55	-0.20	-0.33	-227	-214
	4	-0.59	0.60	0.60	0.45	2.26	0.39	0.46	283	264
3	5	0.75	-0.81	-0.81	-0.68	3.40	-0.56	-0.69	-284	-278
	6	-0.92	0.98	0.98	0.81	4.05	0.74	0.82	284	280
4	7	1.00	-1.04	-1.04	-0.90	4.52	-0.79	-0.92	-293	-292
	8	-1.00	1.02	1.02	0.86	4.28	0.79	0.87	282	283
5	9	1.00	-1.01	-1.01	-0.87	4.37	-0.76	-0.89	-294	-291
	10	-1.00	1.01	1.01	0.84	4.18	0.77	0.86	283	283
6	11	1.00	-1.01	-1.01	-0.88	4.40	-0.76	-0.89	-291	-291
	12	-1.00	1.01	1.01	0.84	4.21	0.78	0.86	279	282
7	13	0.92	-0.92	-0.92	-0.80	3.98	-0.68	-0.80	-287	-287
	14	-0.75	0.73	0.73	0.57	2.84	0.51	0.58	269	272
8	15	0.59	-0.56	-0.56	-0.46	2.28	-0.35	-0.46	-251	-256
	16	-0.42	0.38	0.38	0.24	1.21	0.19	0.25	222	227
9	17	0.26	-0.25	-0.25	-0.20	1.02	-0.11	-0.20	-140	-148
	18	-0.10	0.10	0.10	0.07	0.35	0.05	0.08	80	78

Table 4.14: Test 18, Response data at target displacement peaks

Cycle #	Peak #	D_t [in]	D_{mE} [in]	D_{mW} [in]	D_b [in]	$\|D_b/D_{by}\|$ [in/in]	D_{cc} [in]	D_{RB} [in]	P_{tot} [kips]	P_b [kips]	V_{RB} [kips]
1	1	0.10	-0.08	-0.08	-0.07	0.36	-0.01	-0.08	-18	-15	-3
	2	-0.26	0.20	0.20	0.11	0.55	0.08	0.12	122	115	7
2	3	0.42	-0.31	-0.31	-0.23	1.14	-0.14	-0.24	-175	-167	-8
	4	-0.59	0.44	0.44	0.30	1.51	0.24	0.31	243	229	13
3	5	0.75	-0.58	-0.58	-0.47	2.36	-0.37	-0.49	-264	-244	-19
	6	-0.92	0.75	0.75	0.60	3.02	0.53	0.62	280	254	26
4	7	1.00	-0.82	-0.82	-0.70	3.48	-0.59	-0.71	-289	-261	-28
	8	-1.00	0.83	0.83	0.68	3.39	0.60	0.69	284	256	29
5	9	1.00	-0.82	-0.82	-0.70	3.48	-0.59	-0.71	-288	-260	-28
	10	-1.00	0.83	0.83	0.68	3.39	0.60	0.70	283	255	28
6	11	1.00	-0.82	-0.82	-0.70	3.49	-0.59	-0.71	-288	-260	-28
	12	-1.00	0.83	0.83	0.68	3.39	0.60	0.69	282	254	28
7	13	0.92	-0.74	-0.74	-0.62	3.11	-0.52	-0.64	-280	-255	-25
	14	-0.75	0.59	0.59	0.45	2.24	0.38	0.46	261	242	19
8	15	0.59	-0.44	-0.44	-0.33	1.65	-0.23	-0.34	-232	-219	-13
	16	-0.42	0.31	0.31	0.19	0.93	0.13	0.19	190	181	8
9	17	0.26	-0.20	-0.20	-0.16	0.78	-0.08	-0.16	-111	-107	-4
	18	-0.10	0.07	0.07	0.05	0.27	0.03	0.06	61	54	7

Table 4.15: Test 19, Response data at target displacement peaks

Cycle #	Peak #	D_t [in]	D_{mE} [in]	D_{mW} [in]	D_b [in]	$\lvert D_b/D_{by}\rvert$ [in/in]	D_{cc} [in]	D_{RB} [in]	P_{tot} [kips]	P_b [kips]	V_{RB} [kips]
1	1	0.10	-0.10	-0.10	-0.08	0.42	-0.02	-0.09	-34	-32	-3
	2	-0.26	0.26	0.26	0.15	0.73	0.10	0.15	151	144	7
2	3	0.42	-0.42	-0.42	-0.32	1.59	-0.22	-0.33	-227	-214	-13
	4	-0.59	0.59	0.59	0.44	2.22	0.37	0.46	255	236	19
3	5	0.75	-0.75	-0.75	-0.64	3.21	-0.54	-0.65	-277	-251	-26
	6	-0.92	0.92	0.92	0.77	3.83	0.69	0.78	283	252	31
4	7	1.00	-1.00	-1.00	-0.88	4.39	-0.77	-0.89	-300	-265	-34
	8	-1.00	1.00	1.00	0.85	4.23	0.77	0.86	291	257	34
5	9	1.00	-1.00	-1.00	-0.88	4.39	-0.77	-0.89	-302	-267	-35
	10	-1.00	1.00	1.00	0.85	4.23	0.77	0.86	292	258	34
6	11	1.00	-1.00	-1.00	-0.88	4.38	-0.77	-0.89	-303	-268	-35
	12	-1.00	1.00	1.00	0.85	4.23	0.77	0.86	292	258	34
7	13	0.92	-0.92	-0.92	-0.79	3.97	-0.69	-0.81	-296	-265	-32
	14	-0.75	0.75	0.75	0.60	3.02	0.53	0.62	275	251	25
8	15	0.59	-0.59	-0.59	-0.47	2.37	-0.37	-0.49	-260	-241	-19
	16	-0.42	0.42	0.42	0.28	1.41	0.22	0.29	231	219	12
9	17	0.26	-0.26	-0.26	-0.18	0.88	-0.09	-0.19	-156	-151	-6
	18	-0.10	0.10	0.10	0.08	0.41	0.05	0.09	69	62	7

Table 4.16: Test 20, Response data at target displacement peaks

Cycle #	Peak #	D_t [in]	D_{mE} [in]	D_{mW} [in]	D_b [in]	$\lvert D_b/D_{by}\rvert$ [in/in]	D_{cc} [in]	D_{RB} [in]	P_{tot} [kips]	P_b [kips]	V_{RB} [kips]
1	1	0.34	-0.34	-0.34	-0.25	1.24	-0.15	-0.26	-186	-178	-9
	2	-0.89	0.89	0.89	0.74	3.69	0.67	0.75	284	253	31
2	3	1.47	-1.47	-1.47	-1.33	6.66	-1.22	-1.35	-336	-286	-49
	4	-2.05	2.05	2.05	1.87	9.33	1.78	1.90	350	280	71
3	5	2.63	-2.63	-2.63	-2.46	12.30	-2.34	-2.47	-429	-341	-87
	6	-3.21	3.22	3.22	2.98	14.88	2.88	3.03	415	309	106

Table 4.17: Test 21, Response data at target displacement peaks

Cycle #	Peak #	D_t [in]	D_{mE} [in]	D_{mW} [in]	D_b [in]	$\lvert D_b/D_{by}\rvert$ [in/in]	D_{cc} [in]	D_{RB} [in]	P_{tot} [kips]	P_b [kips]	V_{RB} [kips]
1	1	0.34	-0.34	-0.34	-0.32	1.61	-0.21	-0.33	-144	-117	-27
	2	-0.89	0.89	0.89	0.88	4.39	0.83	0.89	377	346	31
2	3	1.47	-1.47	-1.47	-1.42	7.11	-1.29	-1.44	-421	-361	-60
	4	-2.05	2.05	2.05	2.02	10.10	1.98	2.04	405	338	67
3	5	2.63	-2.63	-2.63	-2.58	12.89	-2.43	-2.58	-532	-433	-99
	6	-3.21	3.21	3.21	3.15	15.76	3.11	3.19	447	339	108
4	**7[a]**	**3.50**	**-3.50**	**-3.50**	**-3.43**	**17.17**	**-3.29**	**-3.42**	**-618**	**-481**	**-136**
	8	-3.50	3.50	3.50	3.20	16.00	3.37	3.48	158	32	125
5	9	3.50	-3.50	-3.50	-3.70	18.52	-3.45	-3.44	-300	-167	-133
	10	-3.50	3.50	3.50	3.19	15.97	3.35	3.48	160	37	123
6	11	3.50	-3.50	-3.50	-3.70	18.51	-3.45	-3.44	-265	-132	-133
	12	-3.50	3.50	3.50	3.20	15.99	3.36	3.48	159	37	121
7	13	3.21	-3.22	-3.21	-3.43	17.16	-3.19	-3.16	-175	-60	-115
	14	-2.63	2.63	2.63	2.35	11.74	2.51	2.63	111	24	87
8	15	2.05	-2.05	-2.05	-2.28	11.39	-2.03	-2.02	-90	-15	-75
	16	-1.47	1.47	1.47	1.20	6.02	1.37	1.47	69	16	54
9	17	0.89	-0.89	-0.89	-1.13	5.66	-0.89	-0.88	-50	-9	-41
	18	-0.34	0.34	0.34	0.08	0.40	0.24	0.34	22	9	13

[a]Peak before fracture of BRB

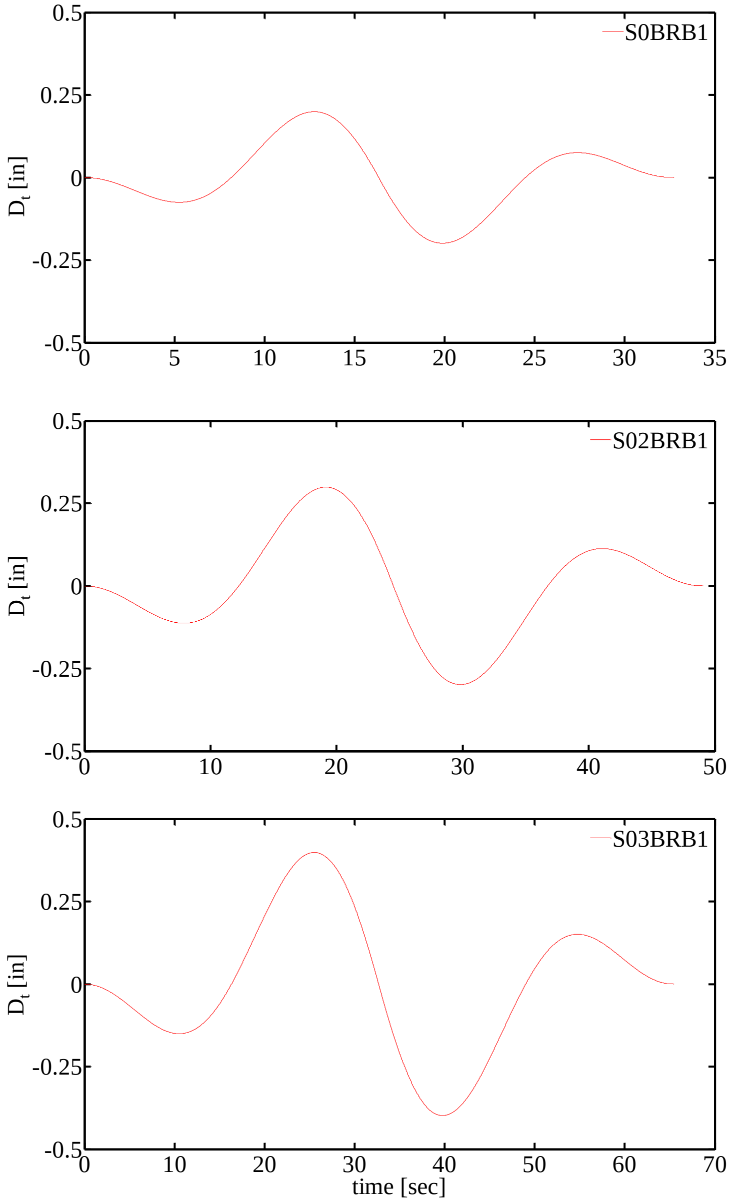

Figure 4.19: Target displacement histories used in phase I-2 to identify the yielding deformation of BRB

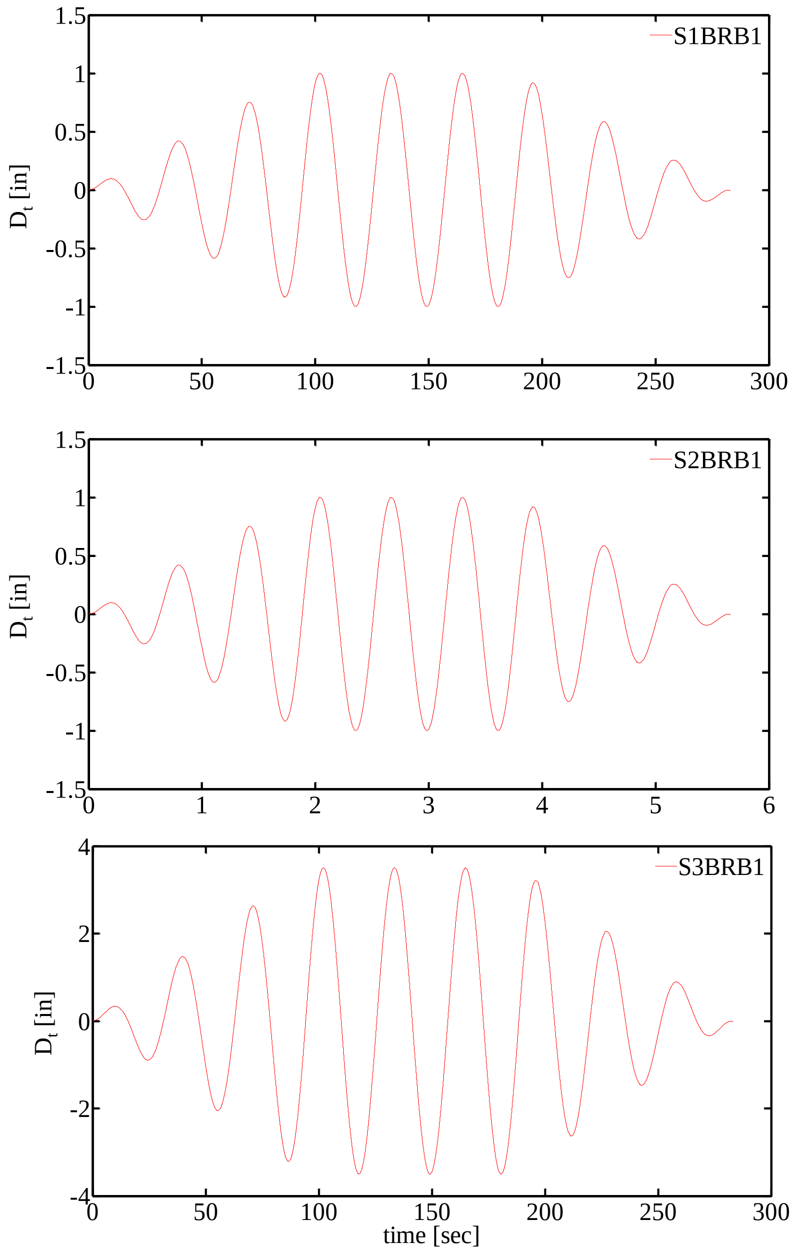

Figure 4.20 : Target sine wave displacement histories used in phase I-2

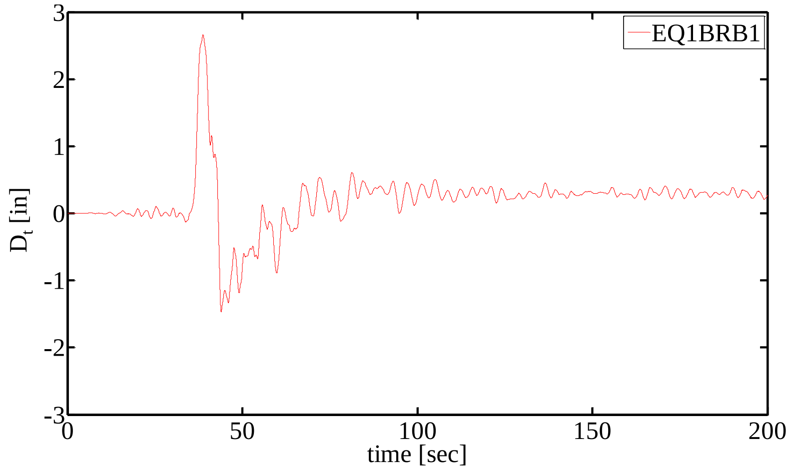

Figure 4.21: Target displacement: Friuli 1976 TMZ000 ground motion (DBE) with 10 times scaled time scale

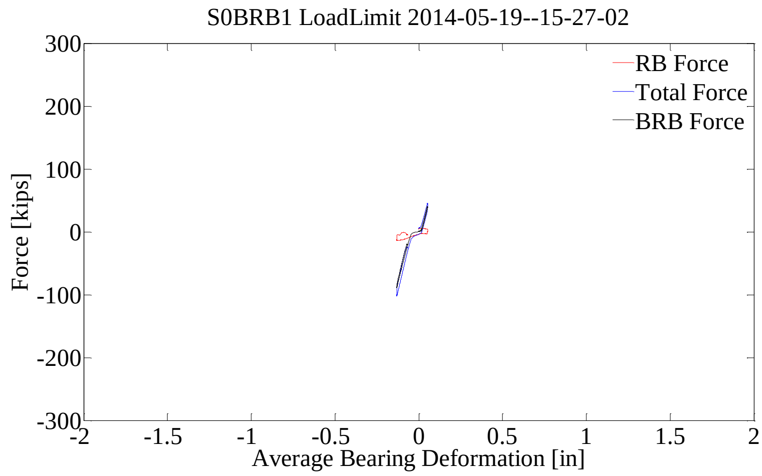

Figure 4.22: Test 9, Force – deformation plots for the deformable connection and its individual components in phase I [pg. 28]

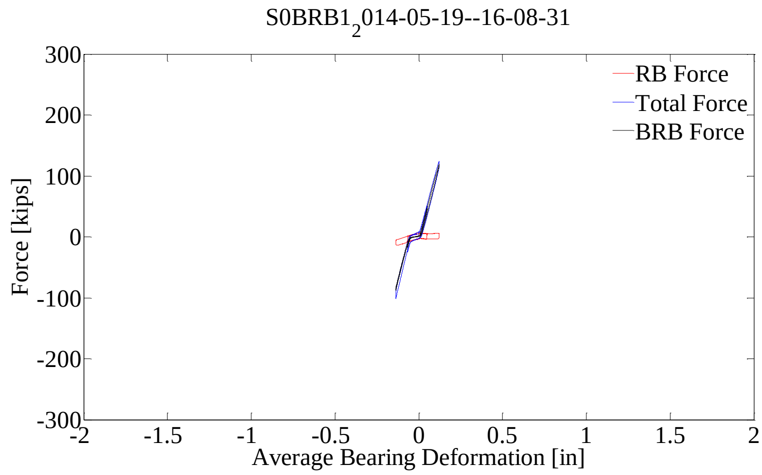

Figure 4.23: Test 10, Force – deformation plots for the deformable connection and its individual components in phase I [pg. 28]

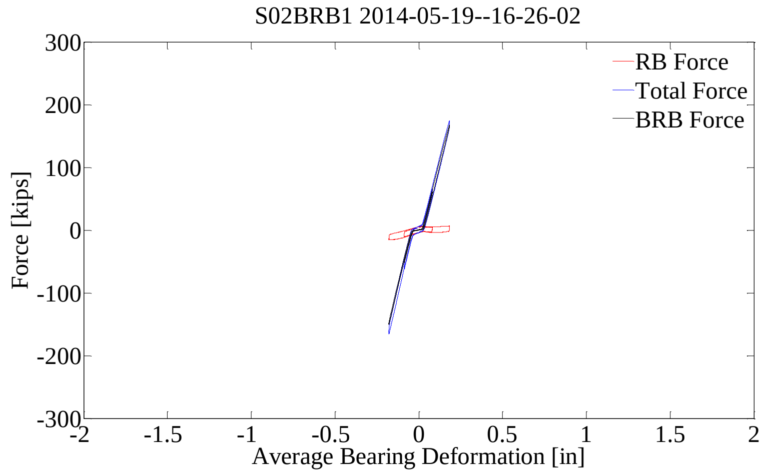

Figure 4.24: Test 11, Force – deformation plots for the deformable connection and its individual components in phase I [pg. 28]

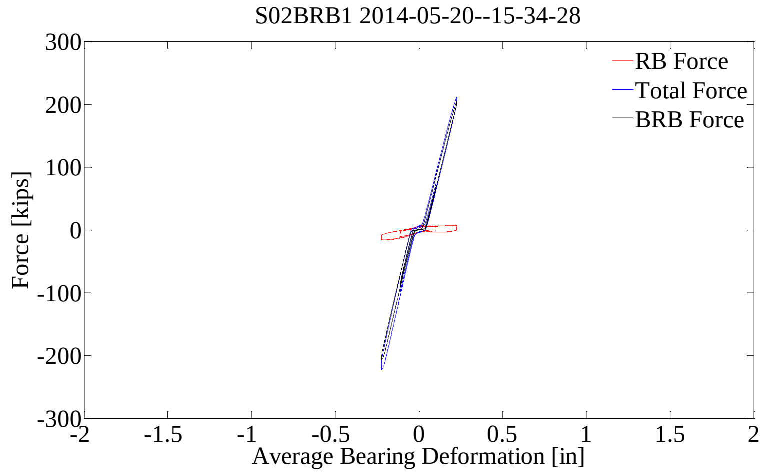

Figure 4.25: Test 12, Force – deformation plots for the deformable connection and its individual components in phase I [pg. 28]

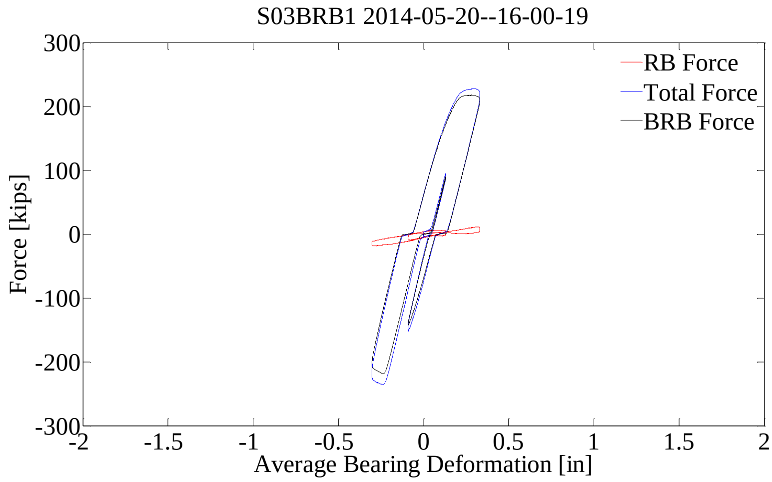

Figure 4.26: Test 13^{y}, Force – deformation plots for the deformable connection and its individual components in phase I. Yielding of BRB [pg. 28; pg. 24]

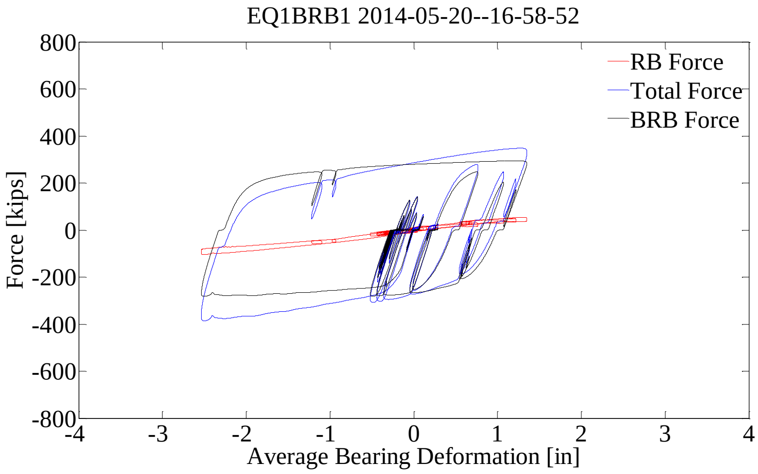

Figure 4.27: Test 14 Force – deformation plots for the deformable connection and its individual components in phase I [pg. 30]

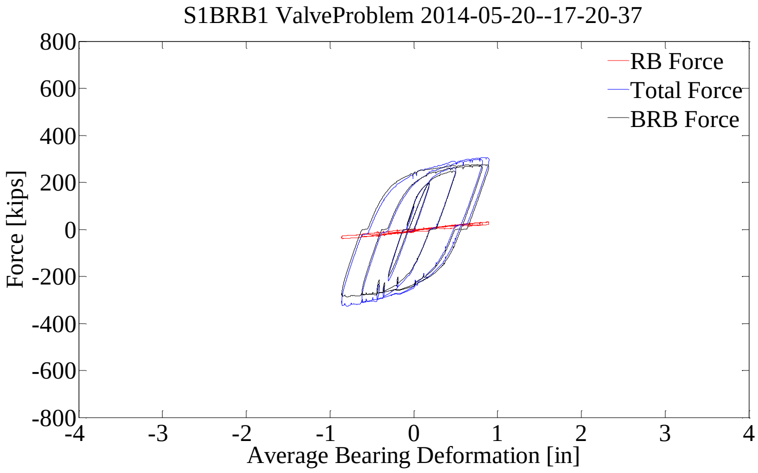

Figure 4.28: Test 15, Force – deformation plots for the deformable connection and its individual components in phase I [pg. 29; pg. 24]

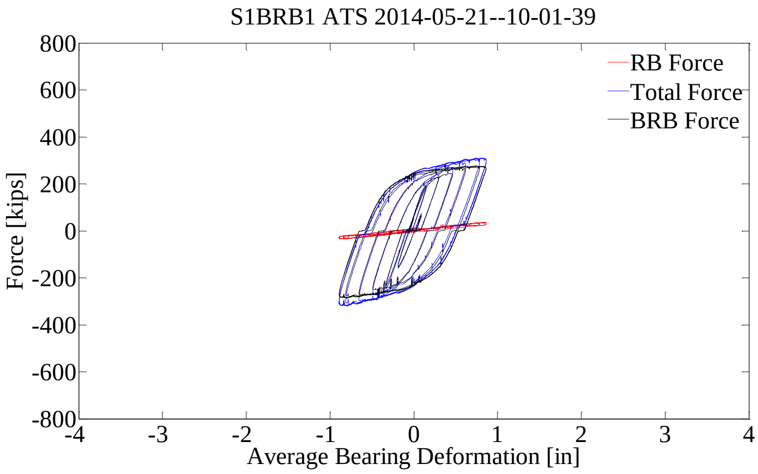

Figure 4.29: Test 16, Force – deformation plots for the deformable connection and its individual components in phase I [pg. 29; pg. 24]

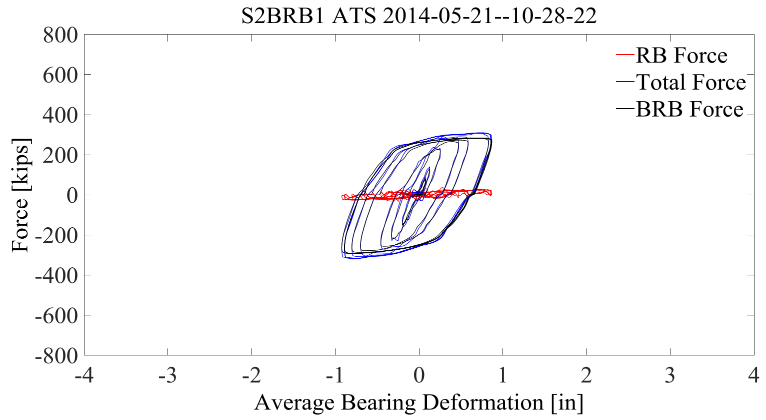

Figure 4.30: Test 17, Force – deformation plots for the deformable connection and its individual components in phase I [pg. 29; pg. 25]

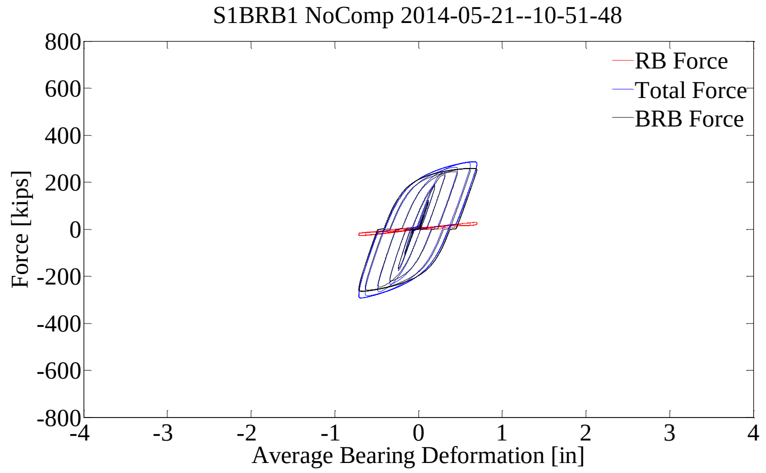

Figure 4.31: Test 18, Force – deformation plots for the deformable connection and its individual components in phase I [pg. 29; pg. 25]

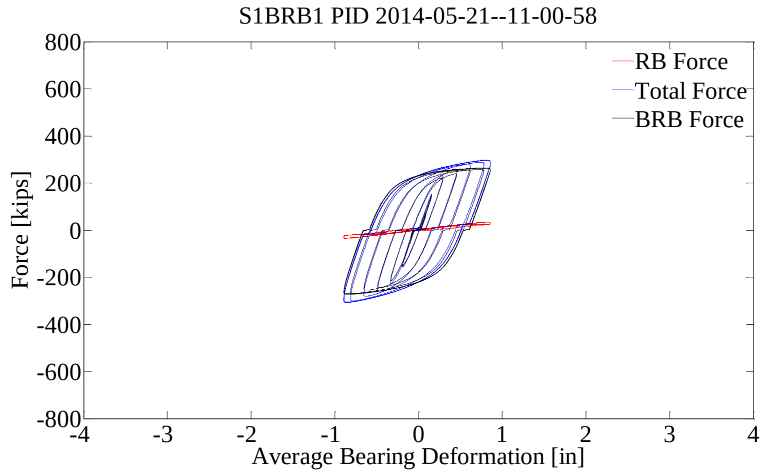

Figure 4.32: Test 19, Force – deformation plots for the deformable connection and its individual components in phase I [pg. 29; pg. 26]

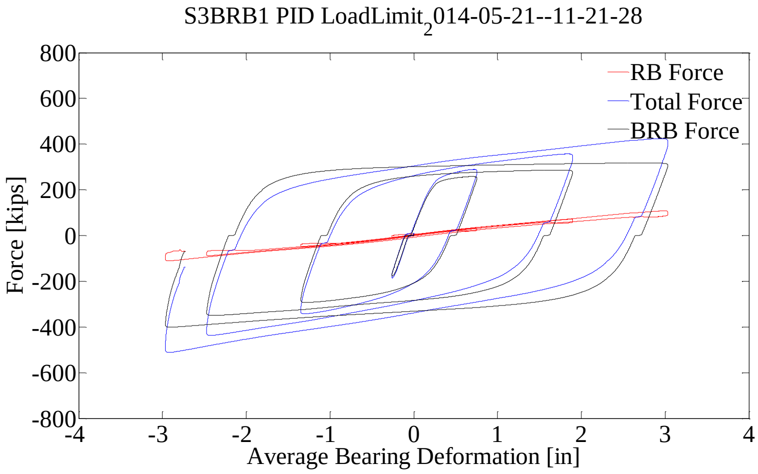

Figure 4.33: Test 20, Force – deformation plots for the deformable connection and its individual components in phase I [pg. 29; pg. 26]

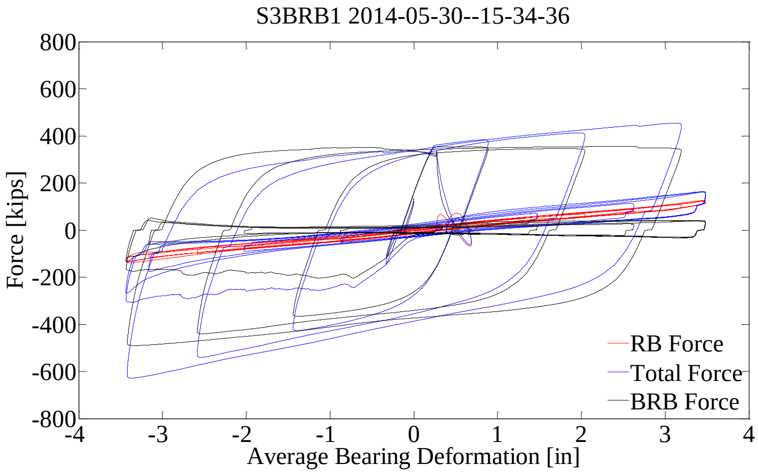

Figure 4.34: Test 21, Force – deformation plots for the deformable connection and its individual components in phase I [pg. 29; pg. 27]

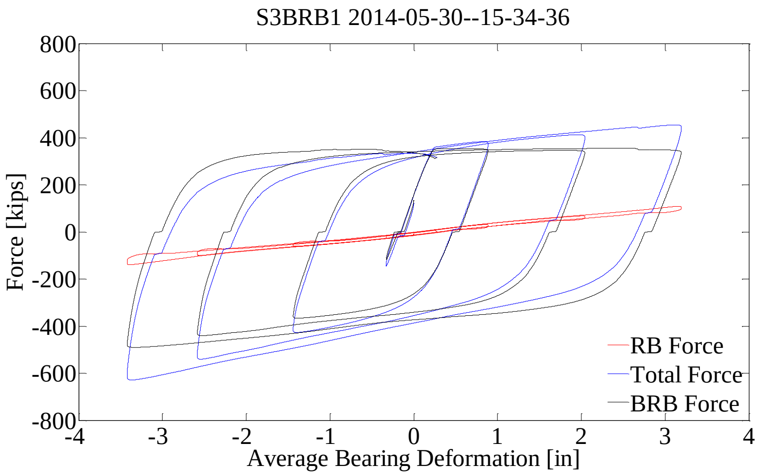

Figure 4.35: Test 21^{fr}, Force – deformation plots for the deformable connection and its individual components in phase I [pg. 29; pg. 27]

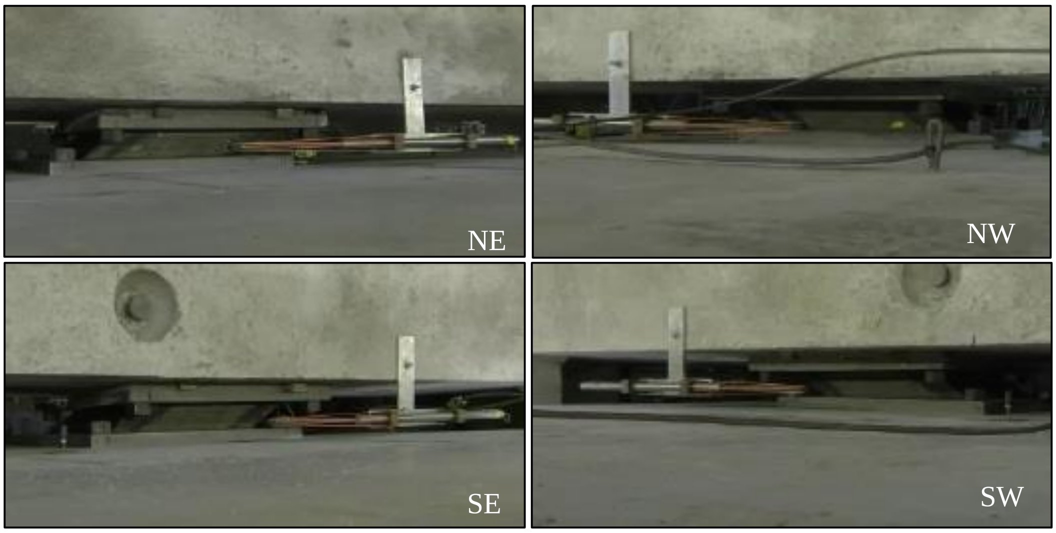

Figure 4.36: Steel reinforced RB at target displacement peak

4.3.9 Phase I-3

In phase I-3 the steel reinforced RB used in phase I-1 and I-2 were used. The BRB was replaced with a second BRB that has identical characteristics with the one used in phase I-2 (see section 4.3.1).

The testing sequence of phase I-3 is shown in Table 4.18.

4.3.9.1 Test 22 through 24^y

Test 22 and 23 assessed the functionality of the sensors before initiating the tests in phase I-3. The force-deformation plots of the deformable connection for test 23 are show in Figure 4.42.

Test 24^y was used to identify the yielding strength of the BRB. The displacement target is shown in Figure 4.37. By observing the force-deformation response of the BRB it can be seen that the experimental elastic stiffness and yielding force are K_b = 1100 kips/in and P_{by} = 217 kips, respectively, which results in the yielding deformation D_{by} = 0.20 inches. In this test yielding occurred in tension. The force-deformation plots of the deformable connection are shown in Figure 4.43. Information about the force and deformation data at the target displacement peaks are shown in Table 4.19.

4.3.9.2 Test 25: EQ7 EQ1BRB2

Test 25 was completed successfully. The low frequency earthquake displacement history EQ7 EQ1BRB2 was used. The displacement target is shown in Figure 4.40. The force-deformation response of the deformable connection is presented in Figure 4.44.

4.3.9.3 Test 26: EQ1 EQ2BRB2

Test 26 was completed successfully. The EQ1 EQ2BRB2 earthquake displacement history was used. This history is the same with EQ1BRB1 used in phase I-2. The displacement target is shown in Figure 4.41. The deformable connection force-deformation response is shown in Figure 4.45.

4.3.9.4 Test 27: S11BRB2

Test 27 completed successfully using sine wave S11BRB2. The displacement target is shown in Figure 4.38. The force-deformation response of the deformable connection shown in Figure 4.46. In the force and deformation data at the target displacement peaks are presented in Table 4.20.

4.3.9.5 Test 28: S12BRB2

Test 28 was completed successfully using sine wave S12BRB2. The displacement target is shown in Figure 4.38. The force-deformation plots of the deformable connection are shown in Figure 4.47. In Table 4.21 his force and deformation data at the target displacement peaks are presented.

4.3.9.6 Test 29: S12BRB2 (UpdateA1)

Test 29 was completed successfully using sine wave S12BRB2 with updated parameters for the ATS compensation in each location [26]. The displacement target is shown in Figure 4.38. The force-deformation plots of the deformable connection are shown in Figure 4.48. In Table 4.22 the force and deformation data at the target displacement peaks are presented.

4.3.9.7 Test 30: S11BRB2_2

Test 30 was successfully completed using the sine wave S11BRB2. It was a repetition of Test 27 after Tests 28 and 29 to confirm that the response of the deformable connection is unchanged. The displacement target is shown in Figure 4.38. The response of the deformable connection was satisfactory and the force-deformation plots are shown in Figure 4.49. In Table 4.23 the force and deformation data at the target displacement peaks are presented.

4.3.9.8 Test 31: S21BRB2

Test 31 was successfully completed. The maximum deformation for this test was 10 times the yielding deformation of the BRB. The design deformation limit was 2.0 inches which is approximately 8 times the yielding deformation. No fracture occurred. LV71 did not work properly and its measurement for this test is not valid. For the average bearing deformation D_{RB} the three LVDTs LV61, LV62, LV72 were used. The displacement target is shown in Figure 4.39. The force-deformation plots are shown in Figure 4.50. In Table 4.24 the force and deformation data at the target displacement peaks are presented.

4.3.9.9 Test 32: S22BRB2

Test 32 was completed successfully using sine wave S22BRB2 which led to the fracture of the BRB. The displacement target is shown in Figure 4.39. The force-deformation plots are shown in Figure 4.51. In Figure 4.53, the two ends of the phase I-3 fractured BRB are shown. It can be observed that the yielding zone plate has fractured at the South end of the BRB which is attached at the shear wall. In Figure 4.54 the steel reinforced RB are shown in deformed position at the end of phase I. In Table 4.25, the force and deformation data at the target displacement peaks are presented.

Table 4.18: Phase I-3 testing sequence

Day	Test	Name	$D_{t,max}$ [in]	$V_{t,max}$ [in/sec]	f [Hz]	# Ramp up cycles	# Ramp down cycles	# Max. amplitude cycles
05-27-2014	22	S0BRB2_ControlTest	0.15	0.04	0.03	1	1	0
05-29-2014	23	S0BRB2	0.15	0.04	0.03	1	1	0
	24^y	S02BRB2	0.35	0.08	0.03	1	1	0
	25	EQ7 EQ1BRB2	1.68	0.66	-	-	-	-
	26	EQ1 EQ2BRB2	2.66	0.45	-	-	-	-
	27	S11BRB2	1.50	0.30	0.03	3	3	3
	28	S12BRB2	1.50	15.00	1.59	3	3	3
	29	S12BRB2 (UpdatedA1)	1.50	15.00	1.59	3	3	3
	30	S11BRB2_2	1.50	0.30	0.03	3	3	3
	31	S21BRB2	2.50	0.50	0.03	3	3	3
05-30-2014	32	S22BRB2	2.50	15.00	0.95	3	3	3

Table 4.19: Test 24^y, Response data at target displacement peaks

Cycle #	Peak #	D_t [in]	D_{mE} [in]	D_{mW} [in]	D_b [in]	$\|D_b/D_{by}\|$ [in/in]	D_{cc} [in]	D_{RB} [in]	P_{tot} [kips]	P_b [kips]	V_{RB} [kips]
1	1	0.13	-0.13	-0.13	-0.12	0.61	-0.08	-0.13	-99	-92	-6
	2	-0.35	0.35	0.35	0.34	1.71	0.27	0.35	227	213	13
2	3	0.35	-0.35	-0.35	-0.33	1.64	-0.27	-0.35	-219	-204	-15
	4	-0.13	0.13	0.13	0.12	0.62	0.06	0.12	178	172	6

Table 4.20: Test 27, Response data at target displacement peaks

Cycle #	Peak #	D_t [in]	D_{mE} [in]	D_{mW} [in]	D_b [in]	$\|D_b/D_{by}\|$ [in/in]	D_{cc} [in]	D_{RB} [in]	P_{tot} [kips]	P_b [kips]	V_{RB} [kips]
1	1	0.14	-0.14	-0.15	-0.13	0.63	-0.07	-0.14	-10	0	-10
	2	-0.38	0.38	0.38	0.36	1.80	0.34	0.38	244	233	11
2	3	0.63	-0.63	-0.63	-0.59	2.94	-0.48	-0.62	-307	-281	-27
	4	-0.88	0.88	0.88	0.84	4.22	0.81	0.87	300	270	30
3	5	1.13	-1.13	-1.13	-1.07	5.36	-0.96	-1.11	-336	-293	-43
	6	-1.38	1.38	1.38	1.33	6.65	1.29	1.38	329	283	46
4	7	1.50	-1.50	-1.50	-1.43	7.13	-1.31	-1.48	-363	-308	-55
	8	-1.50	1.50	1.50	1.45	7.26	1.41	1.50	338	289	49
5	9	1.50	-1.50	-1.50	-1.43	7.13	-1.31	-1.48	-367	-312	-55
	10	-1.50	1.50	1.50	1.45	7.25	1.41	1.50	338	289	49
6	11	1.50	-1.50	-1.50	-1.43	7.15	-1.31	-1.48	-368	-313	-55
	12	-1.50	1.50	1.50	1.45	7.25	1.41	1.50	338	289	49
7	13	1.38	-1.38	-1.38	-1.31	6.56	-1.20	-1.36	-361	-310	-51
	14	-1.13	1.13	1.13	1.09	5.46	1.06	1.12	318	282	37
8	15	0.88	-0.88	-0.88	-0.82	4.10	-0.71	-0.86	-321	-287	-35
	16	-0.63	0.63	0.63	0.60	3.02	0.57	0.63	282	263	19
9	17	0.38	-0.38	-0.38	-0.35	1.75	-0.24	-0.37	-259	-242	-16
	18	-0.14	0.14	0.15	0.13	0.65	0.12	0.14	158	157	1

Table 4.21: Test 28, Response data at target displacement peaks

Cycle #	Peak #	D_t [in]	D_{mE} [in]	D_{mW} [in]	D_b [in]	$\|D_b/D_{by}\|$ [in/in]	D_{cc} [in]	D_{RB} [in]	P_{tot} [kips]	P_b [kips]
1	1	0.14	-0.12	-0.13	-0.10	0.52	-0.04	-0.12	-41	-30
	2	-0.38	0.32	0.37	0.31	1.54	0.27	0.33	247	247
2	3	0.63	-0.42	-0.53	-0.42	2.08	-0.33	-0.46	-283	-272
	4	-0.88	0.96	1.02	0.95	4.74	0.90	0.97	308	293
3	5	1.13	-1.00	-1.11	-0.99	4.94	-0.90	-1.03	-324	-309
	6	-1.38	1.59	1.57	1.52	7.59	1.46	1.57	295	287
4	7	1.50	-1.29	-1.42	-1.28	6.40	-1.19	-1.33	-331	-312
	8	-1.50	1.56	1.59	1.53	7.64	1.47	1.58	295	283
5	9	1.50	-1.24	-1.38	-1.23	6.14	-1.14	-1.28	-326	-322
	10	-1.50	1.56	1.58	1.52	7.58	1.46	1.56	296	293
6	11	1.50	-1.24	-1.38	-1.24	6.19	-1.15	-1.28	-327	-319
	12	-1.50	1.56	1.58	1.52	7.58	1.46	1.57	291	291
7	13	1.38	-1.10	-1.25	-1.12	5.58	-1.03	-1.15	-320	-316
	14	-1.13	1.12	1.17	1.10	5.48	1.04	1.14	281	284
8	15	0.88	-0.57	-0.71	-0.60	3.02	-0.52	-0.62	-288	-288
	16	-0.63	0.59	0.62	0.57	2.86	0.52	0.60	256	262
9	17	0.38	-0.10	-0.21	-0.14	0.71	-0.06	-0.15	-210	-216
	18	-0.14	0.24	0.25	0.23	1.15	0.21	0.24	102	101

Table 4.22: Test 29, Response data at target displacement peaks

Cycle #	Peak #	D_t [in]	D_{mE} [in]	D_{mW} [in]	D_b [in]	$\|D_b/D_{by}\|$ [in/in]	D_{cc} [in]	D_{RB} [in]	P_{tot} [kips]	P_b [kips]
1	1	0.14	-0.10	-0.12	-0.10	0.51	-0.05	-0.11	-70	-69
	2	-0.38	0.25	0.30	0.25	1.23	0.19	0.26	222	213
2	3	0.63	-0.47	-0.58	-0.48	2.39	-0.41	-0.51	-304	-280
	4	-0.88	0.85	0.89	0.82	4.10	0.75	0.84	307	295
3	5	1.13	-1.16	-1.29	-1.16	5.80	-1.10	-1.20	-326	-319
	6	-1.38	1.53	1.45	1.43	7.15	1.36	1.48	288	285
4	7	1.50	-1.47	-1.55	-1.44	7.21	-1.38	-1.49	-332	-319
	8	-1.50	1.51	1.47	1.44	7.22	1.38	1.49	288	284
5	9	1.50	-1.40	-1.50	-1.38	6.91	-1.32	-1.42	-335	-328
	10	-1.50	1.50	1.47	1.43	7.14	1.36	1.48	285	288
6	11	1.50	-1.40	-1.51	-1.39	6.95	-1.33	-1.43	-338	-325
	12	-1.50	1.50	1.47	1.44	7.19	1.37	1.48	284	283
7	13	1.38	-1.26	-1.38	-1.26	6.29	-1.20	-1.30	-331	-320
	14	-1.13	1.06	1.05	1.02	5.10	0.95	1.05	274	280
8	15	0.88	-0.72	-0.83	-0.74	3.69	-0.68	-0.76	-291	-293
	16	-0.63	0.51	0.51	0.48	2.42	0.42	0.51	248	264
9	17	0.38	-0.24	-0.33	-0.27	1.33	-0.21	-0.28	-216	-221
	18	-0.14	0.13	0.14	0.13	0.66	0.09	0.13	99	107

Table 4.23: Test 30, Response data at target displacement peaks

Cycle #	Peak #	D_t [in]	D_{mE} [in]	D_{mW} [in]	D_b [in]	$\|D_b/D_{by}\|$ [in/in]	D_{cc} [in]	D_{RB} [in]	P_{tot} [kips]	P_b [kips]	V_{RB} [kips]
1	1	0.14	-0.15	-0.14	-0.13	0.67	-0.13	-0.14	-204	-210	6
	2	-0.38	0.38	0.38	0.34	1.72	0.23	0.37	208	187	21
2	3	0.63	-0.63	-0.63	-0.61	3.07	-0.60	-0.62	-282	-266	-16
	4	-0.88	0.88	0.88	0.81	4.07	0.68	0.87	310	274	36
3	5	1.13	-1.13	-1.13	-1.09	5.46	-1.08	-1.11	-333	-298	-35
	6	-1.38	1.38	1.38	1.31	6.53	1.17	1.37	337	284	53
4	7	1.50	-1.50	-1.50	-1.46	7.28	-1.44	-1.47	-369	-321	-47
	8	-1.50	1.50	1.50	1.43	7.15	1.29	1.51	346	290	56
5	9	1.50	-1.50	-1.50	-1.45	7.26	-1.43	-1.45	-371	-324	-47
	10	-1.50	1.50	1.50	1.43	7.14	1.29	1.52	346	290	56
6	11	1.50	-1.50	-1.50	-1.45	7.25	-1.43	-1.45	-372	-325	-47
	12	-1.50	1.50	1.50	1.42	7.12	1.29	1.52	345	289	56
7	13	1.38	-1.38	-1.38	-1.33	6.66	-1.31	-1.33	-364	-321	-42
	14	-1.13	1.13	1.13	1.06	5.30	0.93	1.15	327	283	44
8	15	0.88	-0.88	-0.88	-0.85	4.26	-0.83	-0.84	-320	-294	-26
	16	-0.63	0.63	0.63	0.58	2.88	0.45	0.65	292	264	28
9	17	0.38	-0.38	-0.38	-0.36	1.81	-0.35	-0.35	-249	-244	-5
	18	-0.14	0.14	0.14	0.11	0.55	0.00	0.17	165	154	12

Table 4.24: Test 31, Response data at target displacement peaks

Cycle #	Peak #	D_t [in]	D_{mE} [in]	D_{mW} [in]	D_b [in]	$\lvert D_b/D_{by}\rvert$ [in/in]	D_{cc} [in]	D_{RB} [in]	P_{tot} [kips]	P_b [kips]	V_{RB} [kips]
1	1	0.24	-0.24	-0.24	-0.23	1.14	-0.21	-0.24	-252	-248	-4
	2	-0.64	0.64	0.64	0.58	2.90	0.47	0.63	269	247	22
2	3	1.05	-1.05	-1.05	-1.01	5.06	-0.99	-1.04	-341	-304	-37
	4	-1.46	1.46	1.46	1.39	6.94	1.26	1.46	331	282	49
3	5	1.88	-1.88	-1.88	-1.82	9.10	-1.79	-1.86	-404	-341	-63
	6	-2.30	2.30	2.30	2.20	10.99	2.07	2.29	376	300	75
4	7	2.50	-2.50	-2.50	-2.43	12.15	-2.40	-2.47	-458	-376	-81
	8	-2.50	2.50	2.50	2.40	12.02	2.27	2.49	390	313	77
5	9	2.50	-2.50	-2.50	-2.42	12.12	-2.38	-2.47	-471	-391	-80
	10	-2.50	2.50	2.50	2.40	12.01	2.26	2.49	399	319	80
6	11	2.50	-2.50	-2.50	-2.42	12.11	-2.38	-2.46	-481	-401	-80
	12	-2.50	2.50	2.50	2.40	12.01	2.26	2.49	402	322	80
7	13	2.30	-2.30	-2.30	-2.22	11.12	-2.18	-2.27	-476	-404	-72
	14	-1.88	1.88	1.88	1.80	9.01	1.66	1.88	379	321	58
8	15	1.46	-1.47	-1.47	-1.41	7.04	-1.37	-1.44	-416	-369	-47
	16	-1.05	1.05	1.05	0.99	4.95	0.85	1.04	339	306	33
9	17	0.64	-0.64	-0.64	-0.61	3.07	-0.58	-0.63	-330	-310	-20
	18	-0.24	0.24	0.24	0.20	1.00	0.09	0.23	241	235	6

Table 4.25: Test 32, Response data at target displacement peaks

Cycle #	Peak #	D_t [in]	D_{mE} [in]	D_{mW} [in]	D_b [in]	$\lvert D_b/D_{by}\rvert$ [in/in]	D_{cc} [in]	D_{RB} [in]	P_{tot} [kips]	P_b [kips]
1	1	0.24	-0.10	-0.15	-0.10	0.51	-0.08	-0.12	-115	-112
	2	-0.64	0.51	0.60	0.51	2.55	0.38	0.53	353	332
2	3	1.05	-0.81	-0.94	-0.77	3.87	-0.73	-0.83	-438	-406
	4	-1.46	1.66	1.69	1.60	7.98	1.46	1.65	398	351
3	5	1.88	-1.68	-1.66	-1.55	7.77	-1.50	-1.62	-477	-443
	6	-2.30	2.47	2.35	2.32	11.61	2.17	2.38	408	350
4	7	2.50	-2.21	-1.99	-1.93	9.66	-1.89	-1.99	-520	-478
	8	-2.50	2.67	2.46	2.48	12.42	2.32	2.51	395	339
5	**9**[a]	2.50	-2.18	-1.94	-1.90	9.49	-1.86	-1.96	-522	-480
	10	-2.50	2.80	2.64	2.66	13.28	2.60	2.72	64	0
6	11	2.50	-2.17	-2.11	-2.12	10.59	-2.08	-2.07	-497	-453
	12	-2.50	2.88	2.84	2.77	13.84	2.68	2.84	145	57
7	13	2.30	-1.91	-2.02	-1.98	9.90	-1.97	-1.93	-348	-280
	14	-1.88	2.07	2.09	2.01	10.06	1.93	2.07	107	39
8	15	1.46	-1.34	-1.35	-1.39	6.93	-1.39	-1.34	-54	-12
	16	-1.05	1.14	1.14	1.08	5.38	0.99	1.13	75	31
9	17	0.64	-0.48	-0.48	-0.53	2.63	-0.53	-0.47	-55	-34
	18	-0.24	0.32	0.34	0.25	1.27	0.17	0.32	49	34

[a]Peak before fracture of BRB

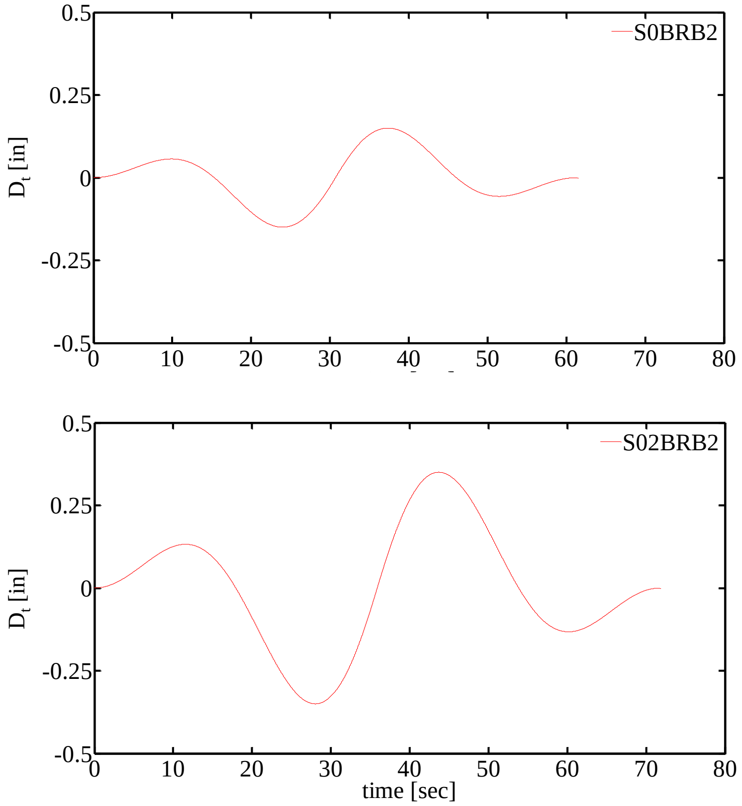

Figure 4.37: Target sine wave displacement histories used in phase I-3 to identify the true yielding deformation of BRB

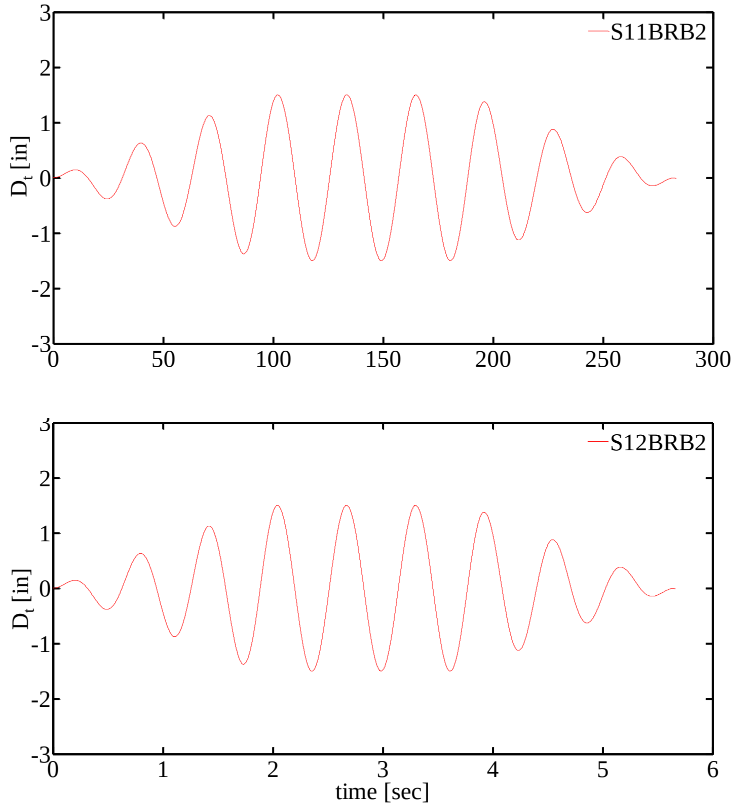

Figure 4.38: Low and high frequency sine waves used in phase I-3 with 1.5 in amplitude

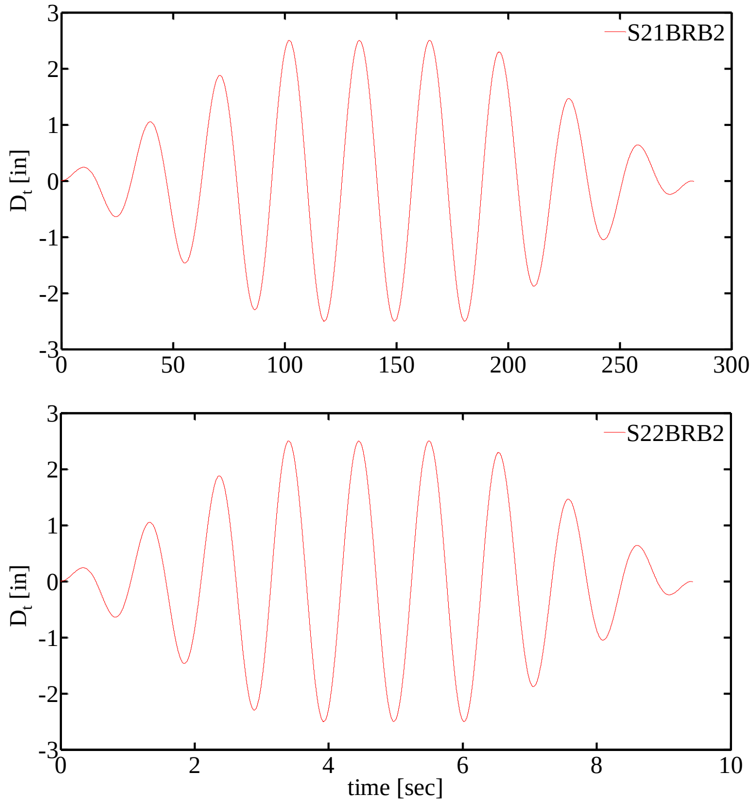

Figure 4.39: Low and high frequency sine wave used in phase I-3 with 2.5 in amplitude

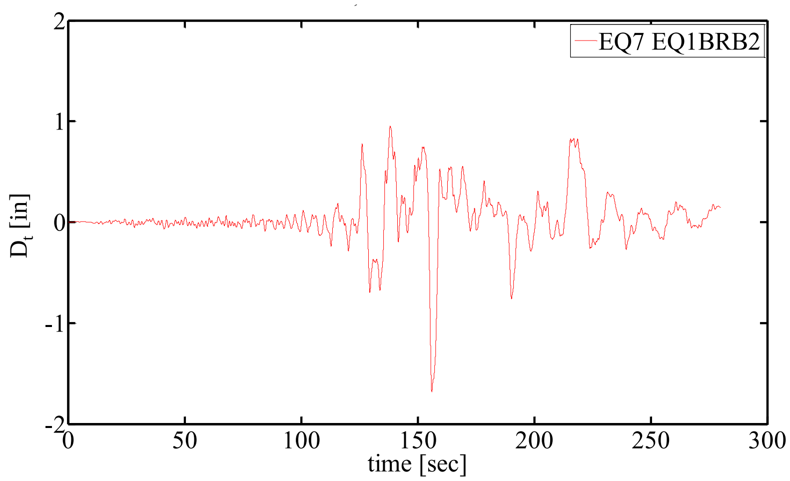

Figure 4.40: DBE level Landers 1992 YER270 ground motion with 10 times longer time scale

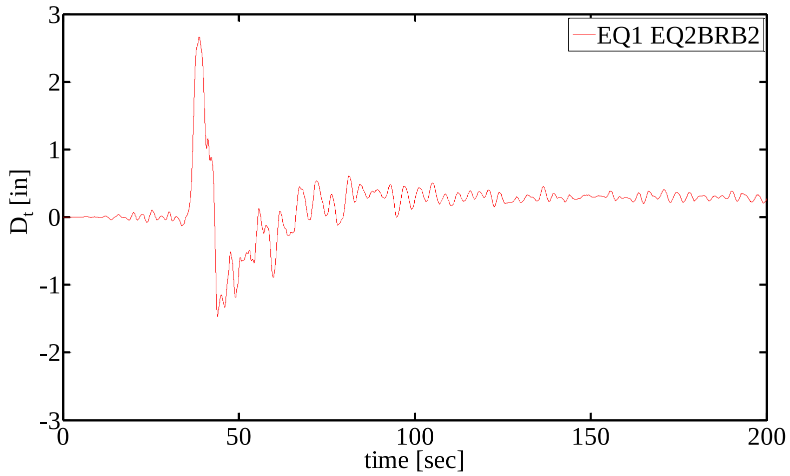

Figure 4.41: DBE level Friuli 1976 TMZ000 ground motion with 10 times longer time scale

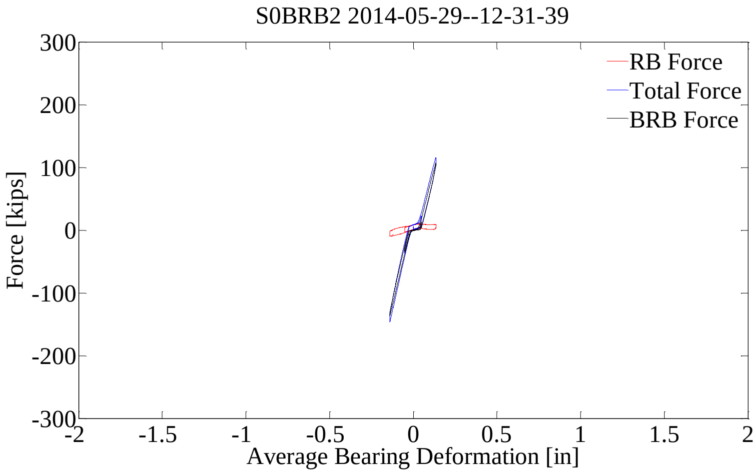

Figure 4.42: Test 23, Force – deformation plots for the deformable connection and its individual components in phase I [pg. 42]

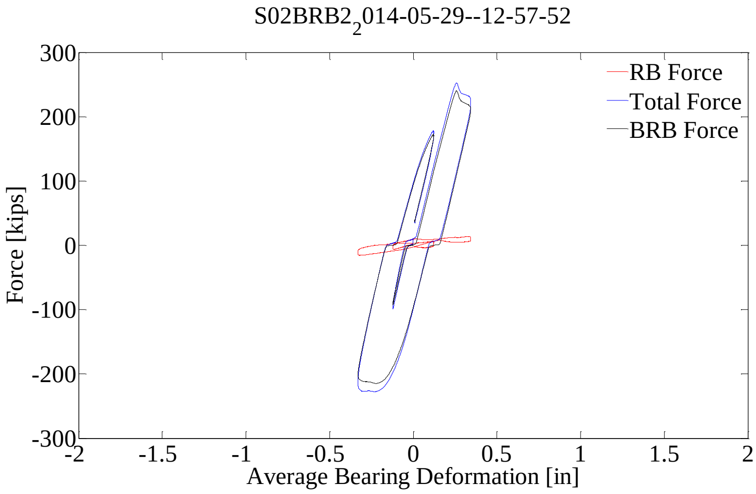

Figure 4.43: Test 24[y], Force – deformation plots for the deformable connection and its individual components in phase I [pg. 42; pg. 38]

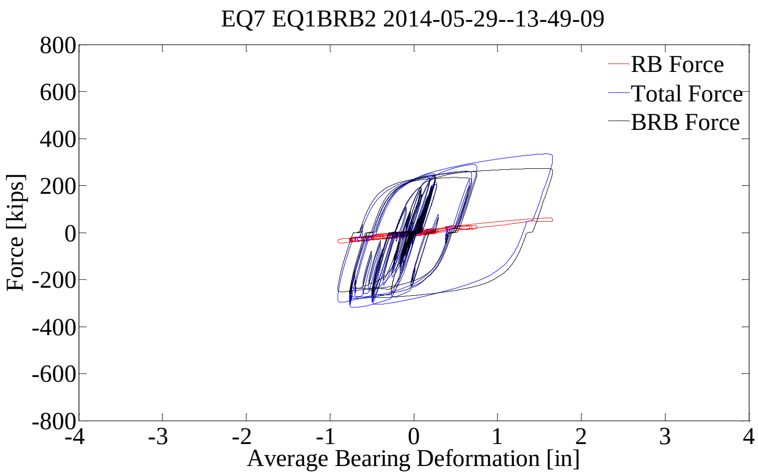

Figure 4.44: Test 25, Force – deformation plots for the deformable connection and its individual components in phase I [pg. 45]

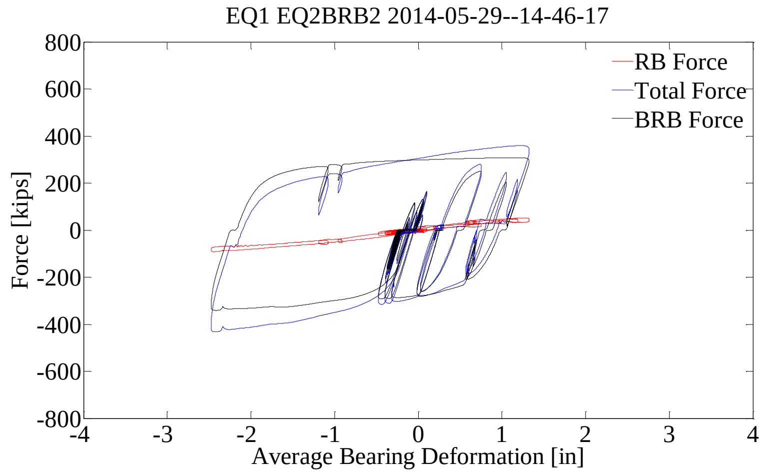

Figure 4.45: Test 26, Force – deformation plots for the deformable connection and its individual components in phase I [pg. 45]

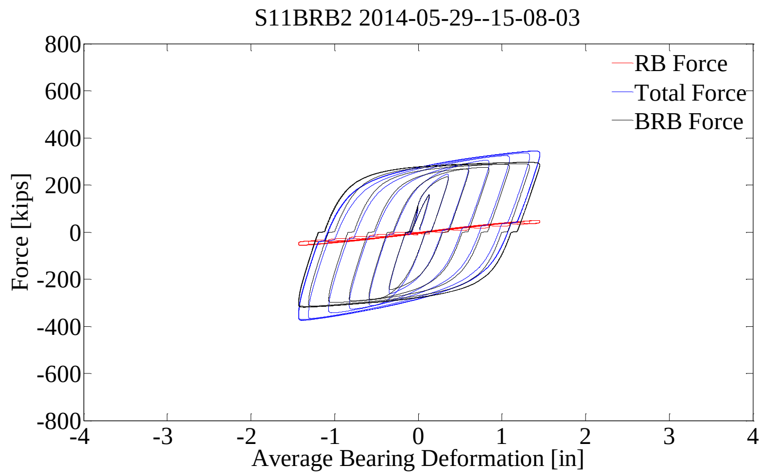

Figure 4.46: Test 27, Force – deformation plots for the deformable connection and its individual components in phase I [pg. 43; pg. 39]

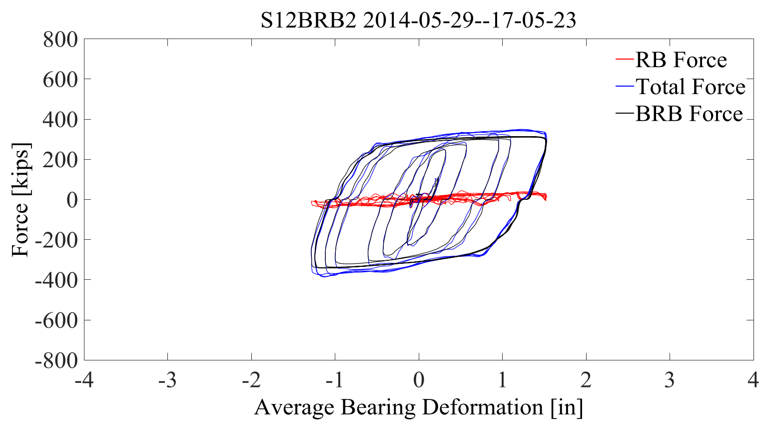

Figure 4.47: Test 28, Force – deformation plots for the deformable connection and its individual components in phase I [pg. 43; pg. 39]

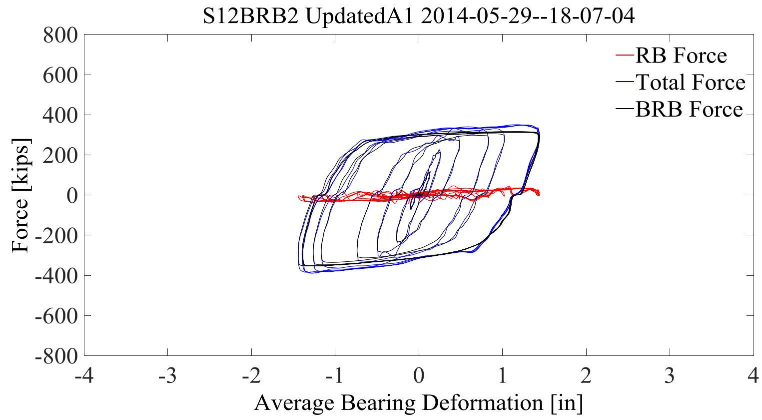

Figure 4.48: Test 29, Force – deformation plots for the deformable connection and its individual components in phase I [pg. 43; pg. 40]

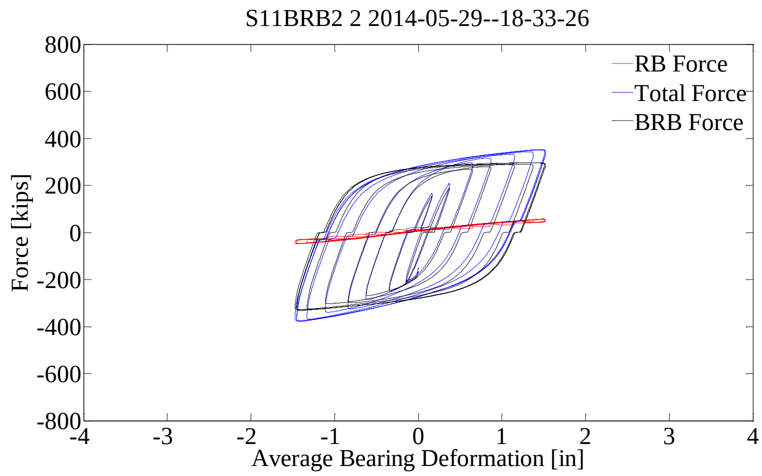

Figure 4.49: Test 30, Force – deformation plots for the deformable connection and its individual components in phase I [pg. 43; pg. 40]

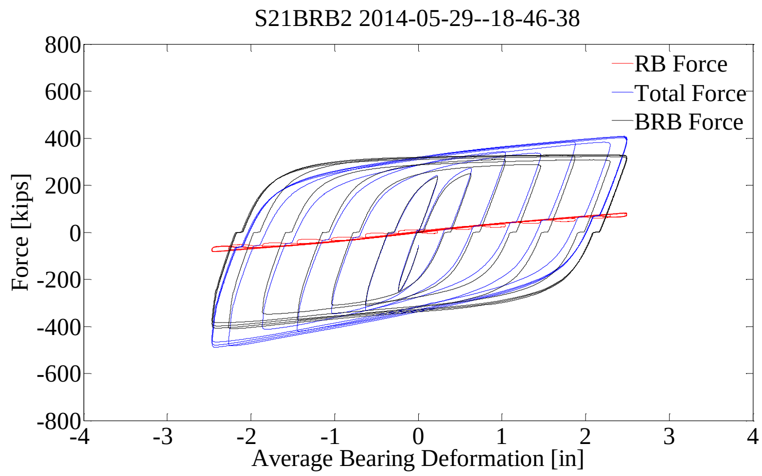

Figure 4.50: Test 31, Force – deformation plots for the deformable connection and its individual components in phase I [pg. 44; pg. 41]

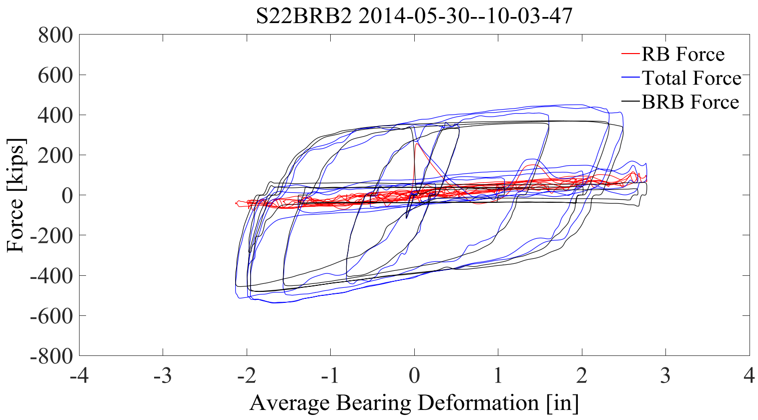

Figure 4.51: Test 32, Force – deformation plots for the deformable connection and its individual components in phase I [pg. 44; pg. 41]

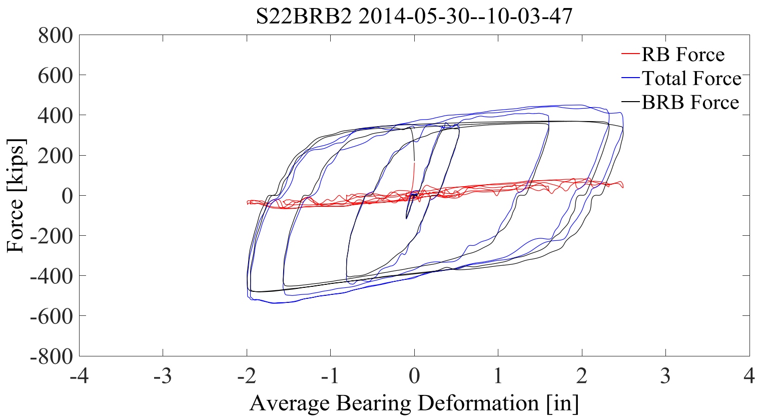

Figure 4.52: Test 32[fr], Force – deformation plots for the deformable connection and its individual components in phase I [pg. 44; pg. 41]

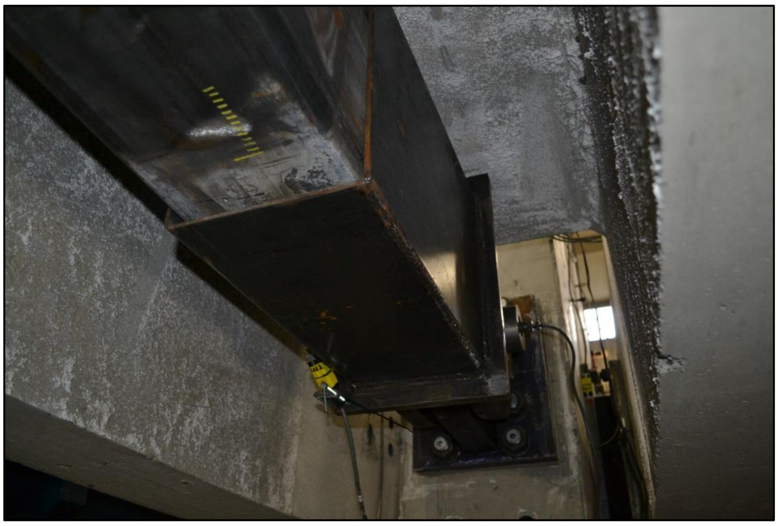

Figure 4.53: South (shear wall) end of fractured BRB, Phase I-3

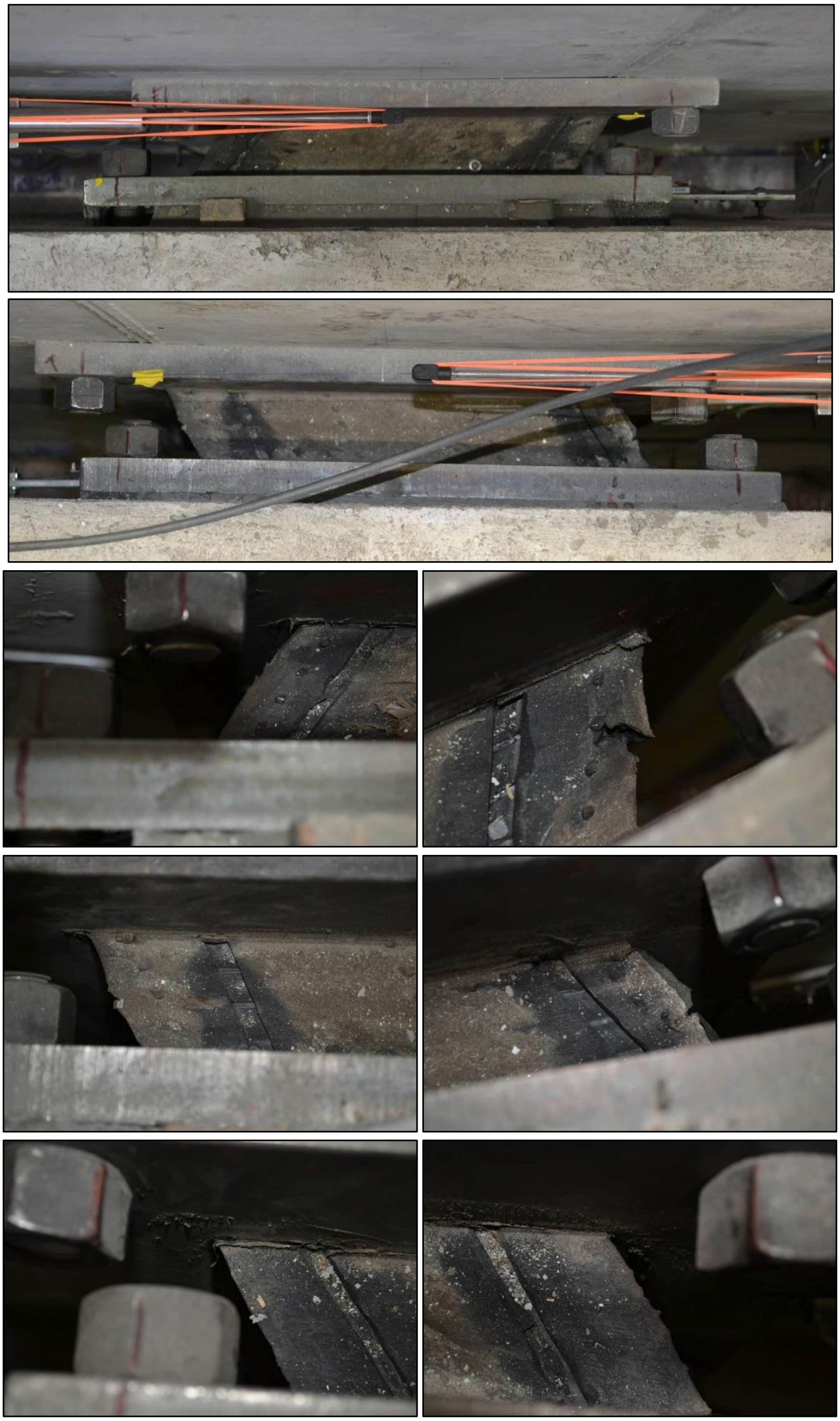

Figure 4.54: Steel reinforced RB in deformed position at the end of Phase I

4.4 Phase II

Phase II assessed the response of the second configuration of the deformable connection. One set of carbon fiber reinforced RB was used. Different friction plates were used for the FD in each subphase. There were four subphases of phase II.

Phase II-1 assessed the response of the deformable connection with low and high friction forces in the FD. The AFT200 composite material [27] is used for the friction plates of the FD.

Phase II-2 assessed the response of the deformable connection with a full-scale friction force in the FD, using the RF42 composite material [28] for the friction plates.

Phase II-3 assessed the response of the deformable connection with a full-scale friction force in the FD, using the RF42 composite material [28] for the friction plates. These plates are thicker compared to the plates used in phase II-2.

Phase II-4 assessed the response of the deformable connection with a full-scale friction force in the FD using the Gatke 398 composite material [29] for the friction plates, which had the same thickness as the friction plates used in phase II-3.

Only composite materials were used for the friction plates to avoid the potential for galvanic corrosion at the slip interface between the friction plates, the internal steel plate, and the external steel plates.

The fixture components used in phase II were identical with those in phase I. However, the arrangement was modified to accommodate the reduced length of the FD compared to the length of the BRB. Figure 4.55 shows the arrangement of fixture components for phase II.

Figure 4.55: Experimental set up for phase II

4.4.1 Friction Device

The FD that was developed at Lehigh University is shown in Figure 4.56. The steel plates were not machined flat to reduce the fabrication cost. The FD was connected to the wall and the floor system using clevis connecitons with spherical bearings. The expected friction force can be estimated using Coulomb theory by the following equation.

$$F_s = n_b n_s N_b \mu_s \qquad 4.1$$

Where F_s is the static friction force, n_b is the number of bolts used at the slip connection, n_s is the number of slip interfaces, N_b is the normal force applied by each bolt at the slip interfaces and μ_s is the static coefficient of friction. For the preliminary estimate of static friction force, the static coefficient of friction provided by the manufactures of the friction plates were used. The FD has two slip interfaces ($n_s = 2$). Also the FD designed for this experimental program had six bolts ($n_b = 6$). The friction force varies with the friction coefficient and the normal force applied by the bolts at the slip connection.

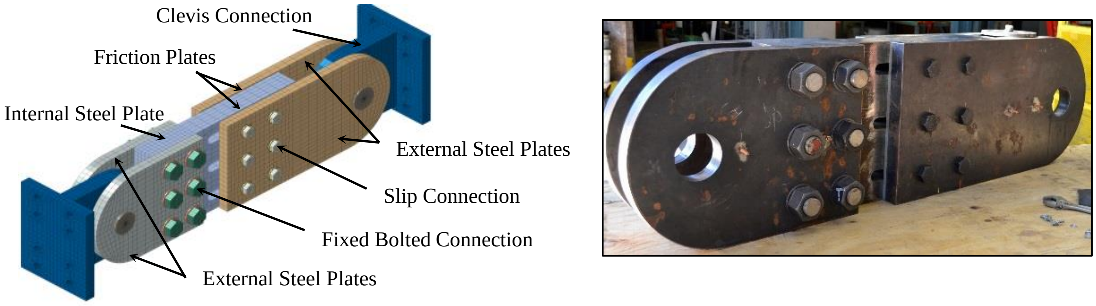

Figure 4.56: Full-scale FD

4.4.2 Carbon Fiber Reinforced Low Damping Rubber Bearings

Carbon fiber reinforced RB (provided by DYMAT™) were used in phase II. Each bearing consisted of 4 layers of carbon fiber reinforced neoprene 50+/-5 Duro Gr. 3 rubber pads with a shear modulus G=0.12 ksi. The carbon fiber reinforced RB were designed for horizontal and vertical shear deformation combined with out-of-plane rotation according to AASHTO specifications [22] [23] and using information from the references [24] [25]. In the present experimental program only the horizontal deformation was applied.

4.4.3 Instrumentation

The instrumentation plan is shown in Figure 4.57. The list of the instruments is shown in Table 4.26. The instruments are the same as those discussed in section 4.3.3 in phase I, except that LV81 and ACC21 were removed. Also, LV41 did not work properly and data from LV41 was not used for phase II.

Table 4.26: Phase II - Instruments list

Serial	Type Of Instrument	Stroke/ Magnitude	Direction	Location	Mounted from	Mounted to
LV11	LVDT	+/- 4"	N -S	NE	Loading Block (Centered to actuator)	Strong floor
LV12	LVDT	+/- 4"	N -S	NW	Loading Block (Centered to actuator)	Strong floor
LV13	LVDT	+/- 4"	N -S	N	Loading Block (centered to section)	Strong floor
LV21	LVDT	+/- 4"	N -S	N	South Collar of BRB	North Collar of BRB
LV22	LVDT	+/-1/8"	N -S	N	Loading Block	Clevis plates of BRB
LV23	LVDT	+/-1/8"	N -S	N	Shear Wall	Clevis plates of BRB
LV31	LVDT	+/- 4"	N -S	N	Shear Wall	Centered on the wall on the top surface of the slab. Far in order to minimize angle effects
LV32	LVDT	+/- 4"	N -S	S	Shear Wall	Centered on the wall on the top surface of the concrete block. Far in order to minimize angle effects
LV41	LVDT	+/-1/8"	N -S	N	Top steel plate of the base of the wall	Strong floor
LV51	LVDT	+/-1/8"	Vertical	N	Top steel plate of the base of the wall	Strong floor
LV52	LVDT	+/-1/8"	Vertical	S	Top steel plate of the base of the wall	Strong floor
LV61	LVDT	+/- 4"	N -S	S	Floor system	Wall
LV62	LVDT	+/- 4"	N -S	S	Floor System	Wall
LP63	Linear Potentiometer (Plastic Slide)	+/-1/2"	N -S	S	Steel Plate of bearing	Wall
LP64	Linear Potentiometer (Plastic Slide)	+/-1/2"	N -S	S	Steel Plate of rubber bearing	Wall
LP65	Linear Potentiometer (Plastic Slide)	+/-1/2"	N -S	S	Steel Plate of rubber bearing	Floor system

Serial	Type Of Instrument	Stroke/ Magnitude	Direction	Location	Mounted from	Mounted to
LP66	Linear Potentiometer (Plastic Slide)	+/-1/2"	N -S	S	Steel Plate of rubber bearing	Floor system
LV71	LVDT	+/- 4"	N -S	N	Floor system	Wall
LV72	LVDT	+/- 4"	N -S	N	Floor system	Wall
LP73	Linear Potentiometer (Plastic Slide)	+/-1/2"	N -S	N	Steel Plate of rubber bearing	Wall
LP74	Linear Potentiometer (Plastic Slide)	+/-1/2"	N -S	N	Steel Plate of rubber bearing	Wall
LP75	Linear Potentiometer (Plastic Slide)	+/-1/2"	N -S	N	Steel Plate of rubber bearing	Floor system
LP76	Linear Potentiometer (Plastic Slide)	+/-1/2"	N -S	N	Steel Plate of rubber bearing	Floor system
ACC11	Accelerometer	-	N -S	NE	-	Top of actuator’s adapter plate
ACC12	Accelerometer	-	N -S	NW	-	Top of actuator’s adapter plate
ACC22	Accelerometer	-	N -S	N	-	Floor system. Centered to wall
ACC23	Accelerometer	-	N -S	S	-	Floor system. Centered to wall
ACC31	Accelerometer	-	N -S	N	-	Top of wall
ACC41	Accelerometer	-	N -S	Middle	-	Top of floor system middle of wall
ACC42	Accelerometer	-	N -S	Middle	-	Top of floor system middle of wall
LC11	Load Cell	N/A	N-S	East	-	East Actuator
LC12	Load Cell	N/A	N-S	West	-	West Actuator
PN11	Load Pin	450 kips	N-S	Middle	-	Clevis at wall's end

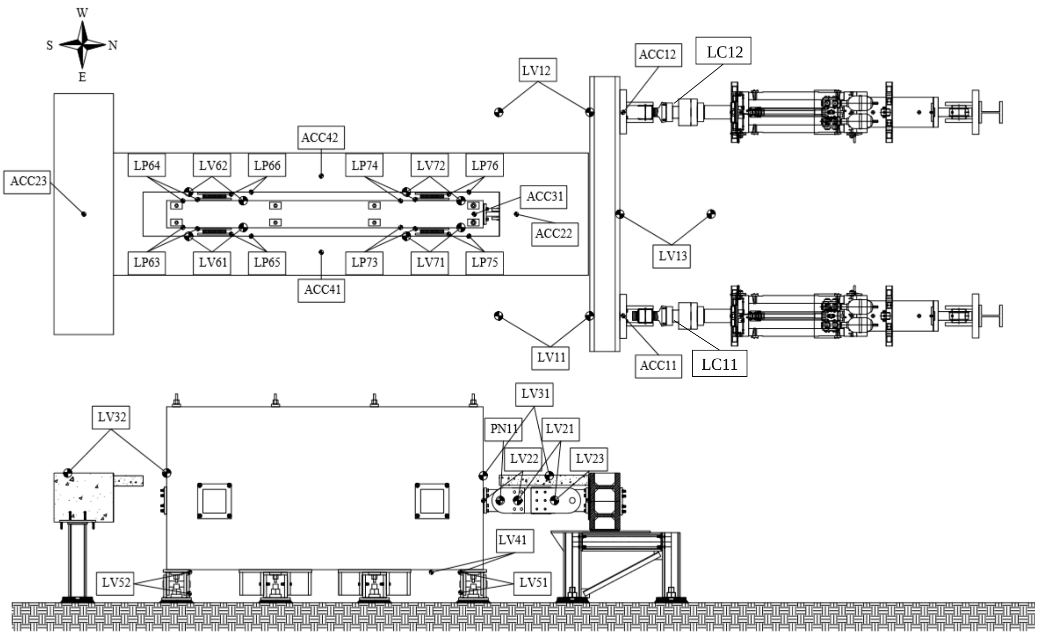

Figure 4.57: Instrumentation plan in phase II

4.4.4 Notation

Total Force, P_{tot} is the sum of the forces measured by the actuator load cells LC11 and LC12. The total force includes the force in the BRB, the force in the steel reinforced RB, any friction force generated at the contact interface between the Teflon and steel at the top of the gravity columns, and the inertial force F_i. The inertial force was estimated by multiplying the total mass of the floor system by the acceleration measured by accelerometers ACC21, ACC22, ACC23, ACC41, and ACC42.

The *Average Bearing Deformation*, D_{RB} is the average of the measurements of the four LVDTs LV61, LV62, LV71, and LV72.

The *BRB Force*, P_b is the axial force in the BRB and was directly measured using the instrumented pin PN11.

The *RB Force*, V_{RB} is the estimated shear force generated by the RB. It is approximated by calculating the difference between the P_{tot} and the P_b ($V_{RB} \approx P_{tot} - P_b$). This approximation is valid for the low frequency tests were the inertial force, F_i, was not significant and any friction force at the top of the gravity columns was small. For the high frequency tests the inertial force was significant compared to the force developed by the RB making the approximation inaccurate.

The *FD Deformation*, D_b is the sum of the measurements of the LVDTs LV21, LV22, and LV23. Also, D_{by} = 0.06 inch is used as the deformation that slip initiates.

The *Target Displacement*, D_t represents the histories shown in Figure 4.64 for phase II-1, in Figure 4.76 through Figure 4.83 for phase II-2, in Figure 4.103 - Figure 4.108 for the phase II-3, and in Figure 4.128 through Figure 4.136 for phase II-4.

Figure 4.15 shows the control scheme used in the testing program and discussed in section 4.3.4.

D_{cE} and D_{cW} are the East and West actuator target displacements, and D_{aE} and D_{aW} are the East and West actuator strokes.

Equations 4.2 and 4.3 give the expressions of the displacements D_{mE} and D_{mW} that were functions of the LVDT measurements. D_{mE} and D_{mW} were feedback to the PID control or ATS compensation. The subscript $_{m}$ next to the name of each LVDT is referring to the measurement by the LVDT.

$$D_{mE} = \frac{\mathrm{LV11_m} - \mathrm{LV12_m}}{2} + \mathrm{LV13_m} - \mathrm{LV41_m} \tag{4.2}$$

$$D_{mW} = \frac{\mathrm{LV12_m} - \mathrm{LV11_m}}{2} + \mathrm{LV13_m} - \mathrm{LV41_m} \tag{4.3}$$

4.4.5 Filtering

The force-deformation plots presented in this section were filtered using a bi-directional 3rd order Butterworth digital filter with zero-phase distortion. 15 Hz and 80Hz were the cut off frequencies for the low and higher frequency tests respectively.

4.4.6 Sign Convention

Positive target displacement led to movement of the floor system towards the North direction which resulted to tension of the FD. For consistency, the force measurements from the instrumented pin PN11 were multiplied by -1.

4.4.7 Phase II-1

Figure 4.58 shows the components of the FD used in phase II-1. Bushings were used in tests 1, 2, and 3 to decrease the tolerance between the slots and the bolts of the FD. In Figure 4.59 the assembled FD is shown before its installation in the specimen. Figure 4.60 shows the installed FD. Table 4.28 gives the properties of the FD including the material of the friction plates and their thickness t_{fp}, the number of Belleville washers used per bolt *BW*, the use of bushings, the number of bolts n_b, the ASTM A325 bolt diameter d_b, the bolt pretension force N_b, the friction coefficient μ_s, and the static friction force based on Coulomb theory F_s.

According to the manufacturer of AFT 200 material of the friction plates:

"*AFT 200 is a heavy-duty material which is able to withstand water and oil applications. AFT-200 is a phenolic treated, brass wire inserted cloth laminated under heat and pressure to a dense, strong composite. AFT-200 provides good fade and wear resistance and may be machined using standard, industry accepted practices. Its high strength makes it suitable for gear and lug driven applications.*"

More information can be found in the product data sheet [27].

The friction plates are shown in Figure 4.61 and their dimensions in Figure 4.62.

A typical carbon fiber reinforced RB is shown installed in Figure 4.63.

Table 4.29 shows the summary of the conditions of the East and West friction plates and the RB after each test. The notation *UC* indicates that the component was in undamaged condition after the test. If significant damage was observed at the end of a test, the description of the damage is given.

The test sequence is shown in Table 4.27.

4.4.7.1 Test 1: 01S3p5S

Test 1 was successfully completed. The displacement target time history is shown in Figure 4.64. The force-deformation plots of the deformable connection and its individual components are shown in Figure 4.65. LV71 did not work properly and its measurement for this test is not valid. For the average bearing deformation D_{RB} data from LVDTs LV61, LV62, and LV72 were used. In Table 4.30 the force and deformation data measured at the target displacement peaks are presented.

4.4.7.2 Test 2: 02S3p5S

Test 2 was successfully completed. The displacement target time history is shown in Figure 4.64. The force-deformation plots of the deformable connection and its individual components are shown in Figure 4.66. In Table 4.31 the force and deformation data measured at the target displacement peaks are presented.

4.4.7.3 Test 3: 03S3p5S

Test 3 was successfully completed. The displacement target time history is shown in Figure 4.64. The force-deformation plots of the deformable connection and its individual components are shown in Figure 4.67. In Table 4.32 the force and deformation data measured at the target displacement peaks are presented.

4.4.7.4 Test 4: 04S3p5S

Test 4 was successfully completed. The displacement target time history is shown in Figure 4.64. The force-deformation plots of the deformable connection and its individual components are shown in Figure 4.68. In Table 4.33 the force and deformation data measured at the target displacement peaks are presented.

4.4.7.5 Test 5: 05S3p5S

Test 5 was not completed due to problems with the actuators. However, four cycles were completed. The complete displacement target time history is shown in Figure 4.64. The force-deformation plots of the deformable connection and its individual components for the completed cycles are shown in Figure 4.69. In Table 4.34 the force and deformation data measured at the target displacement peaks are presented. The response of the deformable connection was as expected even after the friction plates had been damaged from the previous tests. In Figure 4.70(a) the friction plates are shown before the test. Figure 4.70(b) shows the surfaces of the plates which were in contact with the internal steel plates, after the tests. Figure 4.70(c) shows the surfaces of the friction plates which were in contact with the external steel plates, after the tests. The damage suggests that the thickness of the friction plates should be increased or/and the shear, tensile and compressive strength of the material should be increased.

Table 4.27: Phase II-1 testing sequence

Day	Test	Name	$D_{t,max}$ [in]	$V_{t,max}$ [in/sec]	f [Hz]	# Ramp up cycles	# Ramp down cycles	# Max. amplitude cycles
08-08-2014	1	01S3p5S	3.5	0.5	0.02	3	3	3
	2	02S3p5S	3.5	0.5	0.02	3	3	3
	3	03S3p5S	3.5	0.5	0.02	3	3	3
08-11-2014	4	04S3p5S	3.5	0.5	0.02	3	3	3
	5	05S3p5S	3.5	0.5	0.02	3	3	3

Table 4.28: Phase II-1 FD properties

Test	Friction Plate Material	t_{fp} [in]	BW	Bushings	*d_b [in]	n_b [-]	N_b [kips]	μ_s [-]	F_s [kips]
1	AFT200	3/16	1/bolt	Yes	7/8	6	7.2	0.42	36
2	AFT200	3/16	1/bolt	Yes	7/8	2	7.2	0.42	12
3	AFT200	3/16	1/bolt	Yes	7/8	2	7.2	0.42	12
4	AFT200	3/16	1/bolt	No	7/8	6	7.5	0.42	38
5	AFT200	3/16	No	No	7/8	6	39.0	0.42	197

*ASTM A325 bolts were used

Table 4.29: Phase II-1 condition of components of deformable connection

Test	East Friction Plate	West Friction Plate	NE RB	NW RB	SE RB	SW RB
1	*UC	*UC	*UC	*UC	*UC	*UC
2	UC	UC	UC	UC	UC	UC
3	UC	UC	UC	UC	UC	UC
4	UC	UC	UC	UC	UC	UC
5	Elongated holes	UC	UC	UC	UC	UC

**The components was at its initial condition at the beginning of the test*
UC: Undamaged Condition

Table 4.30: Test 1, Response data at target displacement peaks

Cycle #	Peak #	D_t [in]	D_{mE} [in]	D_{mW} [in]	D_b [in]	$\lvert D_b/D_{by}\rvert$ [in/in]	D_s [in]	D_{RB} [in]	P_{tot} [kips]	P_b [kips]	V_{RB} [kips]
1	1	0.34	0.34	0.34	0.34	5.60	0.33	0.34	35	11	24
	2	-0.89	-0.89	-0.89	-0.89	14.88	-0.87	-0.90	-62	-14	-48
2	3	1.47	1.47	1.47	1.47	24.56	1.47	1.47	76	13	62
	4	-2.05	-2.05	-2.05	-2.04	33.98	-2.01	-2.06	-104	-17	-87
3	5	2.63	2.63	2.63	2.61	43.58	2.61	2.62	128	19	109
	6	-3.21	-3.21	-3.21	-3.21	53.44	-3.18	-3.22	-157	-17	-139
4	7	3.50	3.50	3.50	3.43	57.18	3.42	3.43	167	20	148
	8	-3.50	-3.50	-3.50	-3.49	58.11	-3.46	-3.50	-162	-18	-143
5	9	3.50	3.50	3.50	3.43	57.16	3.42	3.43	155	21	133
	10	-3.50	-3.50	-3.50	-3.49	58.13	-3.46	-3.50	-155	-19	-136
6	11	3.50	3.50	3.50	3.43	57.13	3.42	3.43	152	23	129
	12	-3.50	-3.50	-3.50	-3.49	58.14	-3.46	-3.50	-152	-20	-133
7	13	3.21	3.21	3.21	3.14	52.40	3.14	3.16	132	25	107
	14	-2.63	-2.63	-2.63	-2.64	43.99	-2.61	-2.65	-110	-22	-88
8	15	2.05	2.05	2.05	2.02	33.59	2.01	2.02	86	22	64
	16	-1.47	-1.47	-1.47	-1.49	24.77	-1.46	-1.50	-77	-22	-55
9	17	0.89	0.89	0.89	0.86	14.39	0.86	0.87	48	16	31
	18	-0.34	-0.34	-0.34	-0.37	6.19	-0.35	-0.36	-39	-17	-21

Table 4.31: Test 2, Response data at target displacement peaks

Cycle #	Peak #	D_t [in]	D_{mE} [in]	D_{mW} [in]	D_b [in]	$\lvert D_b/D_{by}\rvert$ [in/in]	D_s [in]	D_{RB} [in]	P_{tot} [kips]	P_b [kips]	V_{RB} [kips]
1	1	0.34	0.34	0.34	0.34	5.62	0.34	0.34	29	9	20
	2	-0.89	-0.89	-0.89	-0.89	14.85	-0.86	-0.90	-52	-14	-38
2	3	1.47	1.47	1.47	1.47	24.54	1.47	1.48	65	9	55
	4	-2.05	-2.05	-2.05	-2.03	33.80	-2.00	-2.05	-85	-14	-70
3	5	2.63	2.63	2.63	2.62	43.63	2.62	2.64	105	13	91
	6	-3.21	-3.21	-3.21	-3.19	53.16	-3.15	-3.19	-128	-13	-115
4	7	3.50	3.50	3.50	3.46	57.75	3.47	3.47	147	13	134
	8	-3.50	-3.50	-3.50	-3.46	57.69	-3.43	-3.46	-142	-13	-129
5	9	3.50	3.50	3.50	3.46	57.74	3.47	3.47	142	13	129
	10	-3.50	-3.50	-3.50	-3.46	57.69	-3.43	-3.46	-139	-13	-126
6	11	3.50	3.50	3.50	3.46	57.75	3.47	3.47	141	14	127
	12	-3.50	-3.50	-3.50	-3.46	57.69	-3.43	-3.46	-137	-13	-124
7	13	3.21	3.21	3.21	3.19	53.12	3.19	3.21	120	14	106
	14	-2.63	-2.63	-2.63	-2.61	43.47	-2.57	-2.62	-96	-14	-82
8	15	2.05	2.05	2.05	2.05	34.14	2.05	2.06	78	12	67
	16	-1.47	-1.47	-1.47	-1.46	24.26	-1.42	-1.46	-64	-14	-50
9	17	0.89	0.89	0.89	0.90	14.93	0.89	0.90	45	9	36
	18	-0.34	-0.34	-0.34	-0.34	5.67	-0.31	-0.33	-28	-12	-16

Table 4.32: Test 3, Response data at target displacement peaks

Cycle #	Peak #	D_t [in]	D_{mE} [in]	D_{mW} [in]	D_b [in]	$\|D_b/D_{by}\|$ [in/in]	D_s [in]	D_{RB} [in]	P_{tot} [kips]	P_b [kips]	V_{RB} [kips]
1	1	0.34	0.34	0.34	0.34	5.68	0.34	0.34	28	8	20
	2	-0.89	-0.89	-0.89	-0.89	14.79	-0.86	-0.89	-51	-14	-37
2	3	1.47	1.47	1.47	1.47	24.50	1.47	1.48	64	11	54
	4	-2.05	-2.05	-2.05	-2.02	33.75	-1.99	-2.04	-82	-15	-68
3	5	2.63	2.63	2.63	2.62	43.70	2.62	2.64	101	14	87
	6	-3.21	-3.21	-3.21	-3.19	53.08	-3.15	-3.19	-121	-13	-109
4	7	3.50	3.50	3.50	3.47	57.79	3.47	3.47	140	12	128
	8	-3.50	-3.50	-3.50	-3.46	57.73	-3.43	-3.46	-136	-13	-124
5	9	3.50	3.50	3.50	3.47	57.77	3.47	3.44	136	12	124
	10	-3.50	-3.50	-3.50	-3.47	57.79	-3.43	-3.50	-135	-13	-122
6	11	3.50	3.50	3.50	3.46	57.73	3.46	3.40	136	13	123
	12	-3.50	-3.50	-3.50	-3.47	57.78	-3.43	-3.54	-134	-13	-121
7	13	3.21	3.21	3.21	3.19	53.09	3.18	3.13	120	14	106
	14	-2.63	-2.63	-2.63	-2.61	43.47	-2.57	-2.70	-94	-13	-81
8	15	2.05	2.05	2.05	2.04	34.07	2.04	1.99	78	12	66
	16	-1.47	-1.47	-1.47	-1.45	24.20	-1.42	-1.54	-64	-14	-50
9	17	0.89	0.89	0.89	0.90	14.93	0.89	0.82	44	9	35
	18	-0.34	-0.34	-0.34	-0.34	5.67	-0.31	-0.41	-27	-11	-16

Table 4.33: Test 4, Response data at target displacement peaks

Cycle #	Peak #	D_t [in]	D_{mE} [in]	D_{mW} [in]	D_b [in]	$\|D_b/D_{by}\|$ [in/in]	D_s [in]	D_{RB} [in]	P_{tot} [kips]	P_b [kips]	V_{RB} [kips]
1	1	0.34	0.34	0.34	0.33	5.51	0.32	0.33	51	36	15
	2	-0.89	-0.90	-0.90	-0.88	14.73	-0.85	-0.89	-77	-33	-43
2	3	1.47	1.47	1.47	1.46	24.32	1.45	1.47	87	37	50
	4	-2.05	-2.05	-2.05	-2.01	33.57	-1.98	-2.03	-115	-38	-76
3	5	2.63	2.63	2.63	2.59	43.19	2.58	2.61	124	40	84
	6	-3.21	-3.21	-3.21	-3.16	52.67	-3.12	-3.17	-155	-38	-118
4	7	3.50	3.50	3.50	3.44	57.29	3.43	3.45	156	37	119
	8	-3.50	-3.50	-3.50	-3.45	57.44	-3.40	-3.45	-162	-37	-125
5	9	3.50	3.50	3.50	3.44	57.28	3.43	3.40	153	38	114
	10	-3.50	-3.50	-3.50	-3.45	57.44	-3.40	-3.50	-162	-38	-124
6	11	3.50	3.50	3.50	3.44	57.28	3.43	3.40	151	39	112
	12	-3.50	-3.50	-3.50	-3.45	57.44	-3.40	-3.50	-161	-38	-122
7	13	3.21	3.21	3.21	3.15	52.56	3.14	3.13	140	42	98
	14	-2.63	-2.63	-2.63	-2.58	42.96	-2.54	-2.64	-126	-40	-86
8	15	2.05	2.05	2.05	2.03	33.85	2.02	2.00	99	39	60
	16	-1.47	-1.47	-1.47	-1.43	23.91	-1.40	-1.51	-93	-38	-55
9	17	0.89	0.89	0.89	0.89	14.90	0.88	0.84	63	35	28
	18	-0.34	-0.34	-0.34	-0.32	5.35	-0.30	-0.38	-55	-33	-22

Table 4.34: Test 5, Response data at target displacement peaks

Cycle #	Peak #	D_t [in]	D_{mE} [in]	D_{mW} [in]	D_b [in]	$\|D_b/D_{by}\|$ [in/in]	D_s [in]	D_{RB} [in]	P_{tot} [kips]	P_b [kips]	V_{RB} [kips]
1	1	0.34	0.34	0.34	0.21	3.52	0.17	0.22	193	184	9
	2	-0.89	-0.89	-0.89	-0.79	13.20	-0.74	-0.80	-237	-190	-47
2	3	1.47	1.47	1.47	1.32	21.96	1.27	1.34	243	194	49
	4	-2.05	-2.05	-2.05	-1.93	32.12	-1.87	-1.94	-269	-194	-75
3	5	2.63	2.63	2.63	2.46	41.03	2.42	2.50	272	193	80
	6	-3.21	-3.21	-3.22	-3.10	51.74	-3.03	-3.10	-304	-192	-111
4	7	3.50	3.50	3.50	3.31	55.24	3.27	3.35	305	190	115

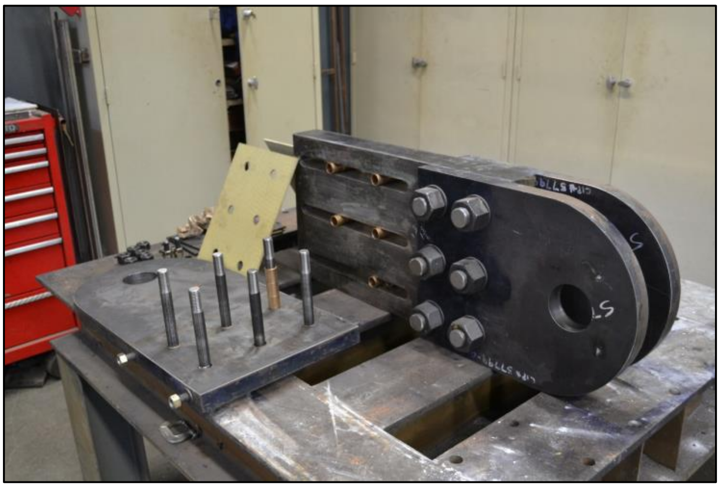

Figure 4.58: Components of the FD for phase II-1

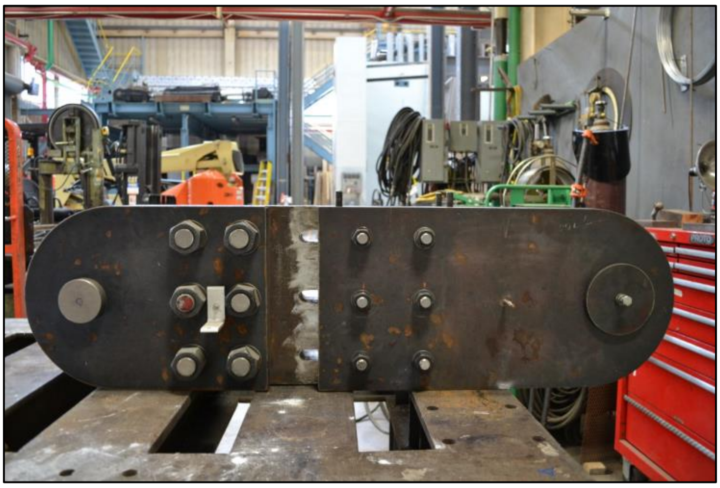

Figure 4.59: Assembled FD for phase II-1

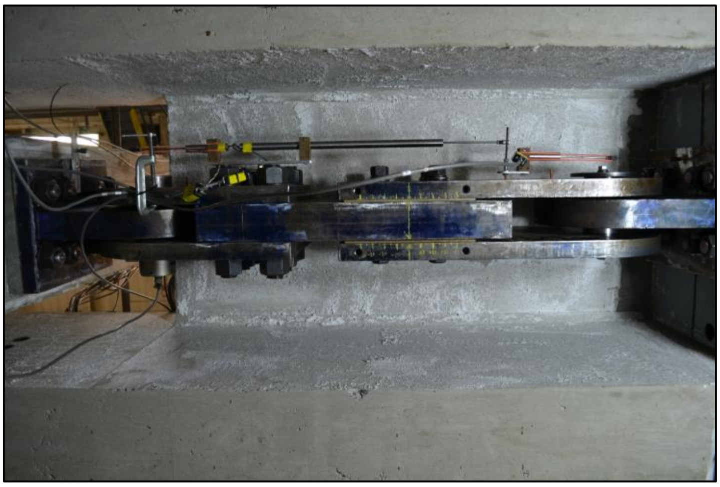

Figure 4.60: Installed FD on the specimen for phase II-1

Figure 4.61: AFT200 friction plates used in phase II-1

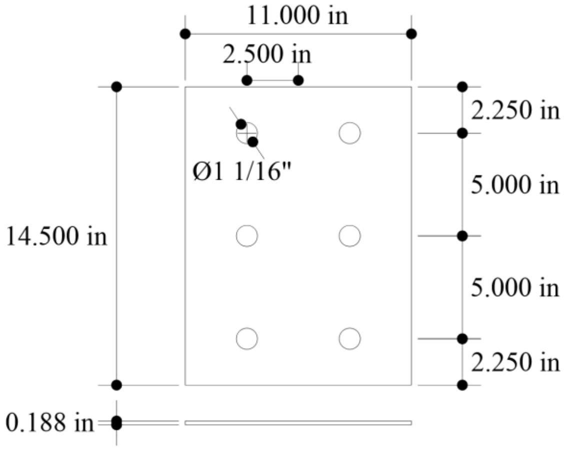

Figure 4.62: Dimensions of AFT200 friction plates used in phase II-1

Figure 4.63: Carbon fiber reinforced low damping rubber bearings for phase II (provided by Dynamat)

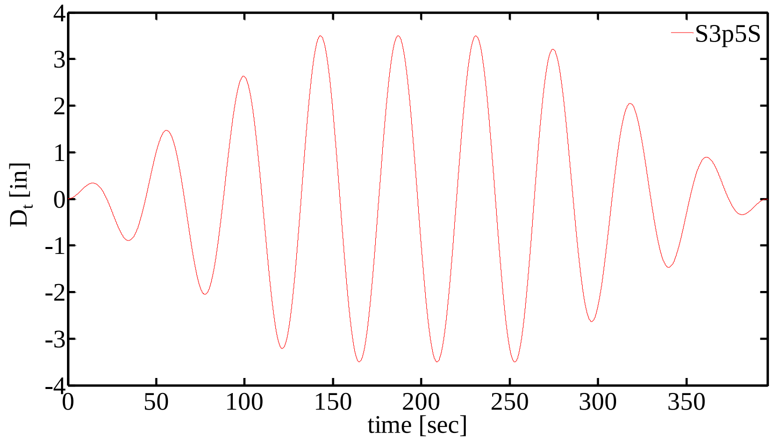

Figure 4.64: Target displacement history use in all five tests conducted in phase II-1

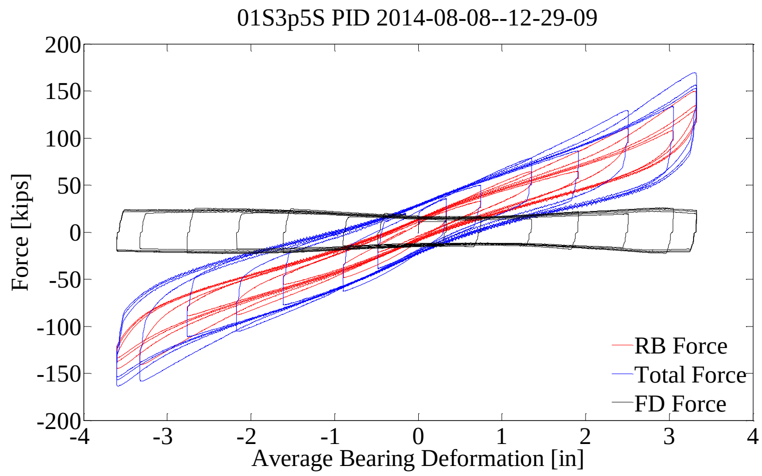

Figure 4.65: Test 1, Force – deformation plots for the deformable connection and its individual components in phase II [pg. 64; pg. 59]

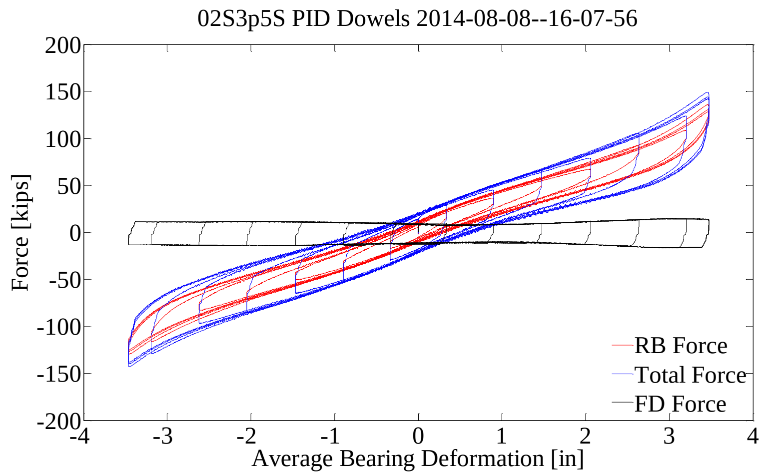

Figure 4.66: Test 2, Force – deformation plots for the deformable connection and its individual components in phase II [pg. 64; pg. 59]

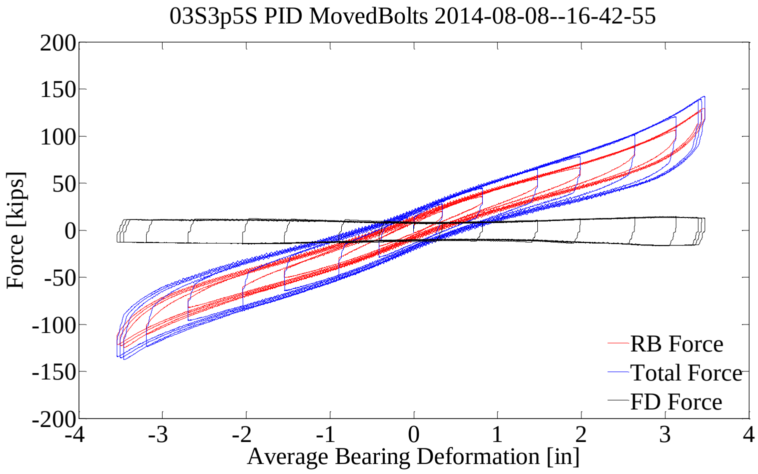

Figure 4.67: Test 3, Force – deformation plots for the deformable connection and its individual components in phase II [pg. 64; pg. 60]

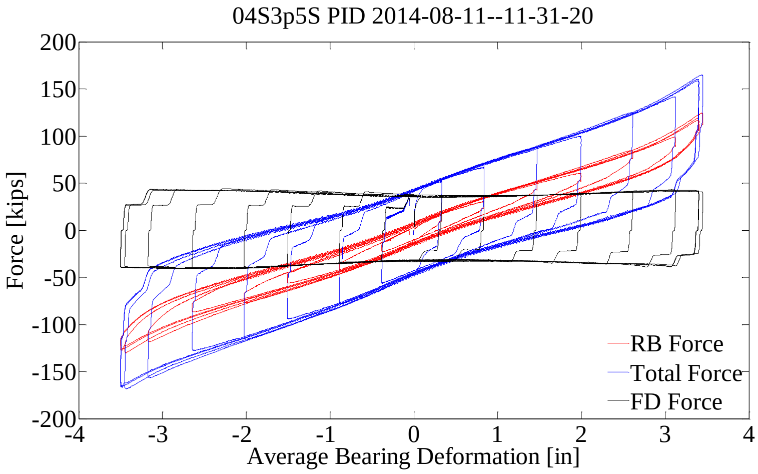

Figure 4.68: Test 4, Force – deformation plots for the deformable connection and its individual components in phase II [pg. 64; pg. 60]

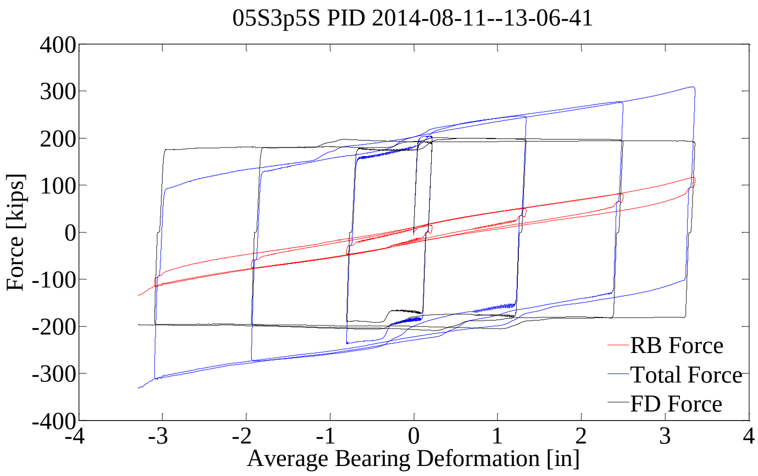

Figure 4.69: Test 5, Force – deformation plots for the deformable connection and its individual components in phase II [pg. 64; pg. 61]

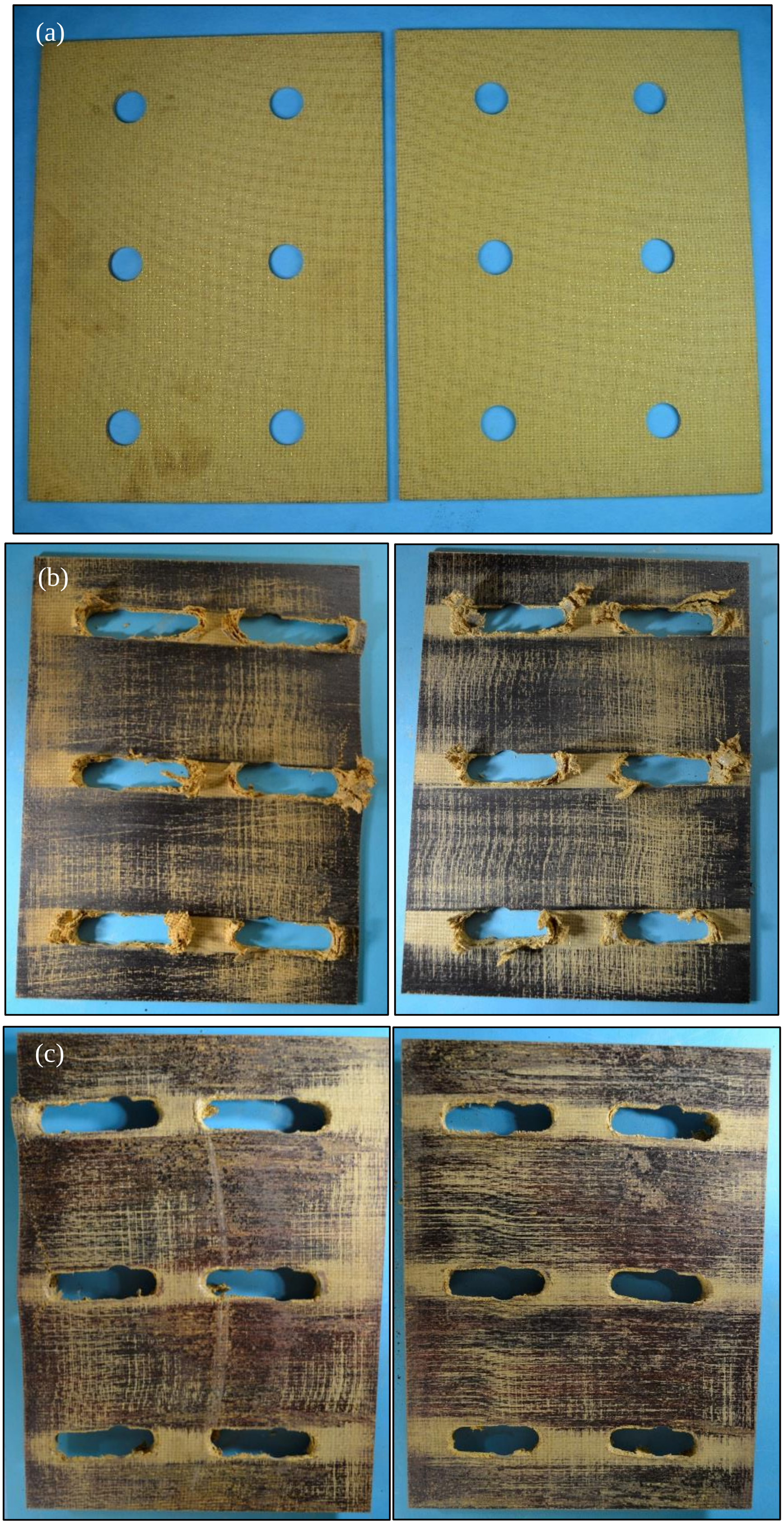

Figure 4.70: Conditions of the AFT200 friction plates used in phase II-1: (a) *before the test; (b) after the test, showing side in contact with internal steel plate; (c) after the test, showing side in contact with external steel plates*

4.4.8 Phase II-2

Phase II-2 used a different material for the friction plates. The RF42 friction plates are shown in Figure 4.71. Their dimensions are presented in Figure 4.72. Figure 4.73 shows the installed friction plates in the FD. According to the manufacturer:

"RF 42 is a rigid molded Non-Asbestos, Non-Metallic friction material suitable for use in Medium Friction brake/clutch applications in a wide variety of equipment including the most severe. RF 42 is recommended for virtually any medium friction application where metal cannot be used. RF 42 can be molded into wide range of shapes and sizes to satisfy virtually all industrial applications."

More information can be found in the product data sheet [28]

Bushings and Belleville washers were not used in phase II-2. The thickness of the friction plates was, t_{fp}=3/16 inches. Six ASTM A325 bolts were used, n_b= 6 with diameter d_b = 1.0 inches. Each bolt was pretensioned at the beginning of phase II-2 to their "minimum pretension" force N_b = 51kips [30] using the hydraulic gun shown in Figure 4.74. The applied pressure was 2900 psi which is associated with a torque 865 lb.-ft. The static friction coefficient reported by the manufacturer is μ_s = 0.43. Thus, the static friction force based on Coulomb theory is $F_s = n_b\, n_s\, N_b\, \mu_s$ = 263 kips.

The carbon fiber reinforced RB used in phase II-1 was used also in phase II-2.

The approximate temperature at the surface of the internal steel plate was measured at the beginning (T_i) and at the end (T_f) of each test using the infrared gun shown in Figure 4.75.

Table 4.35 shows a summary of the conditions of the East and West friction plates and the RB after each test of phase II-2. The notation *UC* indicates that the component was in undamaged condition after the test. If damage was observed at the end of the test, the description of the damage is given.

The test sequence is shown in Table 4.36.

4.4.8.1 Test 6: 06EQ7FD245

Test 6 was successfully completed. The displacement target time history is presented in Figure 4.76. The force-deformation plots are shown in Figure 4.84. The results shown that the actual friction coefficient of the RF42 – steel interface is less than the value provided by the manufacturer. The initial and final temperatures were T_i = 77°F and T_f = 83°F respectively.

4.4.8.2 Test 7: 07S3p5SBrk

Test 7 was successfully completed. The displacement target time history is presented in Figure 4.77. The force-deformation plots are shown in Figure 4.85. The failure of the friction plate shown in Figure 4.86 did not affect the response of the FD. In Table 4.37 the force and deformation data measured at the target displacement peaks are presented. The initial and final temperatures were T_i = 80°F and T_f = 110°F respectively.

4.4.8.3 Test 8: 08S1p0S

Test 8 was successfully completed. The displacement target time history is presented in Figure 4.78. The force-deformation plots are shown in Figure 4.87. In Table 4.38 the force and deformation data measured at the target displacement peaks are presented. The initial and final temperatures were T_i = 95°F and T_f = 95°F respectively.

4.4.8.4 Test 9: 09S1p0D

Test 9 was successfully completed. The displacement target time history is presented in Figure 4.79. The force-deformation plots are shown in Figure 4.88. The inertial force of the floor system was significant. In Table 4.39 the force and deformation data measured at the target displacement peaks are presented. The initial and final temperatures were T_i = 92°F and T_f = 98°F respectively.

4.4.8.5 Test 10: 10S1p0S

Test 10 was successfully completed. The displacement target time history is presented in Figure 4.78. The force-deformation plots are shown in Figure 4.89. In Table 4.40 the force and deformation data measured at the target displacement peaks are presented. The initial and final temperatures were T_i = 93°F and T_f = 102°F respectively.

4.4.8.6 Test 11: 11S2p5S

Test 11 was successfully completed. The displacement target time history is presented in Figure 4.80. The force-deformation plots are shown in Figure 4.90. In Table 4.41 the force and deformation data measured at the target displacement peaks are presented. The initial and final temperatures were T_i = 95°F and T_f = 110°F respectively.

4.4.8.7 Test 12: 12S2p5D

Test 12 was successfully completed. The displacement target time history is presented in Figure 4.81. The force-deformation plots are shown in Figure 4.91. The effect of the inertial force is less than those observed for Test 9 due to the different loading frequency. In Table 4.42 the force and deformation data measured at the target displacement peaks are presented. The initial and final temperatures were T_i = 104°F and T_f = 120°F respectively.

4.4.8.8 Test 13: 13S2p5S

Test 13 was successfully completed. The displacement target time history is presented in Figure 4.80. The force-deformation plots are shown in Figure 4.92. In Table 4.43 the force and deformation data measured at the target displacement peaks are presented. The initial and final temperatures were T_i = 95°F and T_f = 108°F respectively.

4.4.8.9 Test 14: 14S3p5S

Test 14 was successfully completed. The displacement target time history is presented in Figure 4.82. The force-deformation plots are shown in Figure 4.93. Another large piece of the friction plate was detached during this test. The North East and South East RB showed signs of tearing of the elastomer layers. In Table 4.44 the force and deformation data measured at the target displacement peaks are presented. The initial and final temperatures were T_i = 105°F and T_f = 120°F respectively.

4.4.8.10 Test 15: 15S3p5D

Test 15 was successfully completed. The displacement target time history is presented in Figure 4.83. The force-deformation plots are shown in Figure 4.94. In Table 4.45 the force and deformation data measured at the target displacement peaks are presented. The initial and final temperatures were T_i = 112°F and T_f = 126°F respectively.

4.4.8.11 Test 16: 16S3p5S

Test 16 was successfully completed. The displacement target time history is presented in Figure 4.82. The force-deformation plots are shown in Figure 4.95. In Table 4.46 the force and deformation data measured at the target displacement peaks are presented. The initial and final temperatures were T_i = 126°F and T_f = 136°F respectively.

4.4.8.12 Test 17: 17EQ7FD245

Test 17 was successfully completed. The displacement target time history is presented in Figure 4.76. The force-deformation plots are shown in Figure 4.96. The initial and final temperatures were T_i = 78°F and T_f = 92°F respectively.

4.4.8.13 Test 18: 18S3p5SBrk

Test 18 was successfully completed. The displacement target time history is presented in Figure 4.77. The force-deformation plots are shown in Figure 4.97. The high frequency oscillations observed in the results are from problems with the hydraulic power and the actuators. In Figure 4.98, a fractured friction plate is shown. The friction plates are shown in their initial condition in Figure 4.71. In Table 4.47 the force and deformation data measured at the target displacement peaks are presented. The initial and final temperatures were T_i = 83 °F and T_f = 105 °F respectively.

Table 4.35: Phase II-2 condition of components of deformable connection

Test	West FP	East FP	NE RB	NW RB	SE RB	SW RB
6	*UC	*UC	UC	UC	UC	UC
7	Fractured	Elongated bolt holes	Torn rubber	Debonded rubber	Torn rubber	Torn rubber
8	Fractured	Elongated bolt holes	Torn rubber	Debonded rubber	Torn rubber	Torn rubber
9	Fractured	Elongated bolt holes	Torn rubber	Debonded rubber	Torn rubber	Torn rubber
10	Fractured	Elongated bolt holes	Torn rubber	Debonded rubber	Torn rubber	Torn rubber
11	Fractured	Elongated bolt holes	Torn rubber	Debonded rubber	Torn rubber	Torn rubber
12	Fractured	Elongated bolt holes	Torn rubber	Debonded rubber	Torn rubber	Torn rubber
13	Fractured	Elongated bolt holes	Torn rubber	Debonded rubber	Torn rubber	Torn rubber
14	Fractured	Elongated bolt holes	Torn rubber	Debonded rubber	Torn rubber	Torn rubber
15	Fractured	Elongated bolt holes	Torn rubber	Debonded rubber	Torn rubber	Torn rubber
16	Fractured	Elongated bolt holes	Torn rubber	Debonded rubber	Torn rubber	Torn rubber
17	Fractured	Elongated bolt holes	Torn rubber	Debonded rubber	Torn rubber	Torn rubber
18	Fractured	Elongated bolt holes	Torn rubber	Debonded rubber	Torn rubber	Torn rubber

**The components was at its initial condition at the beginning of the test*
UC: Undamaged Condition

Table 4.36: Phase II-2 testing sequence

Day	Test	Name	$D_{t,max}$ [in]	$V_{t,max}$ [in/sec]	f [Hz]	# Ramp up cycles	# Ramp down cycles	# Max. amplitude cycles
08-12-2014	6	06EQ7FD245	2.77	0.90	-	-	-	-
	7	07S3p5SBrk	3.50	0.50	0.02	3	3	6
	8	08S1p0S	1.00	0.50	0.08	3	3	3
	9	09S1p0D	1.00	10.00	1.59	3	3	3
	10	10S1p0S	1.00	0.50	0.08	3	3	3
	11	11S2p5S	2.50	0.50	0.03	3	3	3
	12	12S2p5D	2.50	10.00	0.64	3	3	3
	13	13S2p5S	2.50	0.50	0.03	3	3	3
	14	14S3p5S	3.50	0.50	0.02	3	3	3
	15	15S3p5D	3.50	10.00	0.45	3	3	3
	16	16S3p5S	3.50	0.50	0.02	3	3	3
08-13-2014	17	17EQ7FD245	2.77	0.90	-	-	-	-
	18	18S3p5SBrk	3.50	3.50	0.02	3	3	3

Table 4.37: Test 7, Response data at target displacement peaks

Cycle #	Peak #	D_t [in]	D_{mE} [in]	D_{mW} [in]	D_b [in]	$\|D_b/D_{by}\|$ [in/in]	D_s [in]	D_{RB} [in]	P_{tot} [kips]	P_b [kips]	V_{RB} [kips]
1	1	0.34	0.34	0.34	0.23	3.88	0.16	0.24	141	128	14
	2	-0.89	-0.90	-0.90	-0.89	14.75	-0.88	-0.88	-156	-122	-34
2	3	1.47	1.47	1.47	1.37	22.86	1.29	1.38	172	125	47
	4	-2.05	-2.05	-2.05	-2.01	33.55	-2.01	-2.03	-176	-111	-65
3	5	2.63	2.63	2.63	2.53	42.25	2.46	2.55	201	120	81
	6	-3.21	-3.21	-3.21	-3.18	53.06	-3.17	-3.19	-209	-106	-103
4	7	3.50	3.50	3.50	3.41	56.85	3.33	3.40	231	110	121
	8	-3.50	-3.50	-3.50	-3.49	58.20	-3.46	-3.48	-212	-102	-110
5	9	3.50	3.50	3.50	3.41	56.87	3.33	3.41	225	106	119
	10	-3.50	-3.50	-3.50	-3.50	58.25	-3.46	-3.49	-207	-100	-107
6	11	3.50	3.50	3.50	3.41	56.87	3.33	3.41	216	102	114
	12	-3.50	-3.50	-3.50	-3.49	58.23	-3.46	-3.49	-215	-99	-117
7	13	3.50	3.50	3.50	3.42	56.93	3.34	3.41	213	100	113
	14	-3.50	-3.50	-3.50	-3.50	58.27	-3.46	-3.49	-214	-95	-119
8	15	3.50	3.50	3.50	3.42	56.94	3.34	3.41	201	95	105
	16	-3.50	-3.51	-3.49	-3.50	58.31	-3.46	-3.49	-208	-98	-109
9	17	3.50	3.50	3.50	3.41	56.88	3.34	3.41	199	95	104
	18	-3.50	-3.50	-3.50	-3.50	58.27	-3.46	-3.49	-201	-92	-109
10	19	3.21	3.22	3.21	3.12	51.98	3.05	3.12	185	96	89
	20	-2.63	-2.63	-2.63	-2.60	43.41	-2.60	-2.63	-161	-89	-72
11	21	2.05	2.05	2.05	1.96	32.61	1.88	1.96	152	98	54
	22	-1.47	-1.47	-1.47	-1.45	24.20	-1.45	-1.47	-138	-93	-44
12	23	0.89	0.90	0.90	0.80	13.37	0.73	0.80	127	100	27
	24	-0.34	-0.34	-0.34	-0.33	5.55	-0.33	-0.35	-111	-97	-14

Table 4.38: Test 8, Response data at target displacement peaks

Cycle #	Peak #	D_t [in]	D_{mE} [in]	D_{mW} [in]	D_b [in]	$\lvert D_b/D_{by}\rvert$ [in/in]	D_s [in]	D_{RB} [in]	P_{tot} [kips]	P_b [kips]	V_{RB} [kips]
1	1	0.10	0.10	0.10	0.08	1.26	0.02	0.08	104	101	4
	2	-0.26	-0.26	-0.26	-0.18	2.92	-0.15	-0.17	-133	-117	-16
2	3	0.42	0.42	0.42	0.39	6.58	0.34	0.40	139	124	15
	4	-0.59	-0.59	-0.59	-0.50	8.37	-0.48	-0.50	-151	-124	-27
3	5	0.75	0.75	0.75	0.72	12.05	0.66	0.73	150	126	24
	6	-0.92	-0.92	-0.92	-0.84	13.94	-0.81	-0.84	-156	-120	-36
4	7	1.00	1.00	1.00	0.97	16.16	0.91	0.98	150	120	30
	8	-1.00	-1.00	-1.00	-0.92	15.28	-0.89	-0.92	-151	-113	-38
5	9	1.00	1.00	1.00	0.97	16.23	0.92	0.98	146	116	30
	10	-1.00	-1.00	-1.00	-0.92	15.26	-0.89	-0.92	-149	-111	-38
6	11	1.00	1.00	1.00	0.97	16.24	0.92	0.98	145	115	30
	12	-1.00	-1.00	-1.00	-0.92	15.28	-0.89	-0.92	-148	-110	-38
7	13	0.92	0.92	0.92	0.89	14.88	0.84	0.90	141	114	27
	14	-0.75	-0.75	-0.75	-0.68	11.27	-0.65	-0.67	-140	-110	-30
8	15	0.59	0.59	0.59	0.56	9.35	0.50	0.57	133	115	18
	16	-0.42	-0.42	-0.42	-0.34	5.70	-0.32	-0.34	-132	-112	-20
9	17	0.26	0.26	0.26	0.23	3.76	0.17	0.23	125	117	7
	18	-0.10	-0.10	-0.10	-0.01	0.19	0.01	-0.02	-123	-115	-8

Table 4.39: Test 9, Response data at target displacement peaks

Cycle #	Peak #	D_t [in]	D_{mE} [in]	D_{mW} [in]	D_b [in]	$\lvert D_b/D_{by}\rvert$ [in/in]	D_s [in]	D_{RB} [in]	P_{tot} [kips]	P_b [kips]
1	1	0.10	0.05	0.05	0.02	0.29	0.00	0.02	95	92
	2	-0.26	-0.18	-0.18	-0.13	2.09	-0.07	-0.13	-161	-145
2	3	0.42	0.46	0.46	0.37	6.25	0.33	0.37	150	138
	4	-0.59	-0.60	-0.59	-0.56	9.32	-0.51	-0.57	-124	-98
3	5	0.75	0.72	0.72	0.65	10.79	0.62	0.65	140	95
	6	-0.92	-0.90	-0.90	-0.86	14.37	-0.81	-0.87	-101	-56
4	7	1.00	0.93	0.94	0.85	14.20	0.82	0.86	137	133
	8	-1.00	-0.95	-0.95	-0.92	15.38	-0.88	-0.93	-111	-53
5	9	1.00	0.93	0.94	0.85	14.09	0.81	0.85	130	127
	10	-1.00	-0.95	-0.94	-0.93	15.47	-0.88	-0.93	-105	-55
6	11	1.00	0.94	0.94	0.85	14.08	0.81	0.86	122	118
	12	-1.00	-0.95	-0.95	-0.93	15.51	-0.88	-0.93	-102	-71
7	13	0.92	0.86	0.87	0.79	13.16	0.76	0.80	109	101
	14	-0.75	-0.71	-0.70	-0.71	11.75	-0.66	-0.70	-90	-66
8	15	0.59	0.52	0.52	0.47	7.86	0.45	0.48	97	90
	16	-0.42	-0.37	-0.37	-0.34	5.69	-0.30	-0.34	-106	-89
9	17	0.26	0.18	0.19	0.12	2.00	0.09	0.12	106	103
	18	-0.10	-0.01	-0.01	0.01	0.23	0.06	0.01	-124	-117

Table 4.40: Test 10, Response data at target displacement peaks

Cycle #	Peak #	D_t [in]	D_{mE} [in]	D_{mW} [in]	D_b [in]	$\|D_b/D_{by}\|$ [in/in]	D_s [in]	D_{RB} [in]	P_{tot} [kips]	P_b [kips]	V_{RB} [kips]
1	1	0.10	0.10	0.10	0.05	0.85	0.00	0.06	94	87	7
	2	-0.26	-0.26	-0.26	-0.23	3.82	-0.21	-0.23	-130	-112	-18
2	3	0.42	0.42	0.42	0.34	5.65	0.28	0.35	139	123	16
	4	-0.59	-0.59	-0.59	-0.56	9.30	-0.54	-0.55	-147	-120	-28
3	5	0.75	0.76	0.75	0.68	11.27	0.61	0.68	147	122	25
	6	-0.92	-0.92	-0.92	-0.89	14.79	-0.87	-0.89	-152	-115	-37
4	7	1.00	1.00	1.00	0.92	15.40	0.86	0.93	147	117	31
	8	-1.00	-1.00	-1.00	-0.97	16.14	-0.95	-0.97	-148	-110	-39
5	9	1.00	1.00	1.00	0.92	15.38	0.86	0.93	144	114	31
	10	-1.00	-1.00	-1.00	-0.97	16.16	-0.95	-0.97	-146	-107	-38
6	11	1.00	1.00	1.00	0.92	15.36	0.86	0.93	142	112	30
	12	-1.00	-1.00	-1.00	-0.97	16.21	-0.95	-0.97	-144	-106	-38
7	13	0.92	0.92	0.92	0.84	13.97	0.78	0.85	139	111	28
	14	-0.75	-0.75	-0.75	-0.73	12.16	-0.71	-0.72	-137	-106	-31
8	15	0.59	0.59	0.59	0.51	8.56	0.45	0.52	130	111	19
	16	-0.42	-0.42	-0.42	-0.40	6.59	-0.37	-0.39	-130	-109	-21
9	17	0.26	0.26	0.26	0.17	2.89	0.11	0.18	124	115	8
	18	-0.10	-0.10	-0.10	-0.07	1.12	-0.05	-0.07	-122	-113	-8

Table 4.41: Test 11, Response data at target displacement peaks

Cycle #	Peak #	D_t [in]	D_{mE} [in]	D_{mW} [in]	D_b [in]	$\|D_b/D_{by}\|$ [in/in]	D_s [in]	D_{RB} [in]	P_{tot} [kips]	P_b [kips]	V_{RB} [kips]
1	1	0.24	0.24	0.24	0.17	2.78	0.14	0.17	126	117	9
	2	-0.64	-0.64	-0.64	-0.60	10.05	-0.55	-0.60	-144	-115	-29
2	3	1.05	1.05	1.05	0.98	16.35	0.95	0.98	148	117	31
	4	-1.46	-1.47	-1.47	-1.42	23.63	-1.37	-1.42	-159	-109	-50
3	5	1.88	1.88	1.88	1.81	30.16	1.78	1.82	162	111	51
	6	-2.30	-2.30	-2.30	-2.24	37.32	-2.19	-2.26	-170	-101	-70
4	7	2.50	2.50	2.50	2.43	40.47	2.40	2.45	171	105	66
	8	-2.50	-2.50	-2.50	-2.45	40.81	-2.40	-2.46	-170	-96	-74
5	9	2.50	2.50	2.50	2.43	40.55	2.41	2.45	167	102	65
	10	-2.50	-2.50	-2.50	-2.45	40.78	-2.39	-2.47	-167	-93	-73
6	11	2.50	2.50	2.50	2.43	40.50	2.40	2.45	165	100	65
	12	-2.50	-2.50	-2.50	-2.45	40.83	-2.40	-2.46	-165	-92	-73
7	13	2.30	2.30	2.30	2.23	37.09	2.20	2.24	158	99	59
	14	-1.88	-1.88	-1.88	-1.83	30.54	-1.78	-1.85	-150	-93	-57
8	15	1.46	1.46	1.47	1.40	23.29	1.37	1.41	138	100	39
	16	-1.05	-1.05	-1.05	-1.01	16.89	-0.96	-1.02	-134	-97	-38
9	17	0.64	0.64	0.64	0.58	9.59	0.55	0.58	120	102	18
	18	-0.24	-0.24	-0.24	-0.21	3.48	-0.16	-0.21	-115	-101	-14

Table 4.42: Test 12, Response data at target displacement peaks

Cycle #	Peak #	D_t [in]	D_{mE} [in]	D_{mW} [in]	D_b [in]	$\|D_b/D_{by}\|$ [in/in]	D_s [in]	D_{RB} [in]	P_{tot} [kips]	P_b [kips]
1	1	0.24	0.21	0.21	0.18	2.96	0.15	0.18	141	130
	2	-0.64	-0.62	-0.64	-0.54	8.95	-0.48	-0.54	-138	-112
2	3	1.05	1.06	1.06	1.03	17.22	1.01	1.04	126	100
	4	-1.46	-1.42	-1.44	-1.34	22.26	-1.28	-1.34	-128	-82
3	5	1.88	1.88	1.85	1.84	30.74	1.83	1.86	127	80
	6	-2.30	-2.25	-2.27	-2.16	35.98	-2.10	-2.17	-135	-67
4	7	2.50	2.49	2.46	2.45	40.90	2.44	2.47	133	71
	8	-2.50	-2.45	-2.47	-2.36	39.37	-2.30	-2.37	-132	-60
5	9	2.50	2.49	2.46	2.46	40.93	2.44	2.47	128	67
	10	-2.50	-2.45	-2.47	-2.36	39.41	-2.31	-2.38	-129	-57
6	11	2.50	2.49	2.46	2.45	40.90	2.44	2.47	125	64
	12	-2.50	-2.45	-2.47	-2.36	39.40	-2.31	-2.38	-127	-55
7	13	2.30	2.28	2.26	2.25	37.56	2.24	2.27	120	63
	14	-1.88	-1.83	-1.85	-1.75	29.24	-1.70	-1.76	-111	-55
8	15	1.46	1.45	1.44	1.44	23.98	1.43	1.45	100	62
	16	-1.05	-0.98	-1.00	-0.93	15.49	-0.88	-0.93	-95	-57
9	17	0.64	0.62	0.61	0.64	10.60	0.62	0.63	84	65
	18	-0.24	-0.17	-0.18	-0.13	2.10	-0.08	-0.12	-78	-64

Table 4.43: Test 13, Response data at target displacement peaks

Cycle #	Peak #	D_t [in]	D_{mE} [in]	D_{mW} [in]	D_b [in]	$\|D_b/D_{by}\|$ [in/in]	D_s [in]	D_{RB} [in]	P_{tot} [kips]	P_b [kips]	V_{RB} [kips]
1	1	0.24	0.24	0.24	0.22	3.75	0.21	0.22	91	82	9
	2	-0.64	-0.64	-0.64	-0.58	9.67	-0.52	-0.58	-125	-95	-31
2	3	1.05	1.05	1.05	1.02	16.93	1.00	1.02	130	101	30
	4	-1.46	-1.46	-1.46	-1.38	23.08	-1.32	-1.40	-151	-100	-51
3	5	1.88	1.88	1.88	1.84	30.70	1.82	1.85	154	104	49
	6	-2.30	-2.30	-2.30	-2.21	36.83	-2.14	-2.23	-169	-98	-71
4	7	2.50	2.50	2.50	2.46	41.05	2.45	2.48	167	103	64
	8	-2.50	-2.50	-2.50	-2.41	40.18	-2.34	-2.43	-172	-96	-75
5	9	2.50	2.50	2.50	2.46	41.02	2.45	2.48	166	103	63
	10	-2.50	-2.50	-2.50	-2.42	40.27	-2.35	-2.43	-170	-96	-74
6	11	2.50	2.50	2.50	2.46	41.07	2.45	2.48	165	102	63
	12	-2.50	-2.50	-2.50	-2.41	40.24	-2.35	-2.43	-169	-95	-74
7	13	2.30	2.30	2.30	2.26	37.59	2.24	2.27	158	102	57
	14	-1.88	-1.88	-1.88	-1.80	29.98	-1.73	-1.81	-154	-96	-57
8	15	1.46	1.47	1.47	1.43	23.77	1.41	1.44	140	103	38
	16	-1.05	-1.05	-1.05	-0.98	16.34	-0.92	-0.99	-138	-100	-38
9	17	0.64	0.64	0.64	0.61	10.10	0.59	0.61	123	106	18
	18	-0.24	-0.24	-0.24	-0.17	2.89	-0.11	-0.18	-119	-104	-16

Table 4.44: Test 14, Response data at target displacement peaks

Cycle #	Peak #	D_t [in]	D_{mE} [in]	D_{mW} [in]	D_b [in]	$\|D_b/D_{by}\|$ [in/in]	D_s [in]	D_{RB} [in]	P_{tot} [kips]	P_b [kips]	V_{RB} [kips]
1	1	0.34	0.34	0.34	0.33	5.53	0.32	0.33	116	105	11
	2	-0.89	-0.89	-0.89	-0.80	13.25	-0.73	-0.81	-145	-107	-37
2	3	1.47	1.47	1.47	1.46	24.28	1.44	1.46	149	111	38
	4	-2.05	-2.05	-2.05	-1.94	32.28	-1.87	-1.96	-167	-103	-63
3	5	2.63	2.63	2.63	2.62	43.63	2.61	2.63	173	106	66
	6	-3.21	-3.22	-3.21	-3.11	51.89	-3.03	-3.12	-191	-96	-96
4	7	3.50	3.50	3.50	3.49	58.16	3.48	3.50	197	100	96
	8	-3.50	-3.50	-3.50	-3.42	56.92	-3.30	-3.39	-219	-96	-123
5	9	3.50	3.50	3.50	3.49	58.16	3.48	3.50	188	98	90
	10	-3.50	-3.50	-3.50	-3.42	56.95	-3.30	-3.40	-220	-94	-126
6	11	3.50	3.50	3.50	3.49	58.19	3.48	3.51	178	91	88
	12	-3.50	-3.50	-3.50	-3.42	57.08	-3.31	-3.40	-210	-86	-125
7	13	3.21	3.21	3.21	3.20	53.31	3.19	3.22	164	89	75
	14	-2.63	-2.63	-2.63	-2.52	41.98	-2.45	-2.54	-154	-85	-70
8	15	2.05	2.05	2.05	2.04	34.03	2.03	2.05	135	91	45
	16	-1.47	-1.47	-1.47	-1.37	22.84	-1.30	-1.38	-134	-89	-45
9	17	0.89	0.90	0.89	0.89	14.89	0.88	0.89	115	94	21
	18	-0.34	-0.34	-0.34	-0.25	4.24	-0.19	-0.26	-111	-92	-19

Table 4.45: Test 15, Response data at target displacement peaks

Cycle #	Peak #	D_t [in]	D_{mE} [in]	D_{mW} [in]	D_b [in]	$\|D_b/D_{by}\|$ [in/in]	D_s [in]	D_{RB} [in]	P_{tot} [kips]	P_b [kips]
1	1	0.34	0.32	0.32	0.30	5.00	0.28	0.30	113	102
	2	-0.89	-0.85	-0.86	-0.77	12.83	-0.71	-0.78	-135	-99
2	3	1.47	1.46	1.46	1.43	23.88	1.42	1.45	118	87
	4	-2.05	-1.99	-1.99	-1.89	31.58	-1.83	-1.91	-137	-78
3	5	2.63	2.60	2.58	2.57	42.85	2.56	2.59	134	75
	6	-3.21	-3.04	-3.25	-3.06	50.98	-2.99	-3.07	-156	-65
4	7	3.50	3.49	3.42	3.43	57.24	3.42	3.45	151	67
	8	-3.50	-3.24	-3.64	-3.36	55.93	-3.29	-3.36	-157	-60
5	9	3.50	3.52	3.38	3.44	57.32	3.42	3.46	143	63
	10	-3.50	-3.25	-3.64	-3.36	55.95	-3.29	-3.36	-153	-57
6	11	3.50	3.53	3.38	3.45	57.45	3.43	3.46	140	62
	12	-3.50	-3.25	-3.64	-3.36	56.05	-3.30	-3.36	-150	-56
7	13	3.21	3.26	3.10	3.16	52.73	3.15	3.19	126	59
	14	-2.63	-2.57	-2.59	-2.50	41.59	-2.43	-2.51	-118	-50
8	15	2.05	2.03	2.02	2.02	33.66	2.01	2.04	100	57
	16	-1.47	-1.41	-1.42	-1.35	22.44	-1.29	-1.36	-97	-52
9	17	0.89	0.88	0.87	0.88	14.72	0.87	0.89	81	60
	18	-0.34	-0.27	-0.27	-0.23	3.85	-0.18	-0.23	-77	-59

Table 4.46: Test 16, Response data at target displacement peaks

Cycle #	Peak #	D_t [in]	D_{mE} [in]	D_{mW} [in]	D_b [in]	$\lvert D_b/D_{by}\rvert$ [in/in]	D_s [in]	D_{RB} [in]	P_{tot} [kips]	P_b [kips]	V_{RB} [kips]
1	1	0.34	0.34	0.34	0.33	5.52	0.33	0.33	82	72	10
	2	-0.89	-0.89	-0.89	-0.83	13.89	-0.77	-0.84	-113	-79	-34
2	3	1.47	1.47	1.47	1.44	24.07	1.44	1.45	117	83	33
	4	-2.05	-2.05	-2.05	-1.97	32.88	-1.90	-1.99	-136	-80	-56
3	5	2.63	2.63	2.63	2.60	43.38	2.60	2.62	138	82	56
	6	-3.21	-3.21	-3.22	-3.15	52.52	-3.06	-3.15	-159	-75	-84
4	7	3.50	3.50	3.50	3.47	57.90	3.47	3.49	161	81	80
	8	-3.50	-3.50	-3.50	-3.45	57.57	-3.34	-3.43	-194	-76	-118
5	9	3.50	3.50	3.50	3.48	57.94	3.47	3.49	159	81	78
	10	-3.50	-3.50	-3.50	-3.45	57.55	-3.34	-3.43	-193	-76	-116
6	11	3.50	3.50	3.50	3.47	57.85	3.47	3.49	156	81	75
	12	-3.50	-3.50	-3.50	-3.45	57.52	-3.34	-3.43	-191	-76	-115
7	13	3.21	3.22	3.21	3.18	52.95	3.17	3.20	146	81	65
	14	-2.63	-2.63	-2.63	-2.55	42.56	-2.48	-2.57	-141	-78	-63
8	15	2.05	2.05	2.05	2.02	33.69	2.02	2.04	124	84	39
	16	-1.47	-1.47	-1.47	-1.40	23.29	-1.33	-1.41	-124	-83	-41
9	17	0.89	0.89	0.89	0.87	14.51	0.86	0.87	107	88	19
	18	-0.34	-0.34	-0.34	-0.28	4.72	-0.22	-0.28	-104	-85	-18

Table 4.47: Test 18, Response data at target displacement peaks

Cycle #	Peak #	D_t [in]	D_{mE} [in]	D_{mW} [in]	D_b [in]	$\lvert D_b/D_{by}\rvert$ [in/in]	D_s [in]	D_{RB} [in]	P_{tot} [kips]	P_b [kips]	V_{RB} [kips]
1	1	0.34	0.31	0.31	0.19	3.24	0.12	0.20	137	126	11
	2	-0.89	-0.90	-0.90	-0.89	14.90	-0.89	-0.89	-153	-122	-31
2	3	1.47	1.47	1.47	1.36	22.71	1.28	1.38	163	129	34
	4	-2.05	-2.05	-2.05	-2.03	33.79	-2.02	-2.04	-179	-126	-53
3	5	2.63	2.63	2.63	2.52	41.96	2.44	2.55	181	125	57
	6	-3.21	-3.22	-3.22	-3.20	53.41	-3.18	-3.20	-194	-115	-79
4	7	3.50	3.50	3.50	3.40	56.73	3.33	3.42	201	116	85
	8	-3.50	-3.48	-3.53	-3.52	58.59	-3.47	-3.49	-197	-102	-95
5	9	3.50	3.50	3.50	3.41	56.76	3.33	3.42	192	111	82
	10	-3.50	-3.48	-3.53	-3.51	58.42	-3.47	-3.49	-198	-104	-94
6	11	3.50	3.50	3.50	3.41	56.79	3.34	3.42	187	107	80
	12	-3.50	-3.47	-3.52	-3.50	58.39	-3.46	-3.49	-197	-104	-93
7	13	3.50	3.50	3.50	3.41	56.79	3.34	3.42	183	104	79
	14	-3.50	-3.49	-3.52	-3.51	58.49	-3.47	-3.49	-189	-97	-91
8	15	3.50	3.50	3.50	3.41	56.82	3.34	3.43	180	101	79
	16	-3.50	-3.49	-3.52	-3.52	58.63	-3.48	-3.50	-183	-92	-91
9	17	3.50	3.50	3.50	3.41	56.75	3.33	3.42	177	99	79
	18	-3.50	-3.48	-3.53	-3.51	58.56	-3.47	-3.50	-182	-92	-90
10	19	3.21	3.22	3.22	3.11	51.87	3.04	3.14	161	95	66
	20	-2.63	-2.63	-2.63	-2.62	43.66	-2.61	-2.63	-151	-91	-60
11	21	2.05	2.05	2.05	1.95	32.49	1.88	1.97	132	93	39
	22	-1.47	-1.47	-1.47	-1.47	24.45	-1.46	-1.47	-129	-90	-39
12	23	0.89	0.90	0.90	0.79	13.19	0.72	0.81	113	93	20
	24	-0.34	-0.34	-0.34	-0.35	5.83	-0.35	-0.34	-104	-89	-15

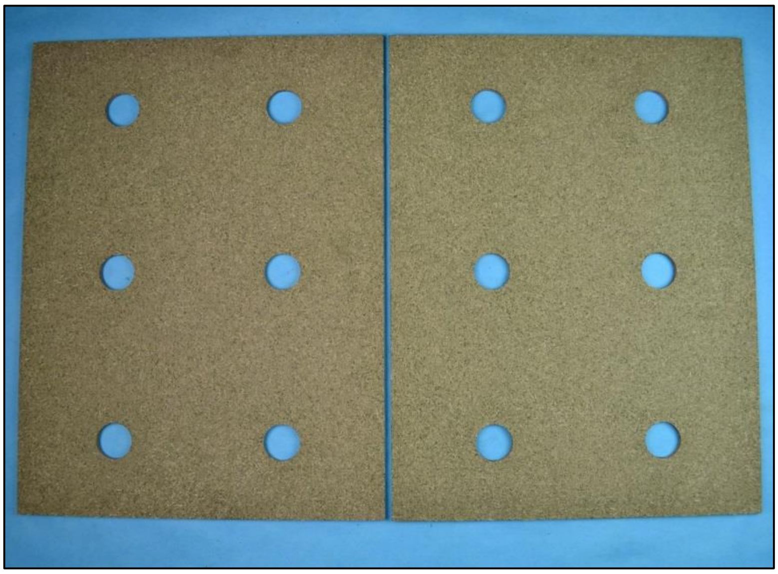

Figure 4.71:RF42 friction plates used in phase II-2

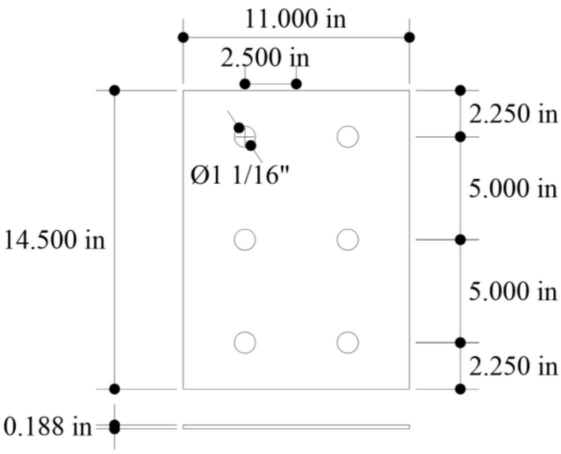

Figure 4.72: Dimensions of RF42 friction plates used in phase II-2

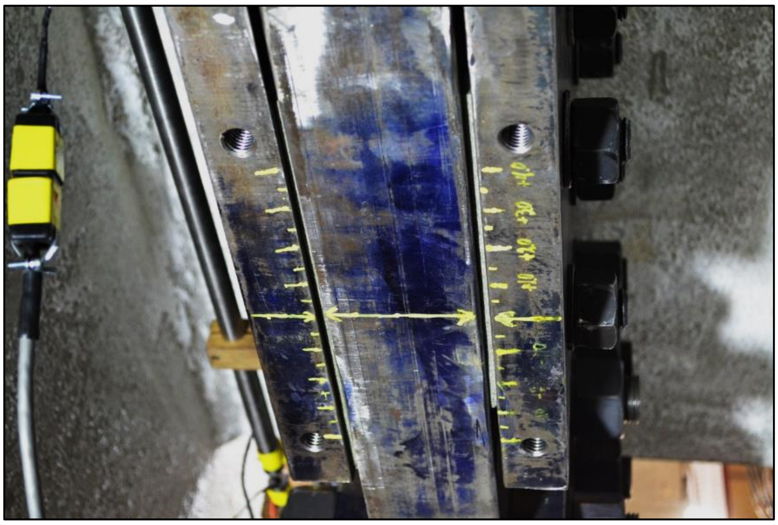

Figure 4.73: Installed FD on the specimen for phase II-2

Figure 4.74: Hydraulic gun used for the bolt pretensioning

Figure 4.75: Infrared gun used to measure the surface temperature of the internal steel plate

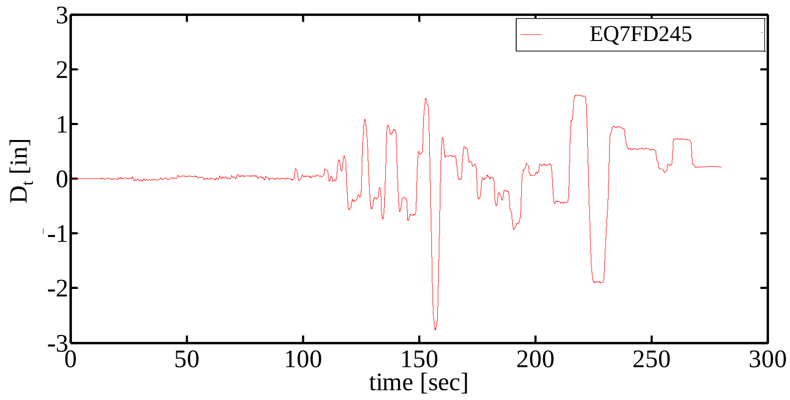

Figure 4.76: Target displacement used in Test 6 and 17 in phase II-2

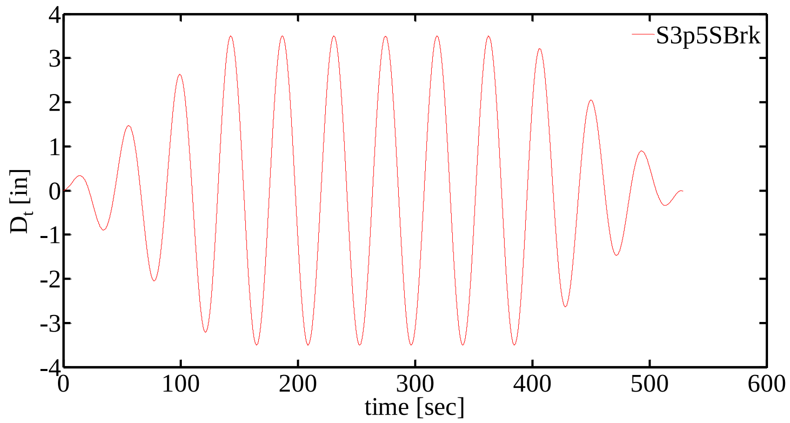

Figure 4.77: Target displacement used in Test 7 and 18 in phase II-2

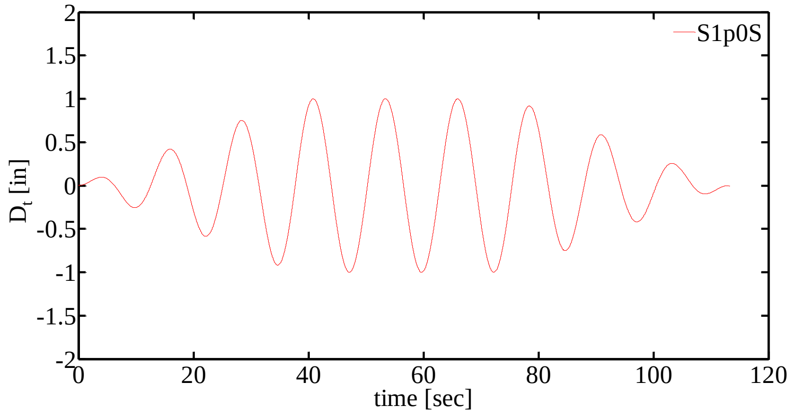

Figure 4.78: Target displacement used in Test 8 and 10 in phase II-2

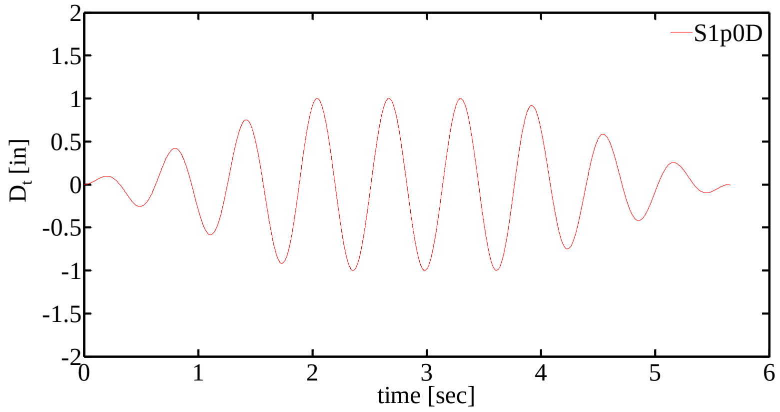

Figure 4.79: Target displacement used in Test 9 in phase II-2

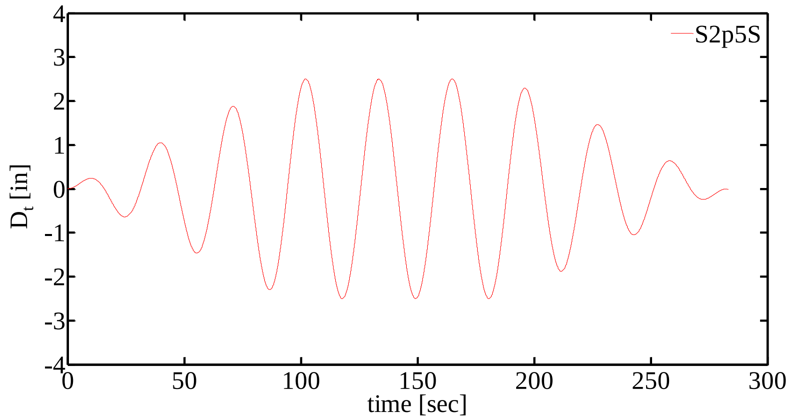

Figure 4.80: Target displacement used in Test 11 and 13 in phase II-2

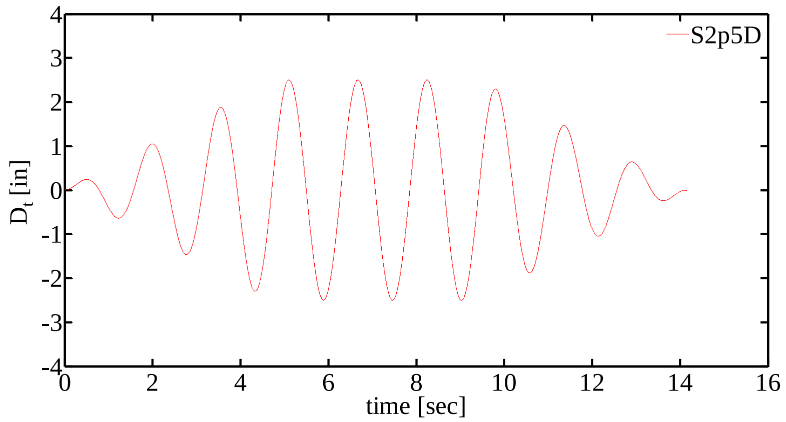

Figure 4.81: Target displacement used in Test 12 in phase II-2

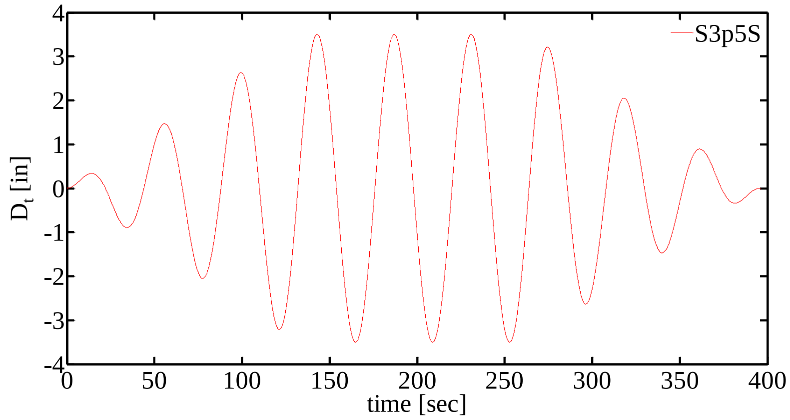

Figure 4.82: Target displacement used in Test 14 and 16 in phase II-2

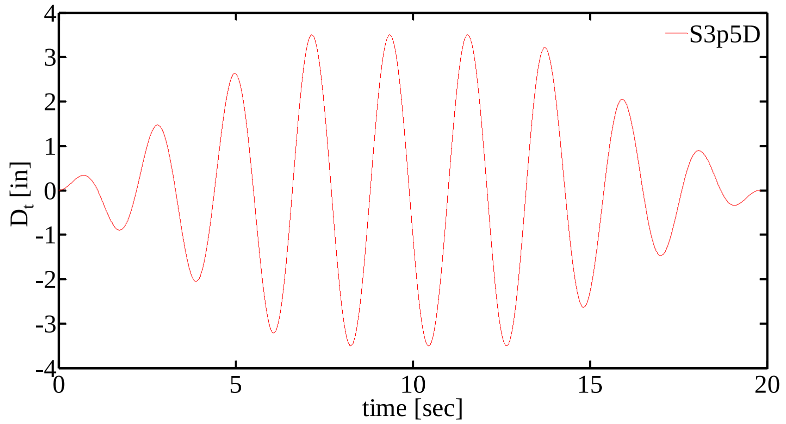

Figure 4.83: Target displacement used in Test 15 in phase II-2

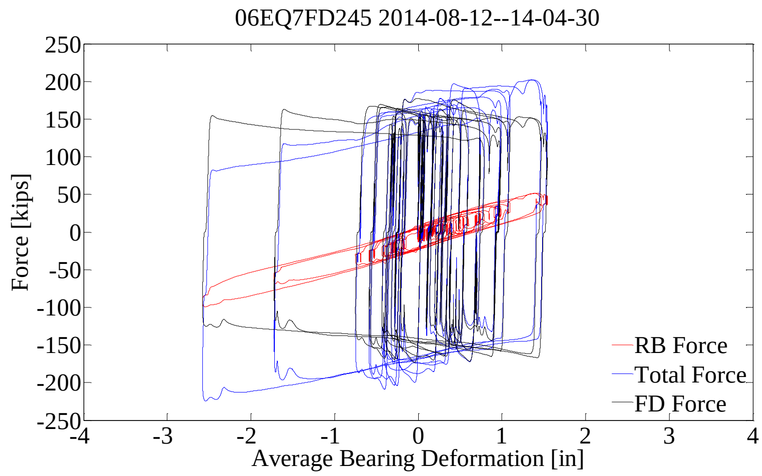

Figure 4.84: Test 6, Force – deformation plots for the deformable connection and its individual components in phase II [pg. 81]

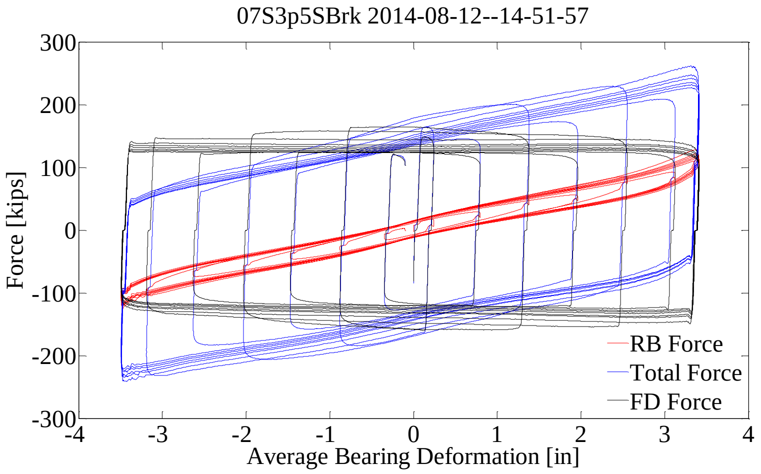

Figure 4.85: Test 7, Force – deformation plots for the deformable connection and its individual components in phase II [pg. 81; pg. 72]

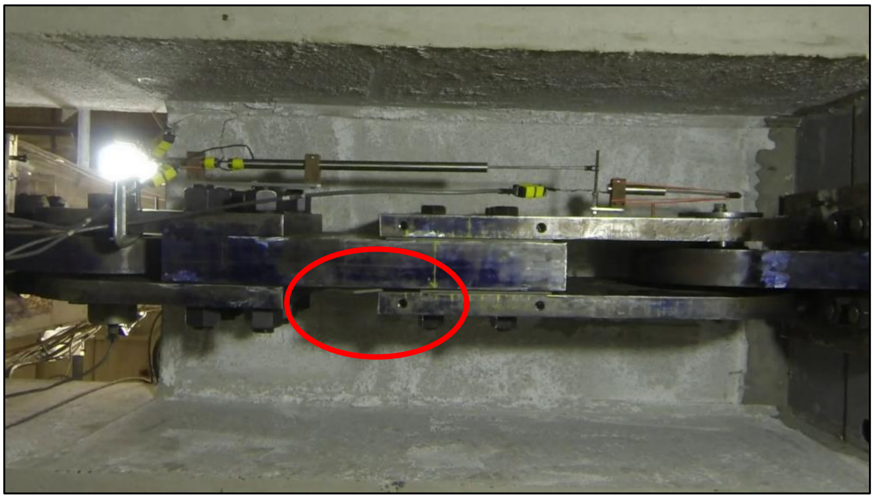

Figure 4.86: Test 7, Fracture of the West friction plate

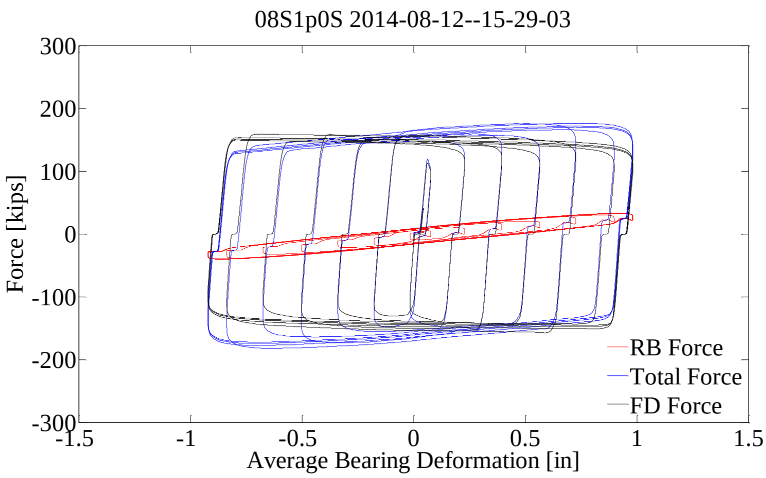

Figure 4.87: Test 8, Force – deformation plots for the deformable connection and its individual components in phase II [pg. 81; pg. 73]

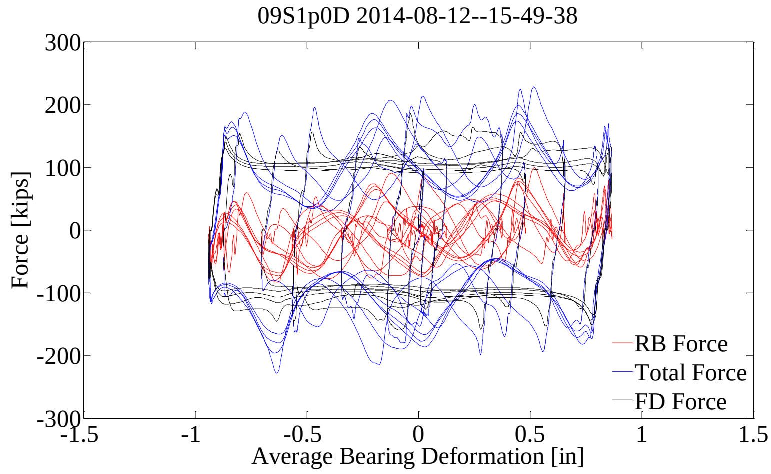

Figure 4.88: Test 9, Force – deformation plots for the deformable connection and its individual components in phase II [pg. 82; pg. 73]

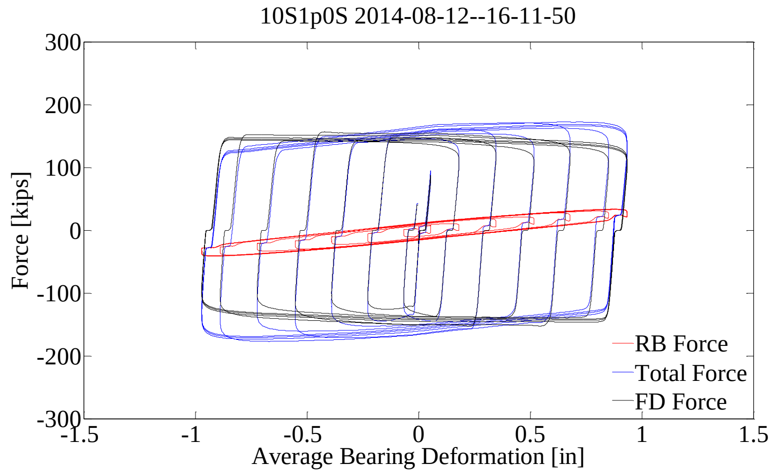

Figure 4.89: Test 10, Force – deformation plots for the deformable connection and its individual components in phase II [pg. 81; pg. 74]

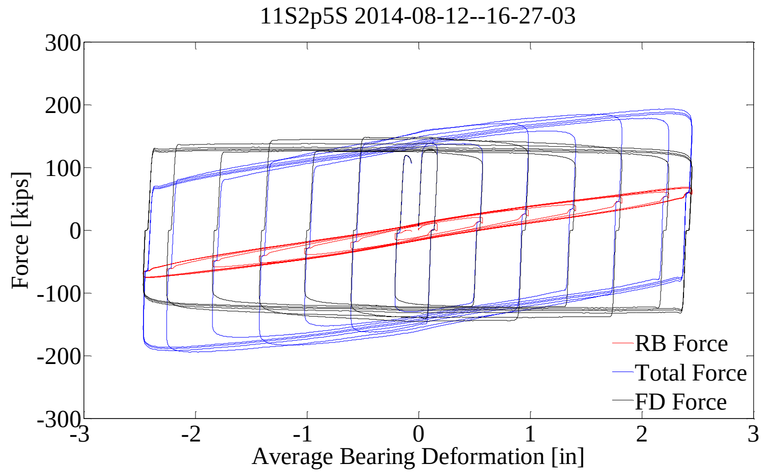

Figure 4.90: Test 11, Force – deformation plots for the deformable connection and its individual components in phase II [pg. 82; pg. 74]

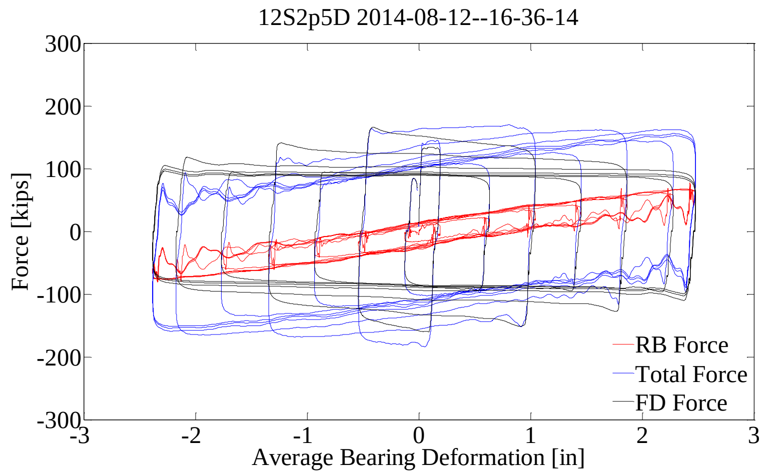

Figure 4.91: Test 12, Force – deformation plots for the deformable connection and its individual components in phase II [pg. 82; pg. 75]

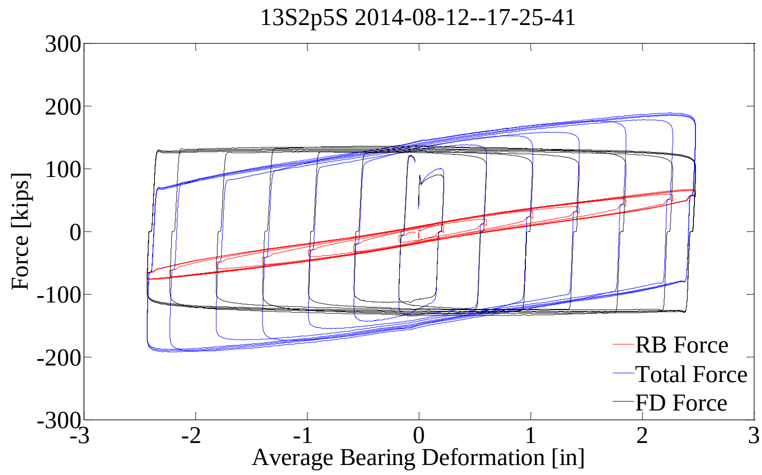

Figure 4.92: Test 13, Force – deformation plots for the deformable connection and its individual components in phase II [pg. 82; pg. 75]

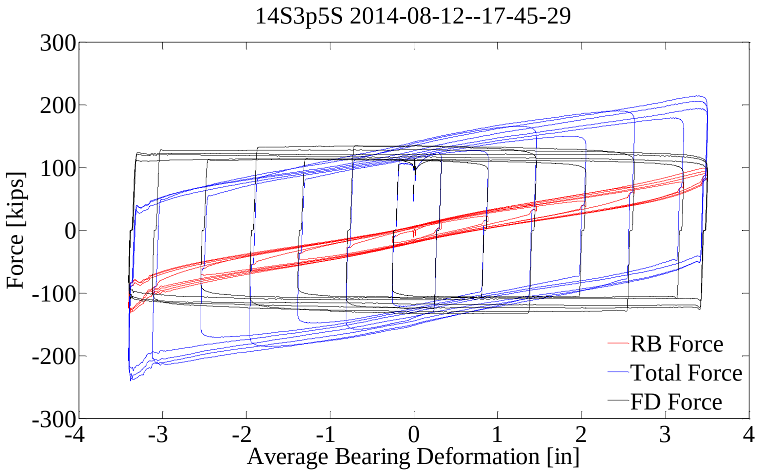

Figure 4.93: Test 14, Force – deformation plots for the deformable connection and its individual components in phase II [pg. 83; pg. 76]

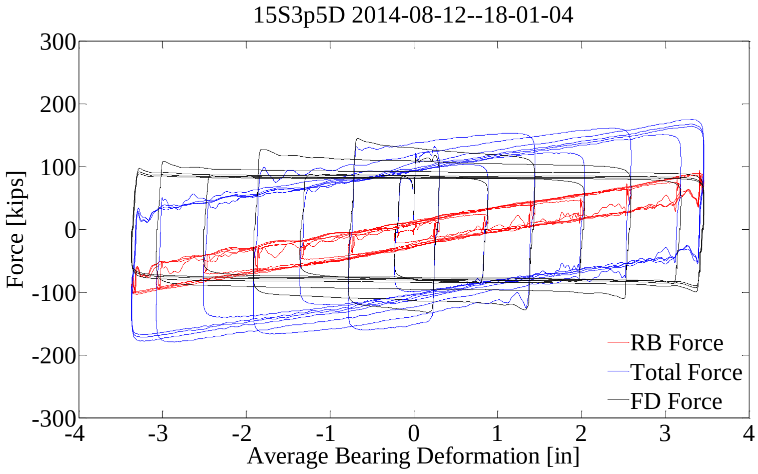

Figure 4.94: Test 15, Force – deformation plots for the deformable connection and its individual components in phase II [pg. 83; pg. 76]

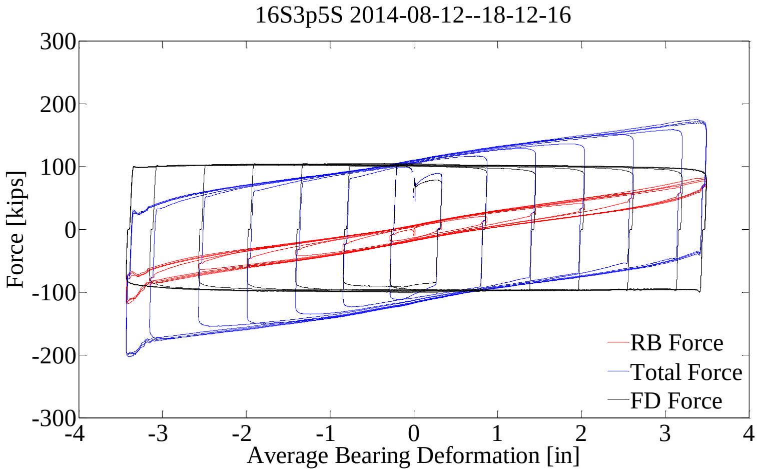

Figure 4.95: Test 16, Force – deformation plots for the deformable connection and its individual components in phase II [pg. 83; pg. 77]

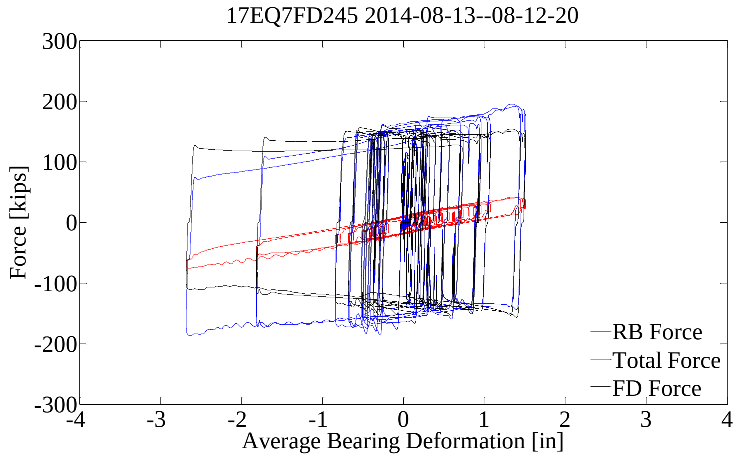

Figure 4.96: Test 17, Force – deformation plots for the deformable connection and its individual components in phase II [pg. 81]

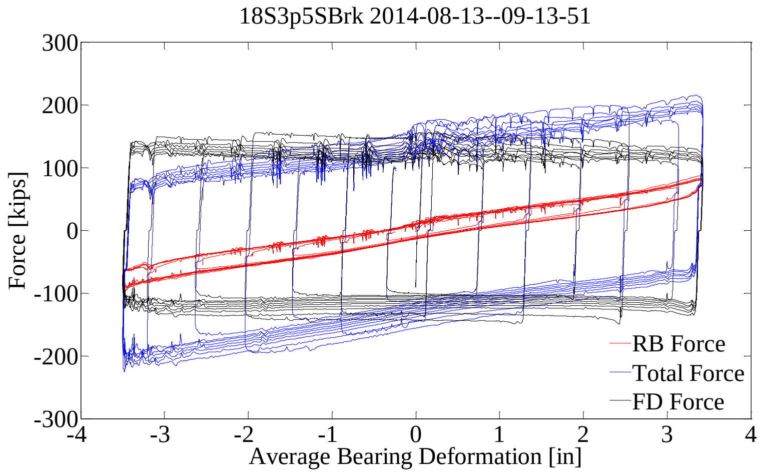

Figure 4.97: Test 18, Force – deformation plots for the deformable connection and its individual components in phase II [pg. 81; pg. 78]

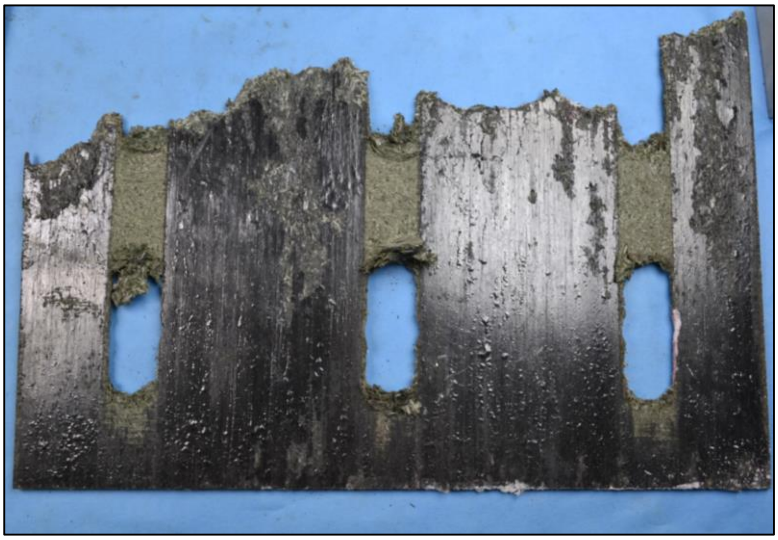

Figure 4.98: Fractured West RF42 friction plate at the end of phase II-2

4.4.9 Phase II-3

In phase II-3 the RF42 friction plates were used in the FD. The material description was provided in section 4.4.8. The friction plates are shown in Figure 4.99 and their dimensions are shown in Figure 4.102. The dimensions of the friction plates have been increased, compared to the dimensions of the friction plates used in phase II-2.

Bushings and Belleville washers were not used in phase II-3. The thickness of the friction plates was, t_{fp}=6/16 inches. Six ASTM A325 bolts were used, n_b= 6 with diameter d_b = 1.0 inches. The bolt force was N_b = 62 kips. Each bolt was pretensioned at the beginning of phase II-3 using the hydraulic gun shown in Figure 4.74. The applied pressure was 3600 psi which is associated with a torque of 1083 lb.-ft. The static friction coefficient reported by the manufacturer is μ_s = 0.43 and the expected static friction force $F_s = n_b\, n_s\, N_b\, \mu_s$ = 320 kips. However, it was observed from the results from phase II-2, that the static friction coefficient between the RF42 and steel interface was approximately 0.26 and not 0.43.

The RB were damaged in phase II-2. However, prior to this damage, these carbon fiber RB were subjected to many large amplitude cycles and their response was good. Thus, to save time and labor cost it was decided to not replace them.

The approximate temperature at the surface of the internal steel plate was measured at the beginning (T_i) and at the end (T_f) of each test using the infrared gun shown in Figure 4.75.

The condition of the surfaces of the internal steel plate before the initiation of the tests are shown in Figure 4.100. Figure 4.101 shows the components, the assembled and installed FD in the fixture.

Table 4.48 shows a summary of the conditions of the East and West friction plates and the RB after each test of phase II-3. The notation *UC* indicates that the component was in an undamaged condition after the test. If damage was observed at the end of the test, the description of the damage is given.

The test sequence is shown in Table 4.49.

4.4.9.1 Test 19: 19EQ7FD245

Test 19 was successfully completed. The displacement target time history is presented in Figure 4.103. The force-deformation plots are shown in Figure 4.109. The initial and final temperatures were T_i = 67°F and T_f = 73°F respectively.

4.4.9.2 Test 20: 20S3p0SBrk

Test 20 was successfully completed. The displacement target time history is presented in Figure 4.104. The force-deformation plots are shown in Figure 4.110. In Table 4.50 the force and deformation data measured at the target displacement peaks are presented. The initial and final temperatures were T_i = 73°F and T_f = 95°F respectively.

4.4.9.3 Test 21: 21S1p0S

Test 21 was successfully completed. The displacement target time history is presented in Figure 4.105. The force-deformation plots are shown in Figure 4.111. In Table 4.51 the force and deformation data measured at the target displacement peaks are presented. The initial and final temperatures were T_i = 91°F and T_f = 93°F respectively.

4.4.9.4 Test 22: 22S1p0D

Test 22 was successfully completed. The displacement target time history is presented in Figure 4.106. The force-deformation plots are shown in Figure 4.112. The bolt holes of the friction plates were elongated as a result of the cumulative applied deformation up to this test. However, it seems that the overall response of the deformable connection was not affected. In Table 4.52

the force and deformation data measured at the target displacement peaks are presented. The initial and final temperatures were T_i = 85℉ and T_f = 92℉ respectively.

4.4.9.5 Test 23: 23S1p0S

Test 7 was successfully completed. The displacement target time history is presented in Figure 4.105. The force-deformation plots are shown in Figure 4.113. In Table 4.53 the force and deformation data measured at the target displacement peaks are presented. The initial and final temperatures were T_i = 95℉ and T_f = 108℉ respectively.

4.4.9.6 Test 24: 24S3p0S

Test 24 was successfully completed. The displacement target time history is presented in Figure 4.107. The force-deformation plots are shown in Figure 4.114. Figure 4.115 shows the FD at the time of fracture of the West friction plate. In Table 4.54 the force and deformation data measured at the target displacement peaks are presented. The initial and final temperatures were T_i = 91℉ and T_f = 103℉ respectively.

4.4.9.7 Test 25: 25S3p0S

Test 25 was successfully completed. The displacement target time history is presented in Figure 4.107. The force-deformation plots are shown in Figure 4.116. In Table 4.55 the force and deformation data measured at the target displacement peaks are presented. The initial and final temperatures were T_i = 102℉ and T_f = 113℉ respectively.

4.4.9.8 Test 26: 26S3p0D

Test 26 was successfully completed. The displacement target time history is presented in Figure 4.108. The force-deformation plots are shown in Figure 4.117. In Table 4.56 the force and deformation data measured at the target displacement peaks are presented. The initial and final temperatures were T_i = 113℉ and T_f = 118℉ respectively.

4.4.9.9 Test 27: 27S3p0D

Test 7 was successfully completed. The displacement target time history is presented in Figure 4.108. The force-deformation plots are shown in Figure 4.118. In Table 4.57 the force and deformation data measured at the target displacement peaks are presented. The initial and final temperatures were T_i = 95℉ and T_f = 102℉ respectively.

4.4.9.10 Test 28: 28S3p0S

Test 7 was successfully completed. The displacement target time history is presented in Figure 4.107. The force-deformation plots are shown in Figure 4.119. In Table 4.58 the force and deformation data measured at the target displacement peaks are presented. The initial and final temperatures were T_i = 100℉ and T_f = 111℉ respectively.

4.4.9.11 Test 29: 29EQ7FD245

Test 29 was successfully completed. The displacement target time history is presented in Figure 4.103. The force-deformation plots are shown in Figure 4.120. Figure 4.121 shows a close up view of the friction plates at the end of phase II-3. Figure 4.121 includes a circle indicating the missing piece of the West friction plate. The East friction plate is shown in Figure 4.122 where the elongated bolt holes can be seen. Figure 4.123 shows the West friction plate that fractured. Figure 4.124 shows the North West RB at the end of phase II-3. Also, rubber particles from wear of the rubber while it was sliding against the external steel plate at the side of the wall are shown in Figure 4.124. The initial and final temperatures for Test 29 were T_i = 109℉ and T_f = 115℉ respectively.

Table 4.48: Phase II-3 condition of components of deformable connection

Test	West FP	East FP	NE RB	NW RB	SE RB	SW RB
19	*UC	*UC	Torn rubber	Debonded rubber	Torn rubber	Torn rubber
20	UC	UC	Torn rubber	Debonded rubber	Torn rubber	Severely Torn
21	UC	UC	Torn rubber	Debonded rubber	Torn rubber	Severely Torn
22	Elongated bolt holes	Elongated bolt holes	Torn rubber	Debonded rubber	Torn rubber	Severely Torn
23	Elongated bolt holes	Elongated bolt holes	Torn rubber	Debonded rubber	Torn rubber	Severely Torn
24	Fractured	Elongated bolt holes	Torn rubber	Debonded rubber	Torn rubber	Severely Torn
25	Fractured	Elongated bolt holes	Torn rubber	Debonded rubber	Torn rubber	Severely Torn
26	Fractured	Elongated bolt holes	Torn rubber	Debonded rubber	Torn rubber	Severely Torn
27	Fractured	Elongated bolt holes	Torn rubber	Debonded rubber	Torn rubber	Severely Torn
28	Fractured	Elongated bolt holes	Torn rubber	Debonded rubber	Torn rubber	Severely Torn
29	Fractured	Elongated bolt holes	Torn rubber	Debonded rubber	Torn rubber	Severely Torn

**The components was at its initial condition at the beginning of the test*
UC: Undamaged Condition

Table 4.49: Phase II-3 testing sequence

Day	Test	Name	$D_{t,max}$ [in]	$V_{t,max}$ [in/sec]	f [Hz]	# Ramp up cycles	# Ramp down cycles	# Max. amplitude cycles
	19	19EQ7FD245	2.77	0.90	-	-	-	-
	20	20S3p0SBrk	3.00	0.50	0.03	3	3	6
	21	21S1p0S	1.00	0.50	0.08	3	3	3
	22	22S1p0D	1.00	10.00	1.59	3	3	3
	23	23S1p0S	1.00	0.50	0.08	3	3	3
09-26-2014	24	24S3p0S	3.00	0.50	0.03	3	3	3
	25	25S3p0S	3.00	0.50	0.03	3	3	3
	26	26S3p0D	3.00	10.00	0.53	3	3	3
	27	27S3p0D	3.00	10.00	0.53	3	3	3
	28	28S3p0S	3.00	0.50	0.03	3	3	3
	29	29EQ7FD245	2.77	0.90	-	-	-	-

Table 4.50: Test 20, Response data at target displacement peaks

Cycle #	Peak #	D_t [in]	D_{mE} [in]	D_{mW} [in]	D_b [in]	$\|D_b/D_{by}\|$ [in/in]	D_s [in]	D_{RB} [in]	P_{tot} [kips]	P_b [kips]	V_{RB} [kips]
1	1	0.29	0.29	0.29	0.03	0.46	0.03	0.13	174	148	27
	2	-0.77	-0.77	-0.77	-0.76	12.62	-0.76	-0.76	-148	-144	-4
2	3	1.26	1.26	1.26	0.99	16.47	0.99	1.10	197	150	47
	4	-1.76	-1.76	-1.76	-1.73	28.88	-1.73	-1.75	-163	-138	-25
3	5	2.26	2.26	2.26	2.00	33.28	2.00	2.11	210	143	67
	6	-2.75	-2.76	-2.76	-2.74	45.63	-2.74	-2.75	-174	-128	-47
4	7	3.00	3.00	3.00	2.74	45.68	2.74	2.82	220	134	87
	8	-3.00	-3.00	-3.00	-2.99	49.81	-2.99	-3.04	-176	-124	-52
5	9	3.00	3.00	3.00	2.75	45.77	2.75	2.82	213	129	83
	10	-3.00	-3.00	-3.00	-2.99	49.87	-2.99	-3.05	-172	-121	-51
6	11	3.00	3.00	3.00	2.75	45.76	2.75	2.83	208	126	82
	12	-3.00	-3.00	-3.00	-2.99	49.82	-2.99	-3.05	-170	-119	-51
7	13	3.00	3.00	3.00	2.75	45.80	2.75	2.83	205	123	82
	14	-3.00	-3.00	-3.00	-2.99	49.89	-2.99	-3.04	-167	-117	-50
8	15	3.00	3.00	3.00	2.75	45.87	2.75	2.83	202	121	82
	16	-3.00	-3.00	-3.00	-3.00	49.94	-3.00	-3.05	-166	-115	-50
9	17	3.00	3.00	3.00	2.75	45.89	2.75	2.83	200	118	81
	18	-3.00	-3.00	-3.00	-2.99	49.88	-2.99	-3.05	-162	-114	-48
10	19	2.75	2.76	2.76	2.51	41.79	2.51	2.58	191	117	74
	20	-2.26	-2.26	-2.26	-2.25	37.49	-2.25	-2.30	-143	-111	-32
11	21	1.76	1.76	1.76	1.51	25.19	1.51	1.58	172	118	54
	22	-1.26	-1.26	-1.26	-1.25	20.89	-1.25	-1.31	-128	-115	-14
12	23	0.77	0.77	0.77	0.52	8.64	0.52	0.57	155	119	36
	24	-0.29	-0.29	-0.29	-0.28	4.75	-0.28	-0.34	-106	-116	9

Table 4.51: Test 21, Response data at target displacement peaks

Cycle #	Peak #	D_t [in]	D_{mE} [in]	D_{mW} [in]	D_b [in]	$\lvert D_b/D_{by}\rvert$ [in/in]	D_s [in]	D_{RB} [in]	P_{tot} [kips]	P_b [kips]	V_{RB} [kips]
1	1	0.10	0.10	0.10	0.00	0.05	0.00	0.06	157	135	22
	2	-0.26	-0.26	-0.26	-0.09	1.50	-0.09	-0.13	-125	-131	6
2	3	0.42	0.42	0.42	0.31	5.25	0.32	0.38	171	141	29
	4	-0.59	-0.59	-0.59	-0.42	7.00	-0.42	-0.46	-142	-140	-2
3	5	0.75	0.75	0.75	0.65	10.79	0.65	0.71	177	140	36
	6	-0.92	-0.92	-0.92	-0.75	12.50	-0.75	-0.79	-147	-137	-10
4	7	1.00	1.00	1.00	0.90	14.95	0.90	0.96	176	134	41
	8	-1.00	-1.00	-1.00	-0.84	13.92	-0.84	-0.88	-143	-132	-11
5	9	1.00	1.00	1.00	0.90	14.93	0.90	0.96	172	131	41
	10	-1.00	-1.00	-1.00	-0.84	13.96	-0.84	-0.88	-142	-130	-11
6	11	1.00	1.00	1.00	0.90	15.01	0.90	0.96	171	129	41
	12	-1.00	-1.00	-1.00	-0.84	13.97	-0.84	-0.88	-140	-129	-11
7	13	0.92	0.92	0.92	0.82	13.63	0.82	0.88	167	128	39
	14	-0.75	-0.75	-0.75	-0.60	9.96	-0.60	-0.64	-132	-127	-6
8	15	0.59	0.59	0.59	0.49	8.17	0.49	0.55	162	130	32
	16	-0.42	-0.42	-0.42	-0.26	4.27	-0.26	-0.30	-124	-127	3
9	17	0.26	0.26	0.26	0.15	2.49	0.15	0.21	157	133	24
	18	-0.10	-0.10	-0.10	0.07	1.14	0.07	0.03	-119	-131	12

Table 4.52: Test 22, Response data at target displacement peaks

Cycle #	Peak #	D_t [in]	D_{mE} [in]	D_{mW} [in]	D_b [in]	$\lvert D_b/D_{by}\rvert$ [in/in]	D_s [in]	D_{RB} [in]	P_{tot} [kips]	P_b [kips]
1	1	0.10	0.06	0.06	0.00	0.05	0.00	0.02	99	77
	2	-0.26	-0.17	-0.18	-0.04	0.75	-0.04	-0.11	-171	-179
2	3	0.42	0.48	0.49	0.26	4.40	0.26	0.33	212	197
	4	-0.59	-0.63	-0.62	-0.50	8.40	-0.50	-0.57	-117	-140
3	5	0.75	0.73	0.73	0.53	8.79	0.53	0.59	201	158
	6	-0.92	-0.88	-0.89	-0.72	12.04	-0.72	-0.79	-192	-200
4	7	1.00	0.98	0.97	0.78	12.97	0.78	0.84	185	119
	8	-1.00	-0.95	-0.95	-0.83	13.76	-0.83	-0.89	-148	-144
5	9	1.00	0.95	0.95	0.78	12.92	0.77	0.83	177	123
	10	-1.00	-0.94	-0.94	-0.83	13.90	-0.83	-0.89	-129	-110
6	11	1.00	0.94	0.94	0.77	12.79	0.77	0.82	163	118
	12	-1.00	-0.93	-0.94	-0.84	14.07	-0.84	-0.90	-116	-91
7	13	0.92	0.87	0.86	0.71	11.78	0.71	0.75	135	87
	14	-0.75	-0.70	-0.70	-0.60	10.06	-0.60	-0.66	-97	-94
8	15	0.59	0.53	0.53	0.34	5.67	0.34	0.39	142	121
	16	-0.42	-0.35	-0.35	-0.24	4.02	-0.24	-0.30	-118	-131
9	17	0.26	0.18	0.18	-0.01	0.15	-0.01	0.05	160	143
	18	-0.10	-0.04	-0.04	0.00	0.06	0.00	-0.04	-88	-100

Table 4.53: Test 23, Response data at target displacement peaks

Cycle #	Peak #	D_t [in]	D_{mE} [in]	D_{mW} [in]	D_b [in]	$\|D_b/D_{by}\|$ [in/in]	D_s [in]	D_{RB} [in]	P_{tot} [kips]	P_b [kips]	V_{RB} [kips]
1	1	0.10	0.10	0.10	0.00	0.06	0.00	0.05	103	79	24
	2	-0.26	-0.26	-0.26	-0.15	2.48	-0.15	-0.19	-143	-148	5
2	3	0.42	0.42	0.42	0.23	3.82	0.23	0.30	191	162	29
	4	-0.59	-0.59	-0.59	-0.47	7.86	-0.47	-0.52	-164	-160	-3
3	5	0.75	0.75	0.75	0.56	9.40	0.56	0.64	197	161	36
	6	-0.92	-0.92	-0.92	-0.80	13.35	-0.80	-0.85	-167	-156	-11
4	7	1.00	1.00	1.00	0.82	13.59	0.82	0.89	194	153	41
	8	-1.00	-1.00	-1.00	-0.88	14.72	-0.88	-0.94	-161	-149	-12
5	9	1.00	1.00	1.00	0.82	13.64	0.82	0.89	189	149	41
	10	-1.00	-1.00	-1.00	-0.89	14.80	-0.89	-0.94	-157	-145	-12
6	11	1.00	1.00	1.00	0.82	13.62	0.82	0.89	187	146	41
	12	-1.00	-1.00	-1.00	-0.89	14.87	-0.89	-0.94	-154	-142	-12
7	13	0.92	0.92	0.92	0.74	12.29	0.74	0.81	182	143	39
	14	-0.75	-0.75	-0.75	-0.65	10.84	-0.65	-0.69	-145	-139	-6
8	15	0.59	0.59	0.59	0.41	6.78	0.41	0.47	177	145	32
	16	-0.42	-0.42	-0.42	-0.31	5.22	-0.31	-0.36	-139	-142	3
9	17	0.26	0.26	0.26	0.07	1.18	0.07	0.14	173	150	23
	18	-0.10	-0.10	-0.10	0.01	0.24	0.01	-0.03	-134	-147	12

Table 4.54: Test 24, Response data at target displacement peaks

Cycle #	Peak #	D_t [in]	D_{mE} [in]	D_{mW} [in]	D_b [in]	$\|D_b/D_{by}\|$ [in/in]	D_s [in]	D_{RB} [in]	P_{tot} [kips]	P_b [kips]	V_{RB} [kips]
1	1	0.29	0.29	0.29	0.10	1.62	0.10	0.15	171	145	26
	2	-0.77	-0.77	-0.77	-0.68	11.31	-0.68	-0.73	-150	-143	-6
2	3	1.26	1.26	1.26	1.06	17.73	1.06	1.13	190	144	46
	4	-1.76	-1.76	-1.76	-1.65	27.55	-1.65	-1.72	-161	-136	-26
3	5	2.26	2.26	2.26	2.07	34.47	2.07	2.14	201	137	64
	6	-2.75	-2.76	-2.76	-2.66	44.32	-2.66	-2.72	-173	-126	-47
4	7	3.00	3.00	3.00	2.81	46.89	2.81	2.90	207	126	81
	8	-3.00	-3.00	-3.00	-2.91	48.49	-2.91	-2.97	-175	-121	-54
5	9	3.00	3.00	3.00	2.82	46.92	2.82	2.90	201	121	80
	10	-3.00	-3.00	-3.00	-2.91	48.54	-2.91	-2.97	-170	-118	-52
6	11	3.00	3.00	3.00	2.82	46.99	2.82	2.90	199	119	79
	12	-3.00	-3.00	-3.00	-2.91	48.53	-2.91	-2.97	-169	-116	-53
7	13	2.75	2.76	2.76	2.57	42.91	2.57	2.65	190	118	72
	14	-2.26	-2.26	-2.26	-2.17	36.19	-2.17	-2.23	-146	-113	-33
8	15	1.76	1.76	1.76	1.58	26.33	1.58	1.65	172	120	52
	16	-1.26	-1.26	-1.26	-1.18	19.60	-1.18	-1.23	-132	-117	-15
9	17	0.77	0.77	0.77	0.59	9.89	0.59	0.64	157	122	35
	18	-0.29	-0.29	-0.29	-0.21	3.54	-0.21	-0.26	-112	-119	7

Table 4.55: Test 25, Response data at target displacement peaks

Cycle #	Peak #	D_t [in]	D_{mE} [in]	D_{mW} [in]	D_b [in]	$\|D_b/D_{by}\|$ [in/in]	D_s [in]	D_{RB} [in]	P_{tot} [kips]	P_b [kips]	V_{RB} [kips]
1	1	0.29	0.29	0.29	0.24	3.98	0.24	0.26	151	126	25
	2	-0.77	-0.77	-0.77	-0.56	9.28	-0.56	-0.64	-135	-129	-6
2	3	1.26	1.26	1.26	1.21	20.09	1.21	1.24	175	131	44
	4	-1.76	-1.76	-1.76	-1.53	25.49	-1.53	-1.62	-149	-123	-26
3	5	2.26	2.26	2.26	2.21	36.80	2.21	2.25	187	125	62
	6	-2.75	-2.76	-2.75	-2.53	42.21	-2.53	-2.62	-162	-118	-44
4	7	3.00	3.00	3.00	2.95	49.21	2.95	3.01	196	117	79
	8	-3.00	-3.00	-3.00	-2.78	46.33	-2.78	-2.87	-170	-115	-55
5	9	3.00	3.00	3.00	2.95	49.17	2.95	3.00	191	113	78
	10	-3.00	-3.00	-3.00	-2.78	46.41	-2.78	-2.87	-167	-114	-53
6	11	3.00	3.00	3.00	2.95	49.23	2.95	3.01	190	112	78
	12	-3.00	-3.00	-3.00	-2.78	46.33	-2.78	-2.87	-164	-112	-52
7	13	2.75	2.76	2.75	2.71	45.16	2.71	2.76	183	111	72
	14	-2.26	-2.26	-2.26	-2.04	34.01	-2.04	-2.13	-141	-109	-32
8	15	1.76	1.76	1.76	1.71	28.56	1.71	1.75	167	115	52
	16	-1.26	-1.26	-1.26	-1.05	17.47	-1.05	-1.13	-129	-114	-15
9	17	0.77	0.77	0.77	0.72	12.08	0.72	0.75	152	117	34
	18	-0.29	-0.29	-0.29	-0.08	1.39	-0.08	-0.16	-107	-114	8

Table 4.56: Test 26, Response data at target displacement peaks

Cycle #	Peak #	D_t [in]	D_{mE} [in]	D_{mW} [in]	D_b [in]	$\|D_b/D_{by}\|$ [in/in]	D_s [in]	D_{RB} [in]	P_{tot} [kips]	P_b [kips]
1	1	0.29	0.28	0.28	0.24	3.95	0.24	0.26	158	131
	2	-0.77	-0.70	-0.71	-0.47	7.83	-0.47	-0.55	-142	-135
2	3	1.26	1.31	1.32	1.28	21.28	1.28	1.30	141	105
	4	-1.76	-1.68	-1.68	-1.45	24.14	-1.45	-1.54	-125	-101
3	5	2.26	2.28	2.25	2.23	37.23	2.23	2.27	156	94
	6	-2.75	-2.62	-2.71	-2.45	40.84	-2.45	-2.53	-131	-86
4	7	3.00	3.03	2.98	2.98	49.59	2.98	3.02	159	80
	8	-3.00	-2.82	-3.00	-2.70	45.01	-2.70	-2.78	-129	-78
5	9	3.00	3.04	2.96	2.98	49.71	2.98	3.02	153	75
	10	-3.00	-2.83	-3.01	-2.71	45.12	-2.71	-2.79	-125	-74
6	11	3.00	3.04	2.97	2.99	49.76	2.99	3.03	149	72
	12	-3.00	-2.82	-3.00	-2.71	45.15	-2.71	-2.79	-122	-72
7	13	2.75	2.80	2.73	2.75	45.82	2.75	2.78	144	72
	14	-2.26	-2.17	-2.19	-1.98	32.98	-1.98	-2.06	-100	-68
8	15	1.76	1.77	1.76	1.76	29.41	1.76	1.78	127	74
	16	-1.26	-1.17	-1.18	-0.98	16.30	-0.98	-1.06	-88	-72
9	17	0.77	0.78	0.78	0.78	13.03	0.78	0.79	115	79
	18	-0.29	-0.19	-0.19	0.00	0.01	0.00	-0.07	-75	-81

Table 4.57: Test 27, Response data at target displacement peaks

Cycle #	Peak #	D_t [in]	D_{mE} [in]	D_{mW} [in]	D_b [in]	$\lvert D_b/D_{by}\rvert$ [in/in]	D_s [in]	D_{RB} [in]	P_{tot} [kips]	P_b [kips]
1	1	0.29	0.28	0.28	0.19	3.23	0.19	0.21	172	142
	2	-0.77	-0.67	-0.70	-0.49	8.20	-0.49	-0.57	-158	-149
2	3	1.26	1.34	1.33	1.26	20.95	1.26	1.28	142	107
	4	-1.76	-1.66	-1.67	-1.47	24.57	-1.47	-1.56	-128	-104
3	5	2.26	2.29	2.26	2.21	36.89	2.21	2.24	163	102
	6	-2.75	-2.61	-2.70	-2.47	41.19	-2.47	-2.55	-138	-91
4	7	3.00	3.04	2.99	2.95	49.15	2.95	2.99	170	91
	8	-3.00	-2.80	-2.99	-2.72	45.33	-2.72	-2.80	-139	-87
5	9	3.00	3.05	2.97	2.95	49.13	2.95	2.99	165	87
	10	-3.00	-2.80	-2.99	-2.73	45.49	-2.73	-2.80	-135	-84
6	11	3.00	3.06	2.97	2.96	49.27	2.96	2.99	161	84
	12	-3.00	-2.80	-3.00	-2.73	45.50	-2.73	-2.80	-131	-81
7	13	2.75	2.82	2.73	2.72	45.35	2.72	2.75	153	82
	14	-2.26	-2.15	-2.17	-1.99	33.24	-1.99	-2.07	-108	-76
8	15	1.76	1.78	1.77	1.73	28.80	1.73	1.75	135	82
	16	-1.26	-1.15	-1.17	-1.00	16.60	-1.00	-1.07	-96	-80
9	17	0.77	0.80	0.78	0.75	12.47	0.75	0.75	122	88
	18	-0.29	-0.16	-0.17	-0.01	0.09	-0.01	-0.08	-86	-92

Table 4.58: Test 28, Response data at target displacement peaks

Cycle #	Peak #	D_t [in]	D_{mE} [in]	D_{mW} [in]	D_b [in]	$\lvert D_b/D_{by}\rvert$ [in/in]	D_s [in]	D_{RB} [in]	P_{tot} [kips]	P_b [kips]	V_{RB} [kips]
1	1	0.29	0.29	0.29	0.23	3.86	0.23	0.24	133	107	26
	2	-0.77	-0.77	-0.77	-0.60	9.92	-0.60	-0.67	-127	-119	-8
2	3	1.26	1.26	1.26	1.19	19.85	1.19	1.21	168	124	45
	4	-1.76	-1.76	-1.76	-1.56	26.04	-1.56	-1.66	-148	-121	-27
3	5	2.26	2.26	2.26	2.18	36.38	2.18	2.22	185	123	61
	6	-2.75	-2.76	-2.76	-2.56	42.75	-2.56	-2.65	-171	-123	-49
4	7	3.00	3.00	3.00	2.92	48.73	2.92	2.97	198	121	77
	8	-3.00	-3.01	-3.00	-2.80	46.75	-2.80	-2.90	-180	-124	-56
5	9	3.00	3.00	3.00	2.93	48.77	2.93	2.97	196	121	76
	10	-3.00	-3.00	-3.00	-2.81	46.81	-2.81	-2.90	-184	-125	-59
6	11	3.00	3.00	3.00	2.92	48.75	2.92	2.97	197	121	76
	12	-3.00	-3.00	-3.00	-2.80	46.73	-2.80	-2.90	-182	-124	-58
7	13	2.75	2.76	2.76	2.68	44.70	2.68	2.72	190	121	69
	14	-2.26	-2.26	-2.26	-2.07	34.46	-2.07	-2.15	-155	-121	-34
8	15	1.76	1.76	1.76	1.68	28.04	1.68	1.71	177	126	51
	16	-1.26	-1.26	-1.26	-1.07	17.77	-1.07	-1.16	-142	-125	-17
9	17	0.77	0.77	0.77	0.69	11.54	0.69	0.71	164	130	34
	18	-0.29	-0.29	-0.29	-0.10	1.67	-0.10	-0.18	-123	-128	5

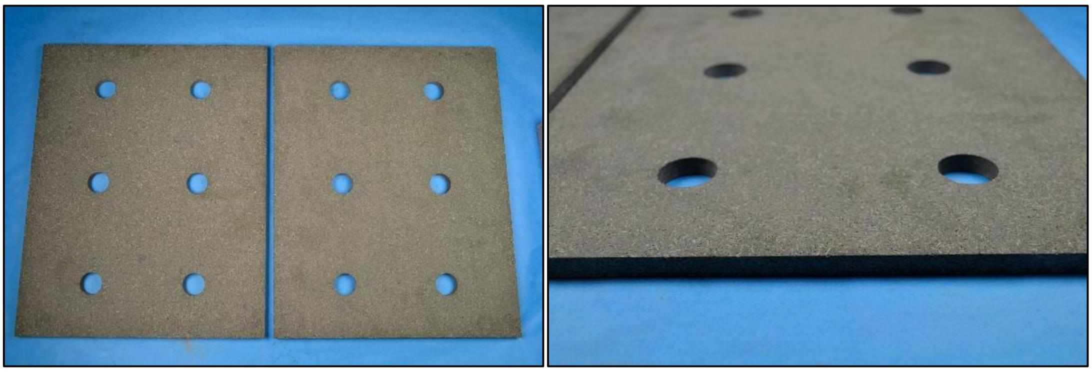

Figure 4.99: RF42 friction plates used in phase II-3

Figure 4.100: Condition of the internal steel plate surfaces at the beginning of Phase II-3

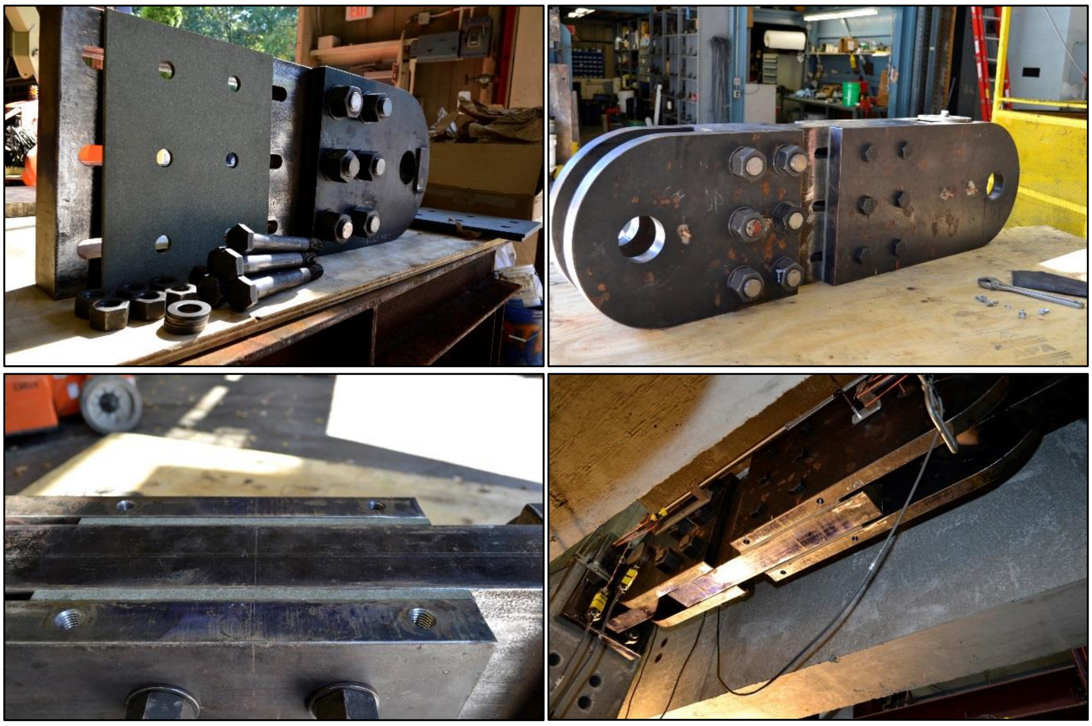

Figure 4.101: Components, assembly and installed FD in phase II-3

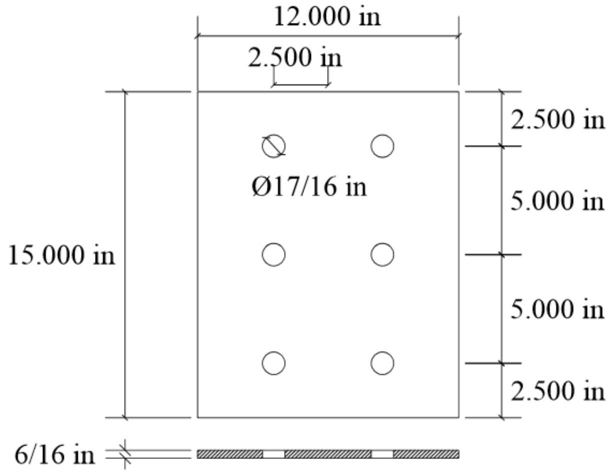

Figure 4.102: Dimensions of RF42 friction plates used in phase II-3

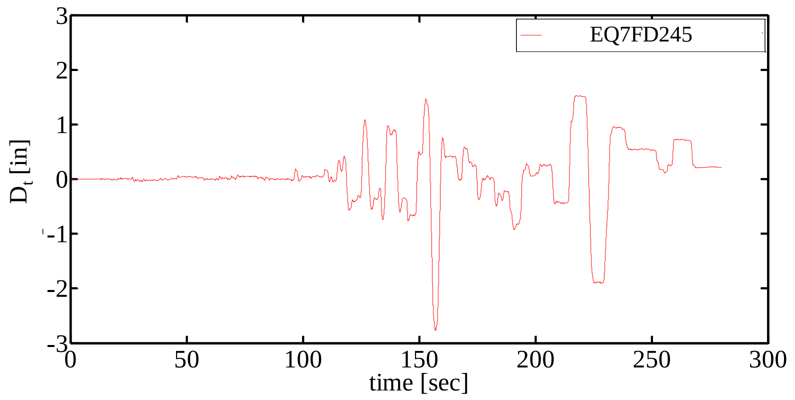

Figure 4.103: Target displacement used in Test 19 and 29 in phase II-3

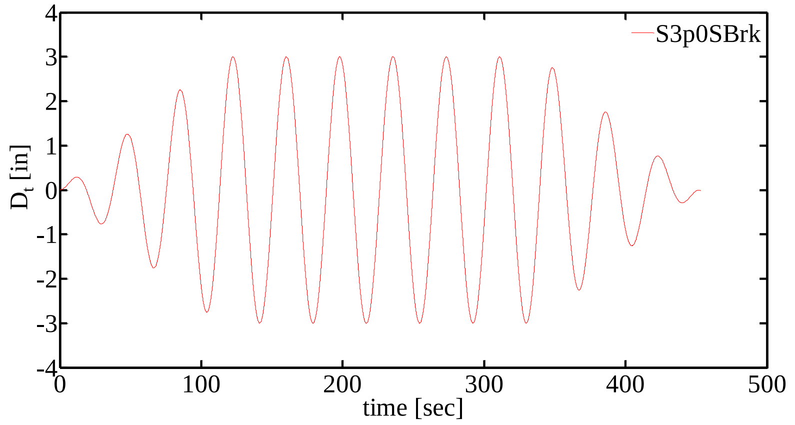

Figure 4.104: Target displacement used in Test 20 in phase II-3

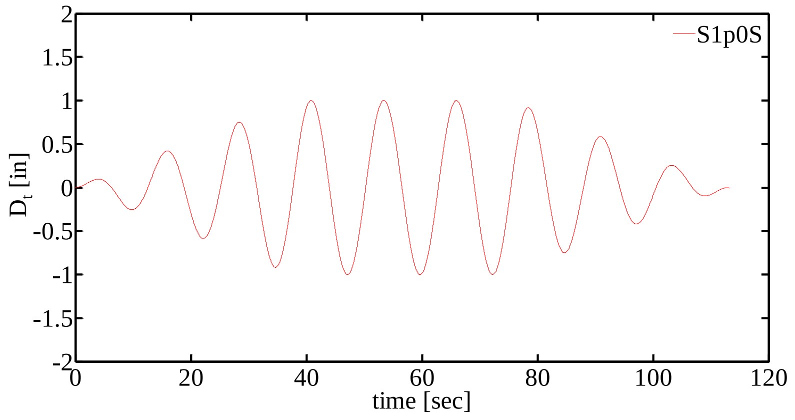

Figure 4.105: Target displacement used in Test 21 and 23 in phase II-3

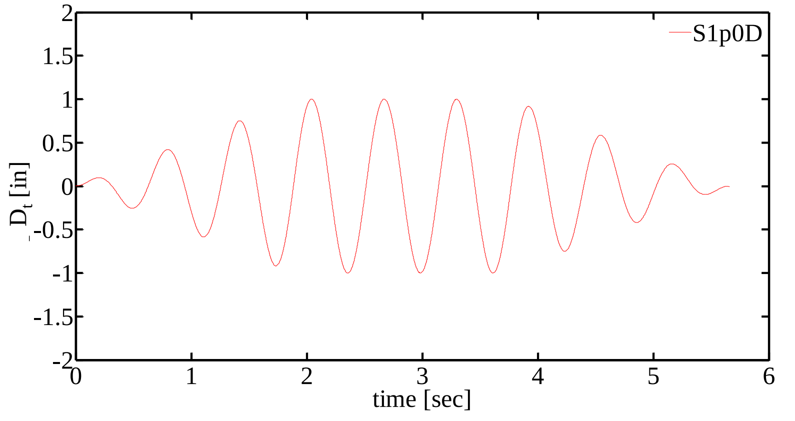

Figure 4.106: Target displacement used in Test 22 in phase II-3

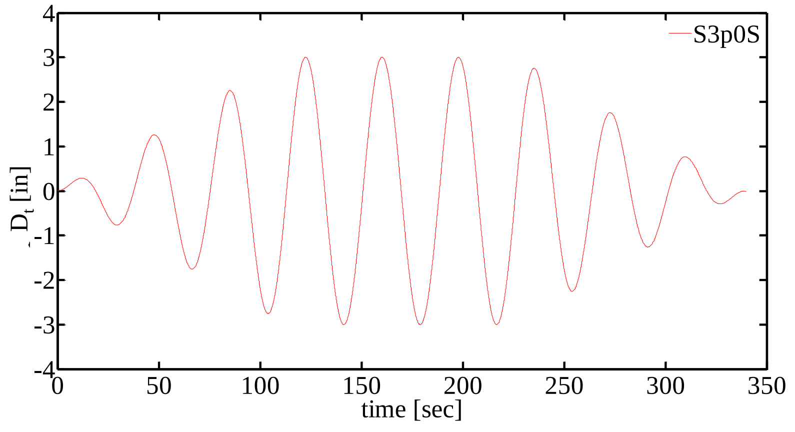

Figure 4.107: Target displacement used in Test 24, 25, and 28 in phase II-3

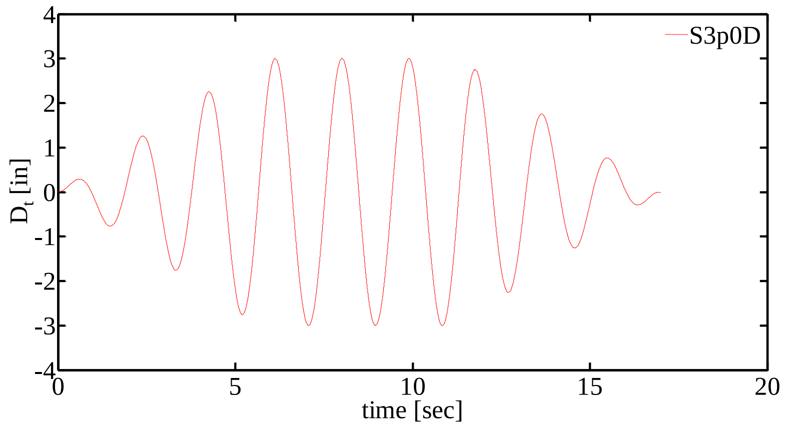

Figure 4.108: Target displacement used in Test 26 and 27 in phase II-3

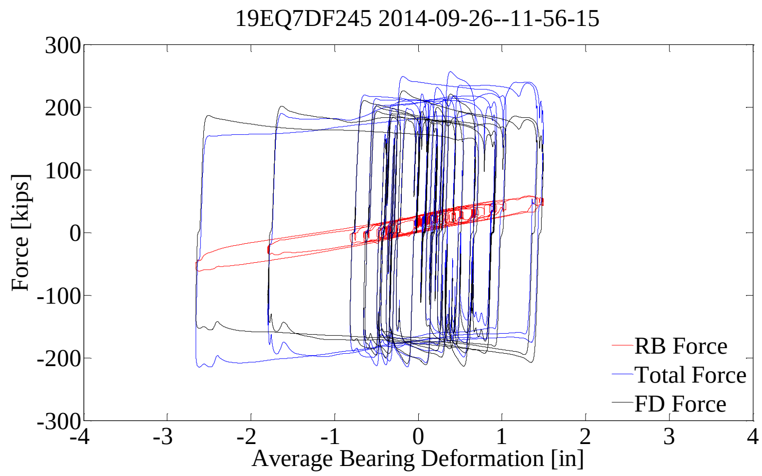

Figure 4.109: Test 19, Force – deformation plots for the deformable connection and its individual components in phase II [pg. 99]

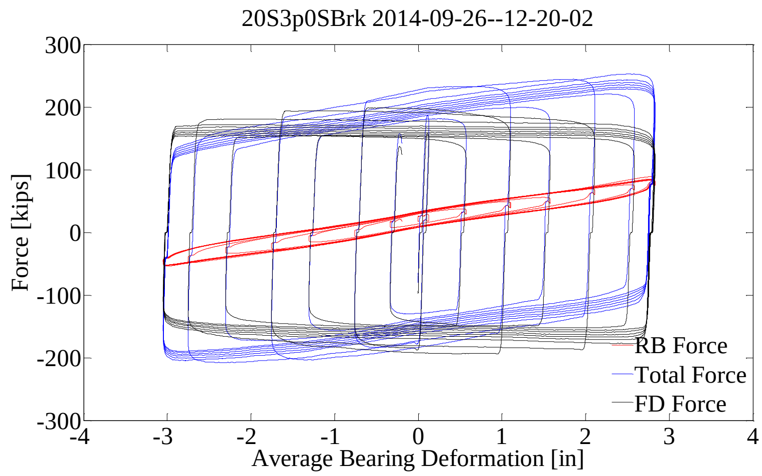

Figure 4.110: Test 20, Force – deformation plots for the deformable connection and its individual components in phase II [pg. 99; pg. 93]

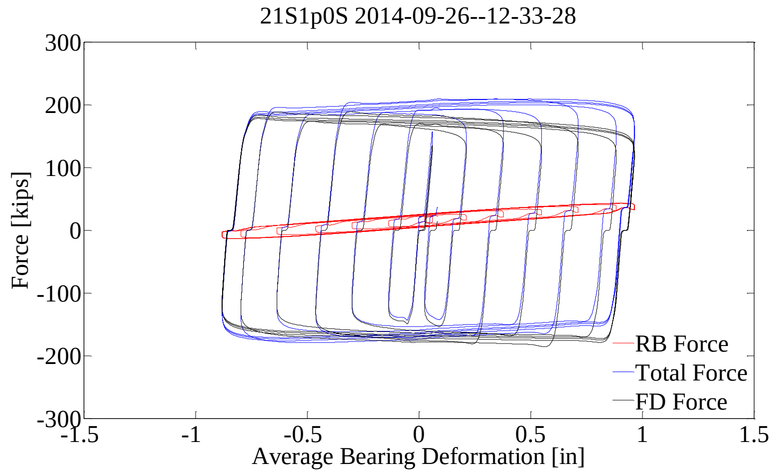

Figure 4.111: Test 21, Force – deformation plots for the deformable connection and its individual components in phase II [pg. 100; pg. 94]

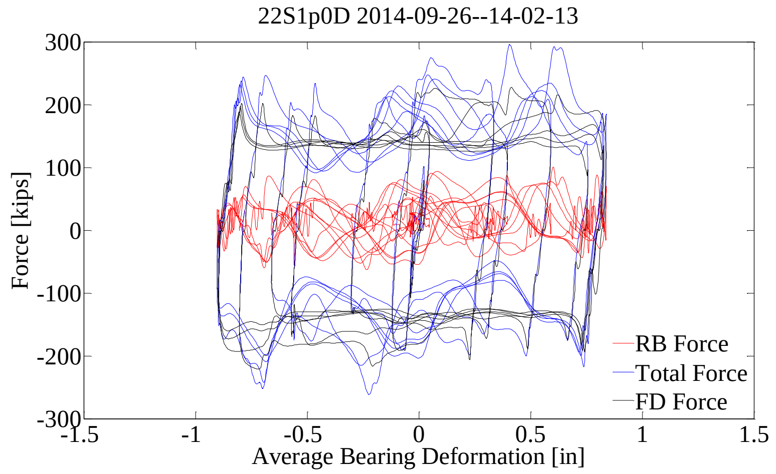

Figure 4.112: Test 22, Force – deformation plots for the deformable connection and its individual components in phase II [pg. 100; pg. 94]

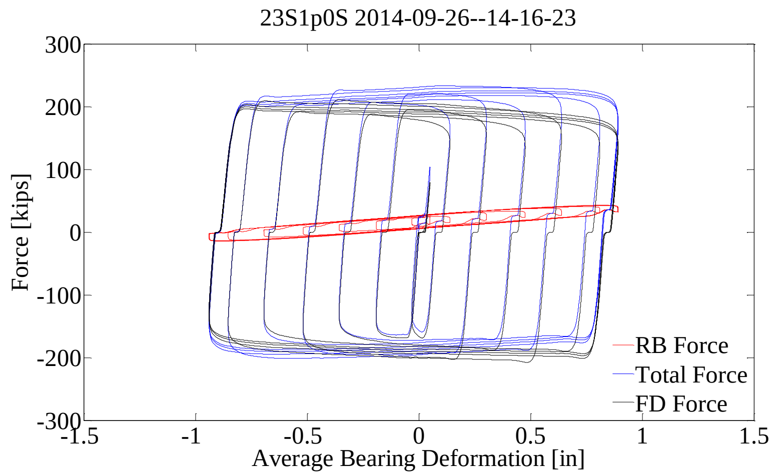

Figure 4.113: Test 23, Force – deformation plots for the deformable connection and its individual components in phase II [pg. 100; pg. 95]

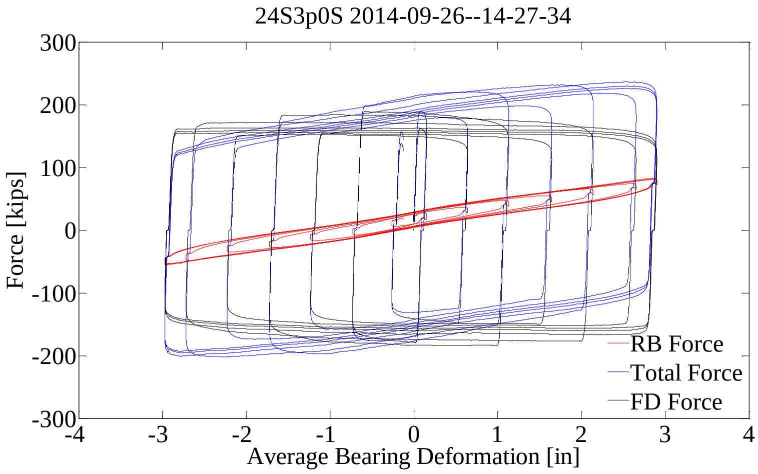

Figure 4.114: Test 24, Force – deformation plots for the deformable connection and its individual components in phase II [pg. 100; pg. 95]

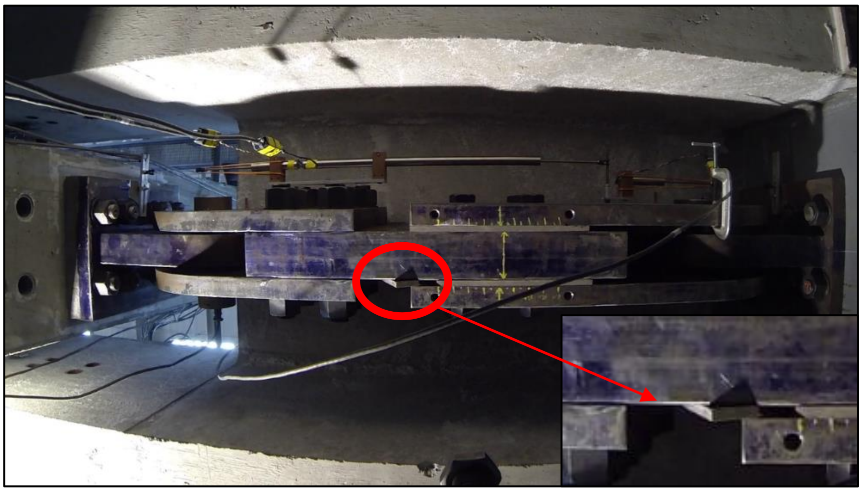

Figure 4.115: Test 24, Fracture of the West friction plate

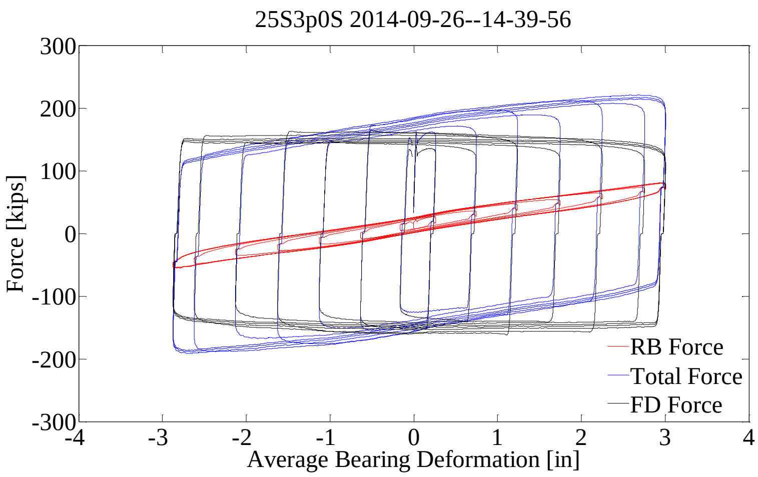

Figure 4.116: Test 25, Force – deformation plots for the deformable connection and its individual components in phase II [pg. 100; pg. 96]

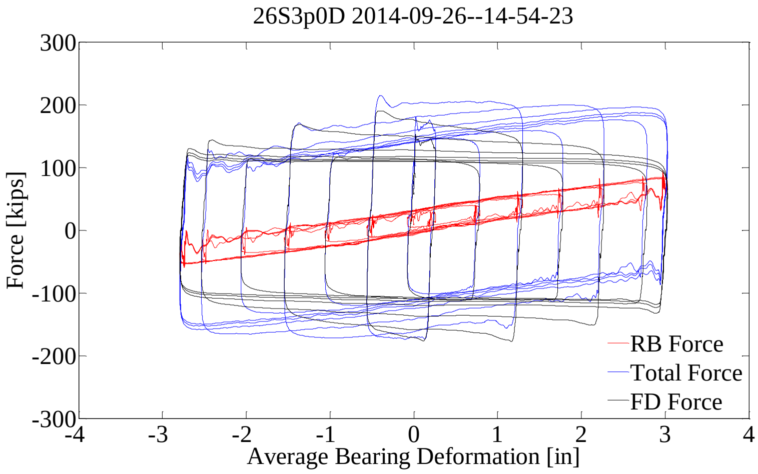

Figure 4.117: Test 26, Force – deformation plots for the deformable connection and its individual components in phase II [pg. 101; pg. 96]

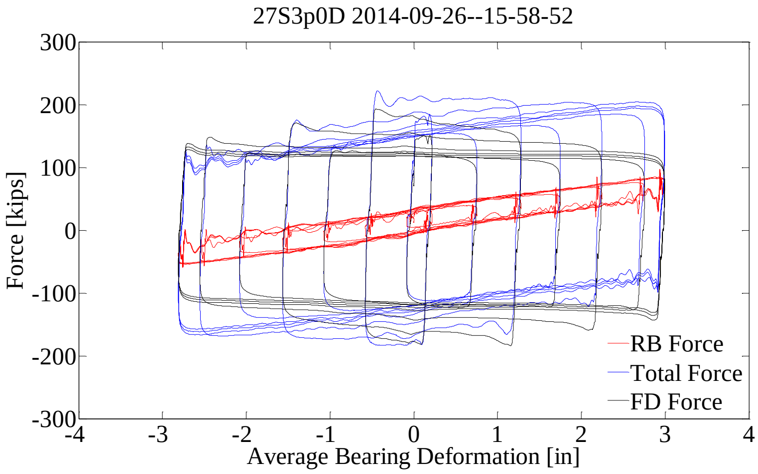

Figure 4.118: Test 27, Force – deformation plots for the deformable connection and its individual components in phase II [pg. 101; pg. 97]

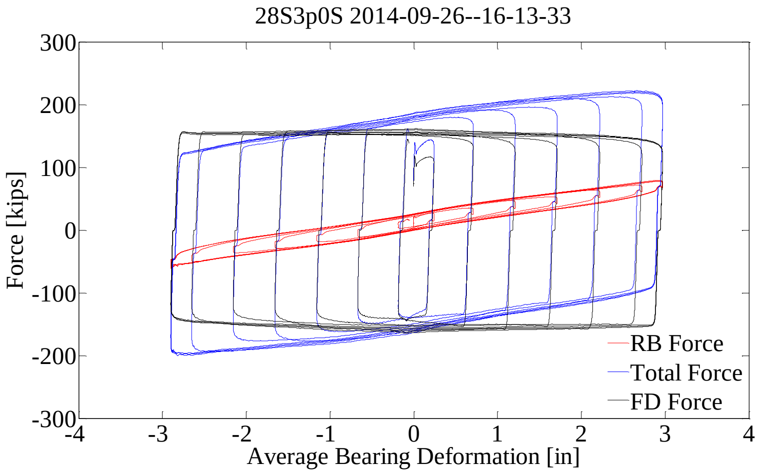

Figure 4.119: Test 28, Force – deformation plots for the deformable connection and its individual components in phase II [pg. 100; pg. 97]

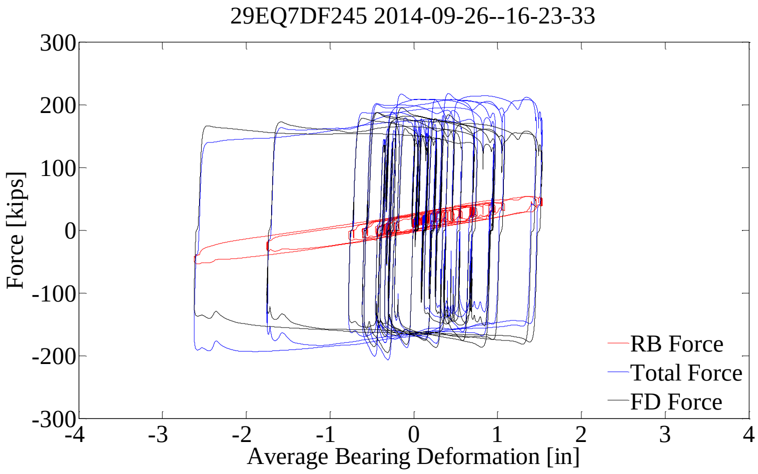

Figure 4.120: Test 29, Force – deformation plots for the deformable connection and its individual components in phase II [pg. 99]

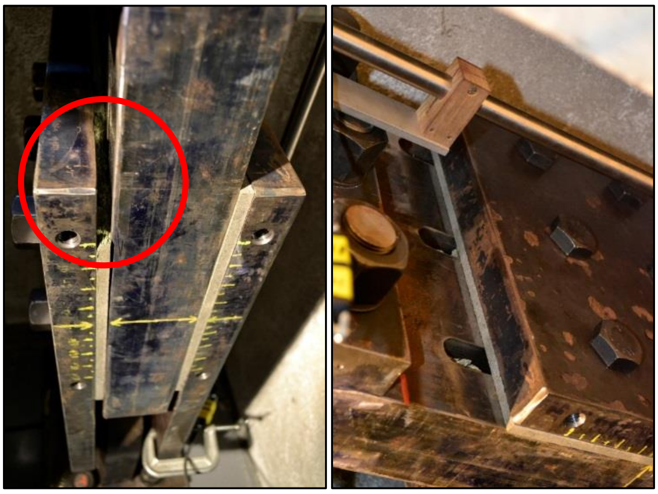

Figure 4.121: FD, close up to the friction plates and the slots of internal steel plate at the end of phase II-3

Figure 4.122: East RF42 friction plate with elongated bolt holes at the end of phase II-3

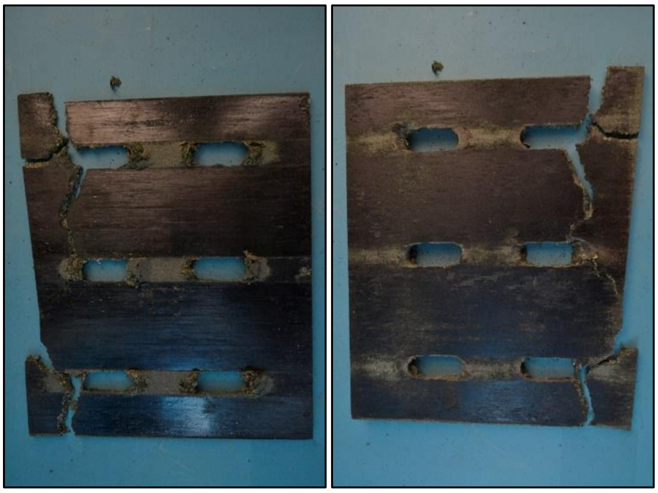

Figure 4.123: Fractured West RF42 friction plate at the end of phase II-3

Figure 4.124: North West rubber bearing and its rubber particles at the end of phase II-3

4.4.10 Phase II-4

In phase II-4, the material Gatke 398 [29] was used for the friction plates. It has greater tensile, compressive, and shear strength than the previously used materials RF42 [28] and AFT200 [27]. The friction plates are shown in Figure 4.125 and their dimensions in Figure 4.126. The FD with the Gatke 398 friction plates is shown in Figure 4.127.

Bushings and Belleville washers were not used in phase II-4. The thickness of the friction plates were, t_{fp}=6/16 inches. Six ASTM A325 bolts were used, n_b= 6 with diameter d_b = 1.0 inches. Each bolt was pretensioned at the beginning of phase II-4 to their "minimum pretension" force N_b = 51kips [30] using the hydraulic gun shown in Figure 4.74. The applied pressure was 2900 psi which is associated with a torque of 865 lb.-ft. The static friction coefficient reported by the manufacturer is within the range of 0.2 to 0.5 [29]. A value μ_s = 0.30 is assumed for the calculation of the expected static friction force $F_s = n_b n_s N_b \mu_s$ = 183.6 kips.

The RB used in the previous tests were used in phase II-4

The approximate temperature at the surface of the internal steel plate was measured at the beginning (T_i) and at the end (T_f) of each test using the infrared gun shown in Figure 4.75.

Table 4.59 shows the summary of the conditions of the East and West friction plates and the RB after each test of phase II-4. The notation *UC* indicates that the component was in an undamaged condition after the test. If damage was observed at the end of the test, the description of the damage is given.

The test sequence is shown in Table 4.60.

4.4.10.1 Test 30: 30EQ7FD245

Test 30 was successfully completed. The displacement target time history is presented in Figure 4.128. The force-deformation plots are shown in Figure 4.137. The high frequency oscillations of force are from problems with the actuators and are not the response of the components of the deformable connection. The initial and final temperatures were T_i = 72 ℉ and T_f = 78 ℉ respectively.

4.4.10.2 Test 31: 31S3p0SBrk

Test 31 was successfully completed. The displacement target time history is presented in Figure 4.129. The force-deformation plots are shown in Figure 4.138. In Table 4.61 the force and deformation data measured at the target displacement peaks are presented. The initial and final temperatures were T_i = 77℉ and T_f = 97℉ respectively.

4.4.10.3 Test 32: 32S3p0S

Test 32 was successfully completed. The displacement target time history is presented in Figure 4.130. The force-deformation plots are shown in Figure 4.139. In Table 4.62 the force and deformation data measured at the target displacement peaks are presented. The initial and final temperatures were T_i = 94℉ and T_f = 108℉ respectively.

4.4.10.4 Test 33: 33S3p0D

Test 33 was successfully completed. The displacement target time history is presented in Figure 4.131. The force-deformation plots are shown in Figure 4.140. In Table 4.63 the force and deformation data measured at the target displacement peaks are presented. The initial and final temperatures were T_i = 91℉ and T_f = 108℉ respectively.

4.4.10.5 Test 34: 34S3p0D

Test 34 was successfully completed. The displacement target time history is presented in Figure 4.131. The force-deformation plots are shown in Figure 4.141. In Table 4.64 the force and deformation data measured at target displacement peaks are presented. The initial and final temperatures were T_i = 105°F and T_f = 118°F respectively.

4.4.10.6 Test 35: 35S3p0S

Test 35 was successfully completed. The displacement target time history is presented in Figure 4.130. The force-deformation plots are shown in Figure 4.142. In Table 4.65 the force and deformation data measured at the target displacement peaks are presented. The initial and final temperatures were T_i = 115°F and T_f = 121°F respectively.

4.4.10.7 Test 36: 36S2p0S

Test 36 was successfully completed. The displacement target time history is presented in Figure 4.132. The force-deformation plots are shown in Figure 4.143. In Table 4.66 the force and deformation data measured at the target displacement peaks are presented. The initial and final temperatures were T_i = 119°F and T_f = 130°F respectively.

4.4.10.8 Test 37: 37S2p0D

Test 37 was successfully completed. The displacement target time history is presented in Figure 4.133. The force-deformation plots are shown in Figure 4.144. In Table 4.67 the force and deformation data measured at the target displacement peaks are presented. The initial and final temperatures were T_i = 127°F and T_f = 135°F respectively.

4.4.10.9 Test 38: 38S2p0S

Test 38 was successfully completed. The displacement target time history is presented in Figure 4.132. The force-deformation plots are shown in Figure 4.145. In Table 4.68 the force and deformation data measured at the target displacement peaks are presented. The initial and final temperatures were T_i = 84°F and T_f = 90°F respectively.

4.4.10.10 Test 39: 39S2p0D

Test 39 was successfully completed. The displacement target time history is presented in Figure 4.133. The force-deformation plots are shown in Figure 4.146. In Table 4.69 the force and deformation data measured at the target displacement peaks are presented. The initial and final temperatures were T_i = 91°F and T_f = 100°F respectively.

4.4.10.11 Test 40: 40EQ7FD245

Test 40 was successfully completed. The displacement target time history is presented in Figure 4.128. The force-deformation plots are shown in Figure 4.147. The initial and final temperatures were T_i = 98°F and T_f = 100°F respectively.

4.4.10.12 Test 41: 41S1p0S

Test 41 was successfully completed. The displacement target time history is presented in Figure 4.134. The force-deformation plots are shown in Figure 4.148. In Table 4.70 the force and deformation data measured at the target displacement peaks are presented. The initial and final temperatures were T_i = 96°F and T_f = 98°F respectively.

4.4.10.13 Test 42: 42S1p0D

Test 41 was successfully completed. The displacement target time history is presented in Figure 4.135. The force-deformation plots are shown in Figure 4.149. In Table 4.71 the force and deformation data measured at the target displacement peaks are presented. The initial and final temperatures were T_i = 86°F and T_f = 90°F respectively.

4.4.10.14 Test 43: 43S0p5D

Test 43 was successfully completed. The displacement target time history is presented in Figure 4.136. The force-deformation plots are shown in Figure 4.150. In Table 4.72 the force and deformation data measured at the target displacement peaks are presented. The initial and final temperatures were T_i = 90°F and T_f = 90°F respectively.

4.4.10.15 Test 44: 44S1p0S

Test 7 was successfully completed. The displacement target time history is presented in Figure 4.134. The force-deformation plots are shown in Figure 4.151. In Figure 4.152 the FD and close up views to the friction plates. Figure 4.153 shows the Gatke 398 friction plates are show after the end of phase II-4 (picture to be taken). In Table 4.73 the force and deformation data measured at the target displacement peaks are presented. The initial and final temperatures were T_i = 90°F and T_f = 93°F respectively.

Table 4.59: Phase II-4 condition of components of deformable connection

Test	West FP	East FP	NE RB	NW RB	SE RB	SW RB
30	*UC	*UC	Torn rubber	Debonded rubber	Torn rubber	Torn rubber
31	UC	UC	Torn rubber	Debonded rubber	Torn rubber	Severely Torn
32	UC	UC	Torn rubber	Debonded rubber	Torn rubber	Severely Torn
33	UC	UC	Torn rubber	Debonded rubber	Torn rubber	Severely Torn
34	UC	UC	Torn rubber	Debonded rubber	Torn rubber	Severely Torn
35	UC	UC	Torn rubber	Debonded rubber	Torn rubber	Severely Torn
36	UC	UC	Torn rubber	Debonded rubber	Torn rubber	Severely Torn
37	UC	UC	Torn rubber	Debonded rubber	Torn rubber	Severely Torn
38	UC	UC	Torn rubber	Debonded rubber	Torn rubber	Severely Torn
39	UC	UC	Torn rubber	Debonded rubber	Torn rubber	Severely Torn
40	UC	UC	Torn rubber	Debonded rubber	Torn rubber	Severely Torn
41	UC	UC	Torn rubber	Debonded rubber	Torn rubber	Severely Torn
42	UC	UC	Torn rubber	Debonded rubber	Torn rubber	Severely Torn
43	UC	UC	Torn rubber	Debonded rubber	Torn rubber	Severely Torn
44	UC	UC	Torn rubber	Debonded rubber	Torn rubber	Severely Torn

**The components was at its initial condition at the beginning of the test*
UC: Undamaged Condition

Table 4.60: Phase II-4 testing sequence

Day	Test	Name	$D_{t,max}$ [in]	$V_{t,max}$ [in/sec]	f [Hz]	# Ramp up cycles	# Ramp down cycles	# Max. amplitude cycles
	30	30EQ7FD245	2.77	0.90	-	-	-	-
	31	31S3p0SBrk	3.00	0.50	0.03	3	3	6
	32	32S3p0S	3.00	0.50	0.03	3	3	3
	33	33S3p0D	3.00	10.00	0.53	3	3	3
	34	34S3p0D	3.00	10.00	0.53	3	3	3
	35	35S3p0S	3.00	0.50	0.03	3	3	3
	36	36S2p0S	2.00	0.50	0.04	3	3	3
09-30-2014	37	37S2p0D	2.00	10.00	1.26	3	3	3
	38	38S2p0S	2.00	0.50	0.04	3	3	3
	39	39S2p0D	2.00	10.00	1.26	3	3	3
	40	40EQ7FD245	2.77	0.90	-	-	-	-
	41	41S1p0S	1.00	0.50	0.08	3	3	3
	42	42S1p0D	1.00	10.00	1.59	3	3	3
	43	43S0p5D	0.50	10.00	3.18	3	3	3
	44	44S1p0S	1.00	0.50	0.08	3	3	3

Table 4.61: Test 31, Response data at target displacement peaks

Cycle #	Peak #	D_t [in]	D_{mE} [in]	D_{mW} [in]	D_b [in]	$\lvert D_b/D_{by}\rvert$ [in/in]	D_s [in]	D_{RB} [in]	P_{tot} [kips]	P_b [kips]	V_{RB} [kips]
1	1	0.29	0.29	0.29	0.07	1.09	0.03	0.11	174	144	30
	2	-0.77	-0.77	-0.77	-0.78	12.93	-0.78	-0.77	-176	-167	-10
2	3	1.26	1.26	1.26	1.04	17.28	1.00	1.08	223	169	54
	4	-1.76	-1.76	-1.76	-1.75	29.22	-1.76	-1.76	-198	-169	-29
3	5	2.26	2.25	2.26	2.04	33.93	2.00	2.08	229	163	66
	6	-2.75	-2.76	-2.76	-2.75	45.87	-2.76	-2.75	-200	-160	-39
4	7	3.00	3.00	3.00	2.78	46.39	2.75	2.84	248	165	83
	8	-3.00	-3.00	-3.00	-3.00	49.94	-3.00	-2.99	-217	-168	-49
5	9	3.00	3.00	3.00	2.78	46.37	2.75	2.83	244	165	79
	10	-3.00	-3.00	-3.00	-3.00	49.99	-3.00	-2.99	-222	-172	-50
6	11	3.00	3.00	3.00	2.78	46.29	2.75	2.83	263	177	86
	12	-3.00	-3.00	-3.00	-3.00	49.95	-3.00	-2.99	-210	-167	-43
7	13	3.00	3.00	3.00	2.78	46.34	2.75	2.83	249	171	78
	14	-3.00	-3.00	-3.00	-2.99	49.86	-2.99	-2.99	-220	-173	-47
8	15	3.00	3.00	3.00	2.77	46.17	2.74	2.83	266	180	87
	16	-3.00	-3.00	-3.00	-2.99	49.91	-3.00	-2.99	-209	-167	-42
9	17	3.00	3.00	3.00	2.77	46.15	2.74	2.83	268	181	87
	18	-3.00	-3.00	-3.00	-3.00	49.95	-3.00	-2.99	-203	-163	-41
10	19	2.75	2.76	2.76	2.53	42.11	2.50	2.59	247	174	73
	20	-2.26	-2.26	-2.26	-2.25	37.57	-2.26	-2.25	-183	-160	-23
11	21	1.76	1.76	1.76	1.52	25.40	1.49	1.57	246	184	61
	22	-1.26	-1.26	-1.26	-1.25	20.86	-1.25	-1.25	-204	-186	-18
12	23	0.77	0.77	0.77	0.53	8.88	0.50	0.57	202	166	36
	24	-0.29	-0.29	-0.29	-0.28	4.72	-0.28	-0.28	-176	-181	5

Table 4.62: Test 32, Response data at target displacement peaks

Cycle #	Peak #	D_t [in]	D_{mE} [in]	D_{mW} [in]	D_b [in]	$\|D_b/D_{by}\|$ [in/in]	D_s [in]	D_{RB} [in]	P_{tot} [kips]	P_b [kips]	V_{RB} [kips]
1	1	0.29	0.29	0.29	0.20	3.42	0.18	0.22	194	168	26
	2	-0.77	-0.77	-0.77	-0.63	10.43	-0.62	-0.63	-157	-158	1
2	3	1.26	1.26	1.26	1.17	19.54	1.15	1.20	218	176	43
	4	-1.76	-1.76	-1.76	-1.60	26.66	-1.59	-1.62	-191	-170	-21
3	5	2.26	2.26	2.26	2.17	36.13	2.15	2.20	257	187	69
	6	-2.75	-2.76	-2.76	-2.60	43.40	-2.60	-2.62	-219	-176	-43
4	7	3.00	3.00	3.00	2.91	48.50	2.89	2.95	267	182	85
	8	-3.00	-3.00	-3.00	-2.85	47.56	-2.85	-2.87	-220	-173	-47
5	9	3.00	3.00	3.00	2.91	48.51	2.89	2.95	271	187	85
	10	-3.00	-3.00	-3.00	-2.84	47.41	-2.84	-2.86	-235	-182	-53
6	11	3.00	3.00	3.00	2.91	48.53	2.89	2.95	252	176	77
	12	-3.00	-3.00	-3.00	-2.85	47.47	-2.84	-2.86	-230	-177	-52
7	13	2.75	2.75	2.75	2.67	44.46	2.65	2.71	241	169	72
	14	-2.26	-2.26	-2.26	-2.10	35.07	-2.10	-2.12	-185	-161	-25
8	15	1.76	1.76	1.75	1.67	27.89	1.65	1.70	226	171	55
	16	-1.26	-1.26	-1.26	-1.10	18.41	-1.09	-1.12	-200	-181	-19
9	17	0.77	0.77	0.77	0.68	11.26	0.65	0.70	222	179	42
	18	-0.29	-0.30	-0.30	-0.14	2.35	-0.13	-0.16	-170	-175	4

Table 4.63: Test 33, Response data at target displacement peaks

Cycle #	Peak #	D_t [in]	D_{mE} [in]	D_{mW} [in]	D_b [in]	$\|D_b/D_{by}\|$ [in/in]	D_s [in]	D_{RB} [in]	P_{tot} [kips]	P_b [kips]
1	1	0.29	0.29	0.28	0.24	3.96	0.23	0.23	208	180
	2	-0.77	-0.71	-0.74	-0.52	8.72	-0.50	-0.56	-180	-173
2	3	1.26	1.32	1.30	1.29	21.49	1.28	1.28	198	160
	4	-1.76	-1.65	-1.67	-1.45	24.18	-1.42	-1.50	-180	-160
3	5	2.26	2.27	2.25	2.25	37.43	2.24	2.25	215	153
	6	-2.75	-2.63	-2.66	-2.45	40.86	-2.42	-2.49	-186	-144
4	7	3.00	3.01	2.97	2.98	49.62	2.98	2.98	224	145
	8	-3.00	-2.87	-2.91	-2.69	44.89	-2.67	-2.73	-186	-139
5	9	3.00	3.01	2.97	2.97	49.50	2.97	2.98	223	145
	10	-3.00	-2.86	-2.91	-2.70	44.93	-2.67	-2.73	-185	-139
6	11	3.00	3.01	2.97	2.96	49.39	2.97	2.97	227	148
	12	-3.00	-2.86	-2.91	-2.69	44.89	-2.66	-2.73	-188	-143
7	13	2.75	2.76	2.73	2.72	45.31	2.73	2.73	215	145
	14	-2.26	-2.14	-2.15	-1.95	32.55	-1.92	-1.99	-170	-140
8	15	1.76	1.76	1.75	1.72	28.70	1.73	1.73	196	144
	16	-1.26	-1.14	-1.15	-0.96	15.94	-0.92	-0.99	-149	-139
9	17	0.77	0.78	0.76	0.74	12.34	0.75	0.74	179	144
	18	-0.29	-0.15	-0.16	0.04	0.61	0.08	0.00	-137	-143

Table 4.64: Test 34, Response data at target displacement peaks

Cycle #	Peak #	D_t [in]	D_{mE} [in]	D_{mW} [in]	D_b [in]	$\lvert D_b/D_{by}\rvert$ [in/in]	D_s [in]	D_{RB} [in]	P_{tot} [kips]	P_b [kips]
1	1	0.29	0.28	0.28	0.16	2.65	0.15	0.16	197	166
	2	-0.77	-0.72	-0.73	-0.60	9.97	-0.57	-0.64	-168	-159
2	3	1.26	1.31	1.30	1.20	20.02	1.19	1.21	189	152
	4	-1.76	-1.66	-1.67	-1.53	25.46	-1.50	-1.58	-176	-155
3	5	2.26	2.26	2.25	2.16	36.08	2.16	2.17	217	155
	6	-2.75	-2.64	-2.66	-2.52	42.03	-2.50	-2.56	-189	-147
4	7	3.00	2.99	2.98	2.89	48.20	2.89	2.91	230	152
	8	-3.00	-2.88	-2.91	-2.77	46.16	-2.75	-2.80	-188	-142
5	9	3.00	2.99	2.97	2.88	48.07	2.88	2.90	230	152
	10	-3.00	-2.88	-2.91	-2.77	46.21	-2.75	-2.81	-189	-143
6	11	3.00	2.99	2.96	2.88	48.04	2.88	2.90	229	152
	12	-3.00	-2.88	-2.91	-2.77	46.20	-2.74	-2.80	-190	-144
7	13	2.75	2.75	2.73	2.64	44.00	2.64	2.66	218	149
	14	-2.26	-2.15	-2.15	-2.02	33.73	-1.99	-2.06	-173	-144
8	15	1.76	1.74	1.75	1.64	27.30	1.64	1.65	202	149
	16	-1.26	-1.15	-1.15	-1.03	17.18	-1.00	-1.07	-152	-141
9	17	0.77	0.76	0.76	0.66	10.96	0.66	0.66	186	149
	18	-0.29	-0.16	-0.16	-0.04	0.63	0.00	-0.08	-140	-146

Table 4.65: Test 35, Response data at target displacement peaks

Cycle #	Peak #	D_t [in]	D_{mE} [in]	D_{mW} [in]	D_b [in]	$\lvert D_b/D_{by}\rvert$ [in/in]	D_s [in]	D_{RB} [in]	P_{tot} [kips]	P_b [kips]	V_{RB} [kips]
1	1	0.29	0.29	0.29	0.18	2.99	0.17	0.18	178	158	20
	2	-0.77	-0.76	-0.77	-0.62	10.35	-0.62	-0.68	-174	-163	-11
2	3	1.26	1.26	1.26	1.17	19.56	1.14	1.16	211	168	43
	4	-1.76	-1.76	-1.76	-1.59	26.57	-1.60	-1.67	-201	-173	-28
3	5	2.26	2.26	2.26	2.17	36.18	2.14	2.16	234	175	59
	6	-2.75	-2.76	-2.76	-2.60	43.28	-2.60	-2.66	-210	-170	-40
4	7	3.00	3.00	3.00	2.92	48.62	2.89	2.91	261	182	79
	8	-3.00	-3.00	-3.00	-2.84	47.37	-2.84	-2.91	-229	-176	-52
5	9	3.00	3.00	3.00	2.91	48.58	2.89	2.92	255	179	75
	10	-3.00	-3.00	-3.00	-2.85	47.49	-2.85	-2.91	-222	-174	-48
6	11	3.00	3.00	3.00	2.91	48.56	2.88	2.91	269	186	83
	12	-3.00	-3.00	-3.00	-2.84	47.29	-2.84	-2.90	-235	-181	-54
7	13	2.75	2.76	2.76	2.67	44.56	2.64	2.67	243	176	68
	14	-2.26	-2.26	-2.26	-2.09	34.85	-2.09	-2.16	-211	-176	-35
8	15	1.76	1.76	1.76	1.67	27.91	1.64	1.66	221	173	48
	16	-1.26	-1.27	-1.27	-1.10	18.38	-1.10	-1.17	-183	-171	-12
9	17	0.77	0.77	0.76	0.68	11.38	0.65	0.66	204	167	37
	18	-0.29	-0.29	-0.29	-0.13	2.20	-0.13	-0.19	-155	-159	3

Table 4.66: Test 36, Response data at target displacement peaks

Cycle #	Peak #	D_t [in]	D_{mE} [in]	D_{mW} [in]	D_b [in]	$\|D_b/D_{by}\|$ [in/in]	D_s [in]	D_{RB} [in]	P_{tot} [kips]	P_b [kips]	V_{RB} [kips]
1	1	0.19	0.19	0.19	0.17	2.79	0.16	0.16	183	166	18
	2	-0.51	-0.51	-0.51	-0.30	4.97	-0.26	-0.34	-156	-161	6
2	3	0.84	0.84	0.84	0.82	13.64	0.81	0.81	212	175	37
	4	-1.17	-1.17	-1.17	-0.95	15.79	-0.92	-0.99	-185	-174	-11
3	5	1.50	1.50	1.50	1.47	24.58	1.47	1.48	232	179	52
	6	-1.84	-1.84	-1.84	-1.61	26.83	-1.58	-1.66	-192	-171	-21
4	7	2.00	2.01	2.00	1.98	33.00	1.98	1.99	233	178	55
	8	-2.00	-2.00	-2.00	-1.77	29.50	-1.74	-1.82	-202	-175	-27
5	9	2.00	2.01	2.00	1.98	33.07	1.98	1.99	227	175	52
	10	-2.00	-2.01	-2.01	-1.78	29.62	-1.75	-1.82	-189	-167	-22
6	11	2.00	2.00	2.00	1.98	32.94	1.97	1.98	225	173	52
	12	-2.00	-2.00	-2.00	-1.77	29.46	-1.74	-1.82	-215	-182	-33
7	13	1.84	1.84	1.84	1.82	30.28	1.81	1.82	220	171	49
	14	-1.50	-1.51	-1.50	-1.28	21.33	-1.25	-1.33	-180	-167	-13
8	15	1.17	1.17	1.17	1.14	19.02	1.14	1.14	226	178	48
	16	-0.84	-0.84	-0.84	-0.62	10.37	-0.59	-0.66	-163	-163	-1
9	17	0.51	0.51	0.51	0.49	8.16	0.48	0.48	183	159	23
	18	-0.19	-0.19	-0.19	0.03	0.55	0.07	-0.01	-169	-172	3

Table 4.67: Test 37, Response data at target displacement peaks

Cycle #	Peak #	D_t [in]	D_{mE} [in]	D_{mW} [in]	D_b [in]	$\|D_b/D_{by}\|$ [in/in]	D_s [in]	D_{RB} [in]	P_{tot} [kips]	P_b [kips]
1	1	0.19	0.17	0.17	0.08	1.39	0.08	0.08	188	160
	2	-0.51	-0.45	-0.47	-0.30	4.95	-0.27	-0.35	-176	-176
2	3	0.84	0.93	0.92	0.85	14.19	0.84	0.84	177	148
	4	-1.17	-1.05	-1.06	-0.88	14.68	-0.85	-0.94	-168	-160
3	5	1.50	1.54	1.53	1.46	24.35	1.45	1.46	199	152
	6	-1.84	-1.70	-1.71	-1.55	25.77	-1.52	-1.60	-165	-146
4	7	2.00	2.02	2.01	1.95	32.43	1.94	1.95	192	141
	8	-2.00	-1.87	-1.87	-1.71	28.52	-1.68	-1.76	-152	-134
5	9	2.00	2.01	2.01	1.94	32.35	1.94	1.94	191	138
	10	-2.00	-1.86	-1.87	-1.71	28.50	-1.68	-1.76	-156	-133
6	11	2.00	2.01	2.01	1.94	32.31	1.94	1.95	191	136
	12	-2.00	-1.86	-1.87	-1.71	28.52	-1.68	-1.76	-155	-133
7	13	1.84	1.84	1.85	1.77	29.55	1.78	1.78	187	137
	14	-1.50	-1.37	-1.37	-1.22	20.41	-1.19	-1.27	-141	-130
8	15	1.17	1.18	1.17	1.10	18.35	1.10	1.10	181	138
	16	-0.84	-0.68	-0.70	-0.56	9.31	-0.52	-0.60	-143	-137
9	17	0.51	0.52	0.52	0.45	7.42	0.45	0.44	172	141
	18	-0.19	-0.05	-0.05	0.09	1.52	0.13	0.05	-120	-136

Table 4.68: Test 38, Response data at target displacement peaks

Cycle #	Peak #	D_t [in]	D_{mE} [in]	D_{mW} [in]	D_b [in]	$\lvert D_b/D_{by}\rvert$ [in/in]	D_s [in]	D_{RB} [in]	P_{tot} [kips]	P_b [kips]	V_{RB} [kips]
1	1	0.19	0.19	0.19	0.04	0.70	0.03	0.06	165	137	28
	2	-0.51	-0.51	-0.51	-0.42	7.00	-0.42	-0.46	-148	-154	6
2	3	0.84	0.84	0.84	0.70	11.71	0.67	0.70	206	165	41
	4	-1.17	-1.18	-1.18	-1.07	17.89	-1.07	-1.12	-179	-164	-15
3	5	1.50	1.50	1.50	1.36	22.65	1.33	1.37	219	169	50
	6	-1.84	-1.84	-1.84	-1.73	28.84	-1.73	-1.78	-196	-170	-26
4	7	2.00	2.00	2.00	1.85	30.92	1.82	1.87	240	178	63
	8	-2.00	-2.00	-2.00	-1.89	31.53	-1.89	-1.94	-209	-177	-32
5	9	2.00	2.00	2.00	1.86	30.95	1.83	1.86	245	183	63
	10	-2.00	-2.00	-2.00	-1.89	31.45	-1.89	-1.94	-217	-184	-33
6	11	2.00	2.00	2.00	1.85	30.84	1.82	1.86	251	188	63
	12	-2.00	-2.00	-2.00	-1.89	31.44	-1.89	-1.94	-221	-188	-33
7	13	1.84	1.84	1.84	1.69	28.17	1.66	1.70	245	188	57
	14	-1.50	-1.51	-1.50	-1.39	23.22	-1.39	-1.44	-190	-176	-14
8	15	1.17	1.17	1.17	1.02	16.95	0.98	1.02	217	179	38
	16	-0.84	-0.84	-0.84	-0.74	12.36	-0.74	-0.78	-169	-169	0
9	17	0.51	0.51	0.51	0.36	5.96	0.32	0.35	213	182	32
	18	-0.19	-0.19	-0.19	-0.08	1.37	-0.08	-0.13	-185	-188	3

Table 4.69: Test 39, Response data at target displacement peaks

Cycle #	Peak #	D_t [in]	D_{mE} [in]	D_{mW} [in]	D_b [in]	$\lvert D_b/D_{by}\rvert$ [in/in]	D_s [in]	D_{RB} [in]	P_{tot} [kips]	P_b [kips]
1	1	0.19	0.14	0.14	0.03	0.50	0.02	0.04	172	146
	2	-0.51	-0.53	-0.54	-0.39	6.53	-0.37	-0.44	-164	-169
2	3	0.84	0.87	0.86	0.76	12.64	0.74	0.75	195	168
	4	-1.17	-1.11	-1.11	-0.97	16.19	-0.94	-1.02	-172	-160
3	5	1.50	1.49	1.49	1.38	23.00	1.37	1.39	199	157
	6	-1.84	-1.76	-1.77	-1.63	27.09	-1.60	-1.68	-168	-147
4	7	2.00	1.96	1.96	1.86	30.95	1.85	1.87	203	151
	8	-2.00	-1.92	-1.93	-1.79	29.86	-1.76	-1.84	-157	-135
5	9	2.00	1.96	1.96	1.85	30.91	1.85	1.87	194	143
	10	-2.00	-1.92	-1.92	-1.79	29.90	-1.77	-1.84	-155	-132
6	11	2.00	1.96	1.96	1.86	30.98	1.86	1.87	193	139
	12	-2.00	-1.92	-1.93	-1.79	29.89	-1.76	-1.84	-156	-133
7	13	1.84	1.80	1.80	1.70	28.27	1.70	1.71	183	137
	14	-1.50	-1.42	-1.42	-1.30	21.60	-1.26	-1.33	-148	-132
8	15	1.17	1.13	1.13	1.03	17.11	1.03	1.03	181	141
	16	-0.84	-0.74	-0.76	-0.64	10.65	-0.60	-0.67	-143	-137
9	17	0.51	0.48	0.47	0.37	6.17	0.37	0.38	174	142
	18	-0.19	-0.09	-0.09	0.03	0.58	0.07	-0.01	-131	-143

Table 4.70: Test 41, Response data at target displacement peaks

Cycle #	Peak #	D_t [in]	D_{mE} [in]	D_{mW} [in]	D_b [in]	$\|D_b/D_{by}\|$ [in/in]	D_s [in]	D_{RB} [in]	P_{tot} [kips]	P_b [kips]	V_{RB} [kips]
1	1	0.10	0.10	0.10	0.02	0.31	0.00	0.05	28	1	27
	2	-0.26	-0.25	-0.25	-0.24	4.04	-0.24	-0.24	-179	-180	1
2	3	0.42	0.42	0.42	0.18	2.97	0.14	0.22	213	178	35
	4	-0.59	-0.59	-0.59	-0.58	9.73	-0.58	-0.58	-162	-163	1
3	5	0.75	0.75	0.75	0.51	8.52	0.47	0.55	217	175	42
	6	-0.92	-0.92	-0.92	-0.92	15.29	-0.92	-0.92	-180	-170	-10
4	7	1.00	1.00	1.00	0.76	12.66	0.72	0.80	214	173	41
	8	-1.00	-1.00	-1.00	-0.99	16.54	-0.99	-0.99	-183	-173	-10
5	9	1.00	1.00	1.00	0.76	12.68	0.72	0.80	222	177	45
	10	-1.00	-1.01	-1.01	-1.00	16.62	-1.00	-1.00	-186	-176	-9
6	11	1.00	1.00	1.00	0.76	12.68	0.72	0.80	218	174	43
	12	-1.00	-1.00	-1.00	-0.99	16.56	-1.00	-1.00	-187	-178	-10
7	13	0.92	0.92	0.92	0.68	11.29	0.64	0.71	227	181	46
	14	-0.75	-0.75	-0.75	-0.74	12.41	-0.75	-0.75	-181	-178	-3
8	15	0.59	0.59	0.59	0.35	5.82	0.31	0.38	213	181	32
	16	-0.42	-0.42	-0.42	-0.40	6.73	-0.40	-0.41	-170	-176	6
9	17	0.26	0.25	0.26	0.01	0.14	-0.03	0.04	214	184	29
	18	-0.10	-0.10	-0.10	-0.08	1.30	-0.08	-0.09	-156	-165	9

Table 4.71: Test 42, Response data at target displacement peaks

Cycle #	Peak #	D_t [in]	D_{mE} [in]	D_{mW} [in]	D_b [in]	$\|D_b/D_{by}\|$ [in/in]	D_s [in]	D_{RB} [in]	P_{tot} [kips]	P_b [kips]
1	1	0.10	0.05	0.06	0.01	0.10	0.00	0.04	26	1
	2	-0.26	-0.20	-0.21	-0.15	2.54	-0.15	-0.16	-190	-197
2	3	0.42	0.37	0.39	0.14	2.41	0.11	0.19	209	190
	4	-0.59	-0.72	-0.71	-0.69	11.45	-0.68	-0.68	-152	-156
3	5	0.75	0.69	0.69	0.48	8.00	0.46	0.52	160	140
	6	-0.92	-0.97	-0.96	-0.94	15.63	-0.92	-0.93	-131	-134
4	7	1.00	0.91	0.90	0.69	11.51	0.67	0.74	157	128
	8	-1.00	-1.02	-1.02	-1.00	16.64	-0.98	-0.99	-132	-134
5	9	1.00	0.89	0.88	0.67	11.12	0.65	0.72	164	137
	10	-1.00	-1.01	-1.02	-1.00	16.72	-0.99	-0.99	-119	-123
6	11	1.00	0.89	0.86	0.66	11.00	0.64	0.71	168	147
	12	-1.00	-1.00	-1.03	-1.01	16.77	-0.99	-0.99	-119	-123
7	13	0.92	0.82	0.78	0.58	9.63	0.56	0.63	162	134
	14	-0.75	-0.73	-0.78	-0.75	12.54	-0.73	-0.73	-117	-125
8	15	0.59	0.48	0.45	0.24	4.04	0.23	0.30	156	134
	16	-0.42	-0.38	-0.43	-0.39	6.52	-0.37	-0.38	-134	-142
9	17	0.26	0.15	0.10	-0.10	1.66	-0.11	-0.04	158	144
	18	-0.10	-0.09	-0.12	-0.14	2.26	-0.12	-0.13	-69	-84

Table 4.72: Test 43, Response data at target displacement peaks

Cycle #	Peak #	D_t [in]	D_{mE} [in]	D_{mW} [in]	D_b [in]	$\|D_b/D_{by}\|$ [in/in]	D_s [in]	D_{RB} [in]	P_{tot} [kips]	P_b [kips]
1	1	0.05	0.03	0.03	0.01	0.11	0.00	0.02	49	27
	2	-0.13	-0.07	-0.08	-0.01	0.19	0.00	-0.04	-93	-101
2	3	0.21	0.16	0.16	0.03	0.44	0.00	0.05	136	129
	4	-0.29	-0.25	-0.27	-0.14	2.26	-0.12	-0.17	-170	-178
3	5	0.38	0.39	0.40	0.22	3.71	0.20	0.24	159	174
	6	-0.46	-0.52	-0.52	-0.41	6.85	-0.40	-0.43	-67	-85
4	7	0.50	0.50	0.49	0.34	5.59	0.32	0.35	129	142
	8	-0.50	-0.48	-0.48	-0.37	6.22	-0.36	-0.40	-112	-143
5	9	0.50	0.48	0.48	0.31	5.16	0.29	0.33	133	138
	10	-0.50	-0.46	-0.46	-0.36	5.95	-0.34	-0.37	-117	-147
6	11	0.50	0.47	0.46	0.30	4.98	0.28	0.32	135	134
	12	-0.50	-0.45	-0.45	-0.35	5.79	-0.33	-0.36	-117	-142
7	13	0.46	0.41	0.41	0.25	4.15	0.23	0.27	145	129
	14	-0.38	-0.32	-0.32	-0.23	3.84	-0.21	-0.24	-110	-116
8	15	0.29	0.24	0.24	0.08	1.30	0.06	0.10	144	139
	16	-0.21	-0.14	-0.14	-0.03	0.54	-0.01	-0.06	-131	-153
9	17	0.13	0.10	0.09	-0.01	0.14	-0.02	0.02	96	97
	18	-0.05	-0.03	-0.03	-0.04	0.68	-0.02	-0.04	-30	-41

Table 4.73: Test 44, Response data at target displacement peaks

Cycle #	Peak #	D_t [in]	D_{mE} [in]	D_{mW} [in]	D_b [in]	$\|D_b/D_{by}\|$ [in/in]	D_s [in]	D_{RB} [in]	P_{tot} [kips]	P_b [kips]	V_{RB} [kips]
1	1	0.10	0.10	0.10	0.02	0.32	0.00	0.04	120	97	23
	2	-0.26	-0.26	-0.26	-0.13	2.23	-0.12	-0.15	-182	-181	-1
2	3	0.42	0.42	0.42	0.29	4.83	0.26	0.31	200	175	25
	4	-0.59	-0.59	-0.59	-0.47	7.83	-0.46	-0.48	-174	-169	-6
3	5	0.75	0.75	0.75	0.63	10.45	0.60	0.65	208	171	37
	6	-0.92	-0.92	-0.92	-0.80	13.35	-0.79	-0.82	-181	-169	-11
4	7	1.00	1.00	1.00	0.87	14.55	0.85	0.90	213	172	41
	8	-1.00	-1.00	-1.00	-0.88	14.62	-0.87	-0.90	-178	-169	-9
5	9	1.00	1.00	1.00	0.88	14.59	0.85	0.90	214	172	42
	10	-1.00	-1.00	-1.00	-0.87	14.51	-0.86	-0.89	-201	-182	-18
6	11	1.00	1.00	1.00	0.87	14.48	0.84	0.89	222	177	45
	12	-1.00	-1.00	-1.00	-0.87	14.55	-0.86	-0.89	-192	-178	-14
7	13	0.92	0.92	0.92	0.79	13.10	0.76	0.81	216	179	37
	14	-0.75	-0.75	-0.75	-0.63	10.55	-0.62	-0.65	-198	-185	-13
8	15	0.59	0.59	0.59	0.45	7.57	0.43	0.48	202	176	26
	16	-0.42	-0.42	-0.42	-0.30	4.92	-0.28	-0.31	-163	-171	7
9	17	0.26	0.26	0.26	0.12	2.02	0.09	0.15	206	182	23
	18	-0.10	-0.10	-0.10	0.03	0.49	0.04	0.00	-123	-141	18

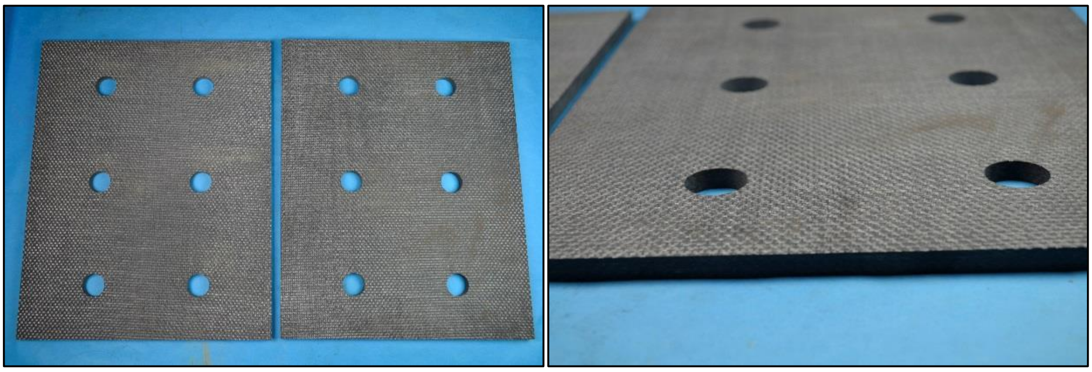

Figure 4.125: Gatke 398 friction plates used in phase II-4

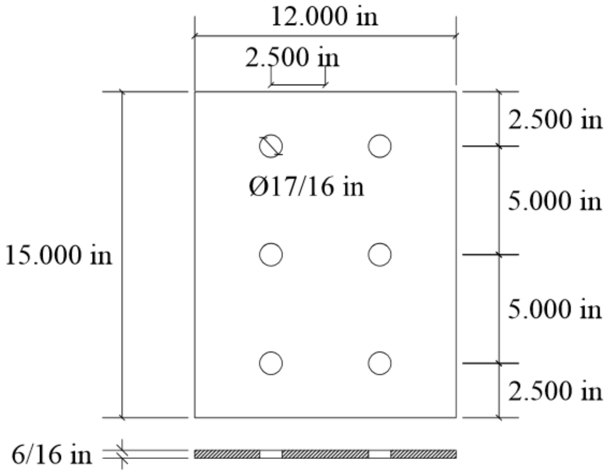

Figure 4.126: Dimensions of Gatke 398 friction plates used in phase II-4

Figure 4.127: Gatke 398 friction plates installed in FD in phase II-4

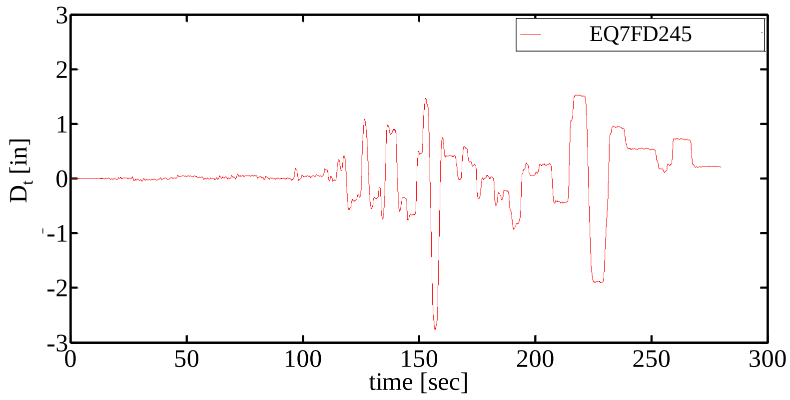

Figure 4.128: Target displacement used in Test 30 and 40 in phase II-4

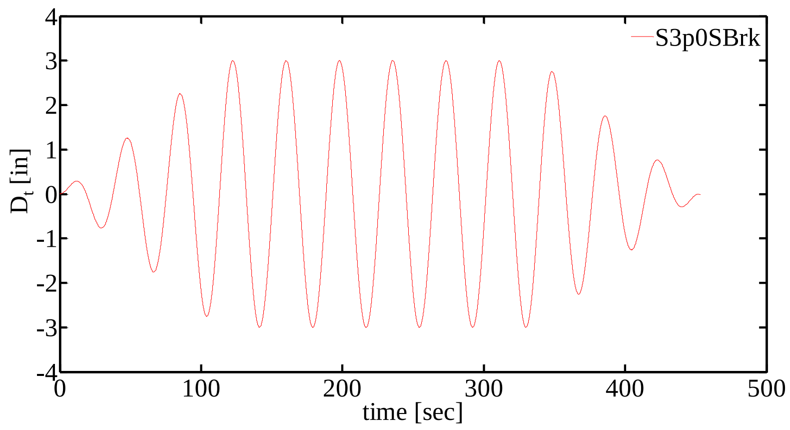

Figure 4.129: Target displacement used in Test 31 in phase II-4

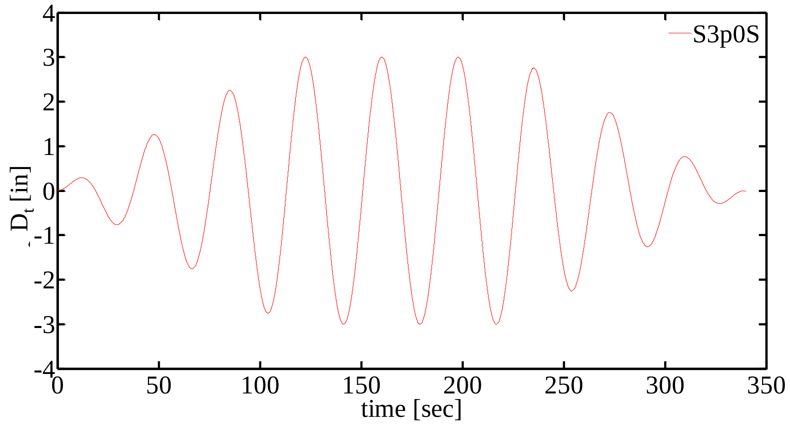

Figure 4.130: Target displacement used in Test 32 and 35 in phase II-4

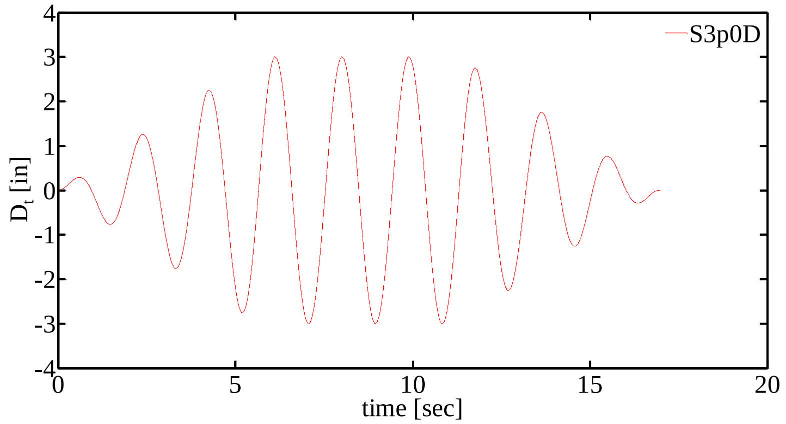

Figure 4.131: Target displacement used in Test 33 and 34 in phase II-4

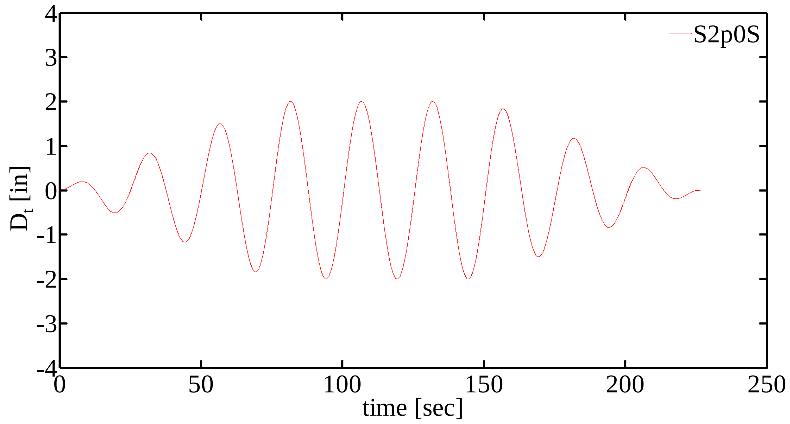

Figure 4.132: Target displacement used in Test 36 and 38 in phase II-4

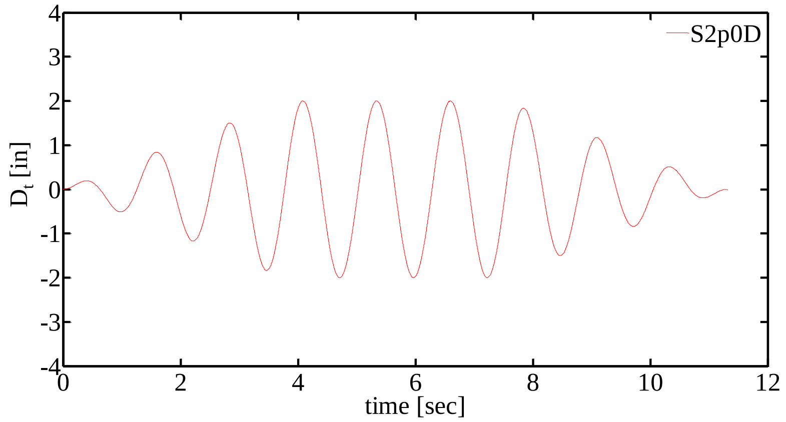

Figure 4.133: Target displacement used in Test 37 and 39 in phase II-4

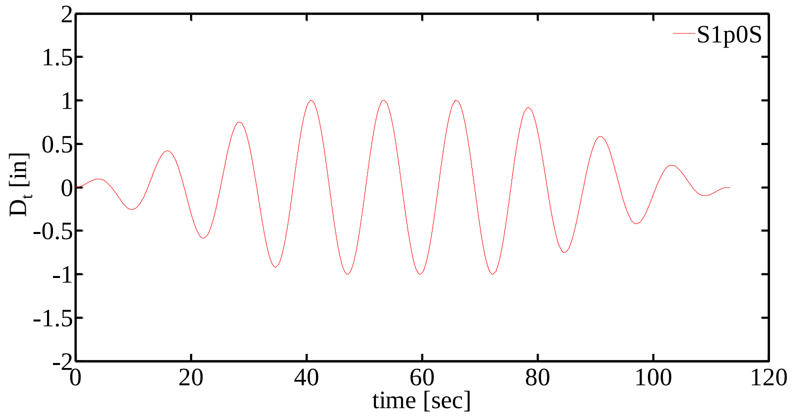

Figure 4.134: Target displacement used in Test 41 and 44 in phase II-4

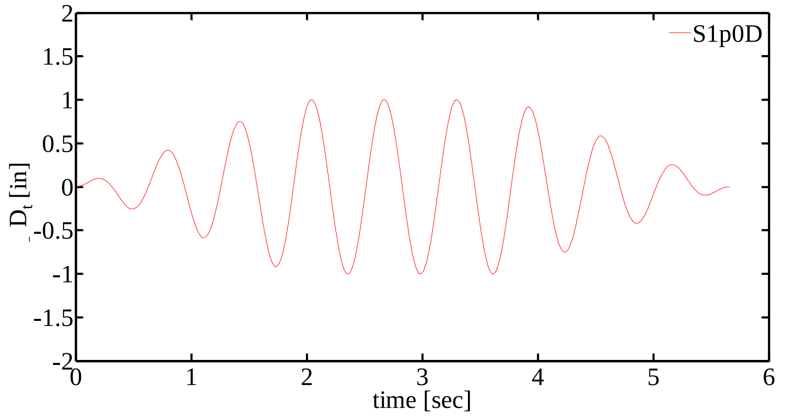

Figure 4.135: Target displacement used in Test 42 in phase II-4

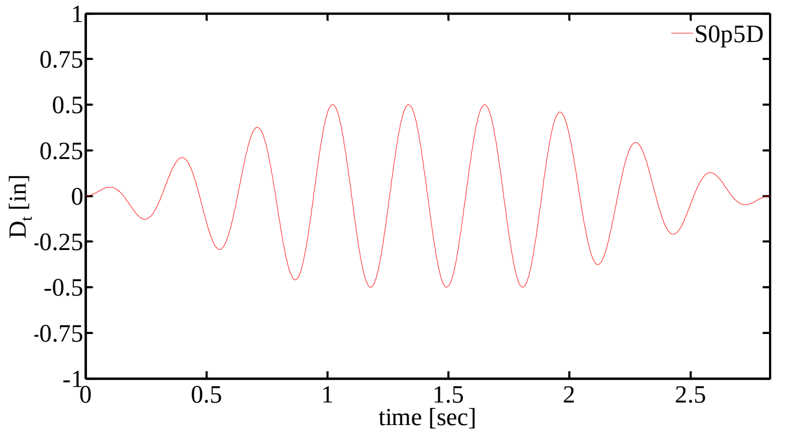

Figure 4.136: Target displacement used in test 43 in phase II-4

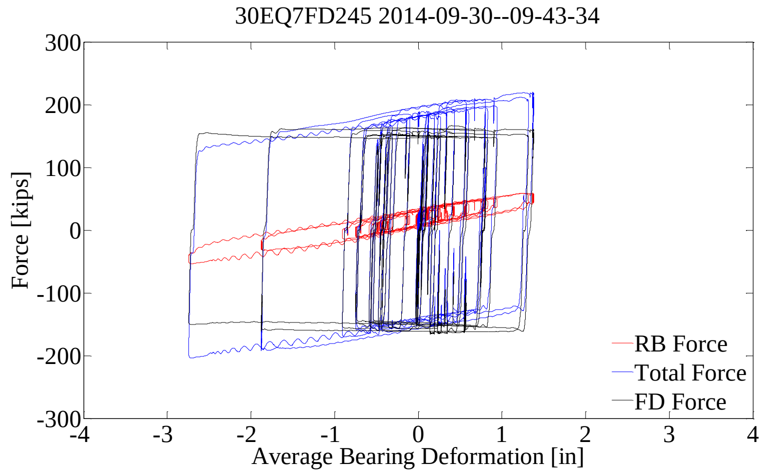

Figure 4.137: Test 30, Force – deformation plots for the deformable connection and its individual components in phase II [pg. 120]

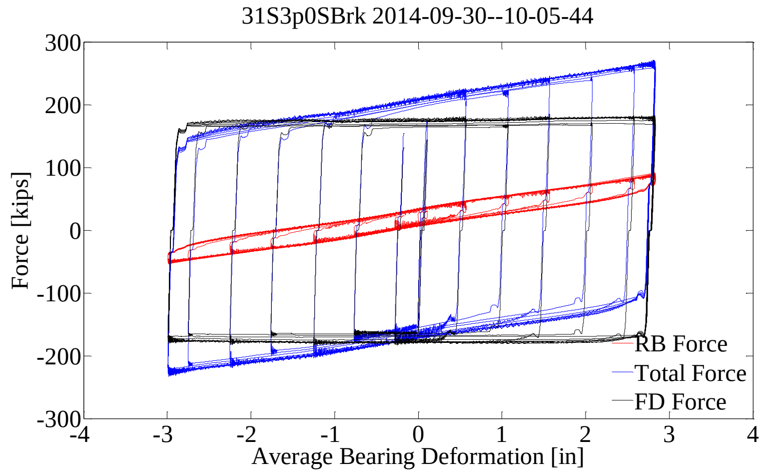

Figure 4.138: Test 31, Force – deformation plots for the deformable connection and its individual components in phase II [pg. 120; pg. 112]

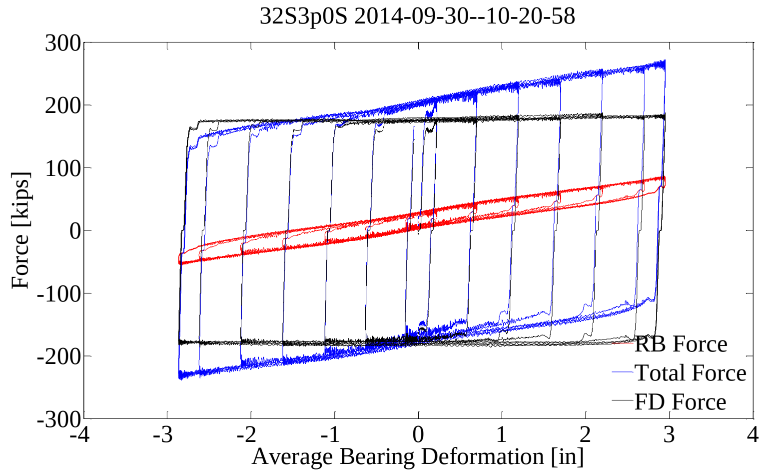

Figure 4.139: Test 32, Force – deformation plots for the deformable connection and its individual components in phase II [pg. 120; pg. 113]

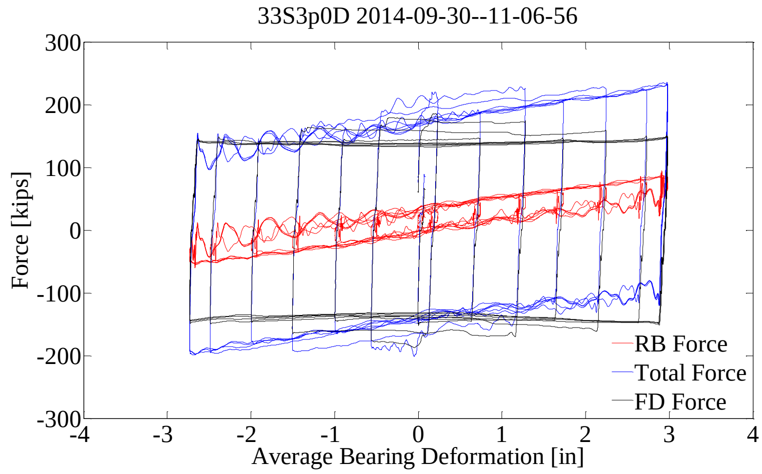

Figure 4.140: Test 33, Force – deformation plots for the deformable connection and its individual components in phase II [pg. 121; pg. 113]

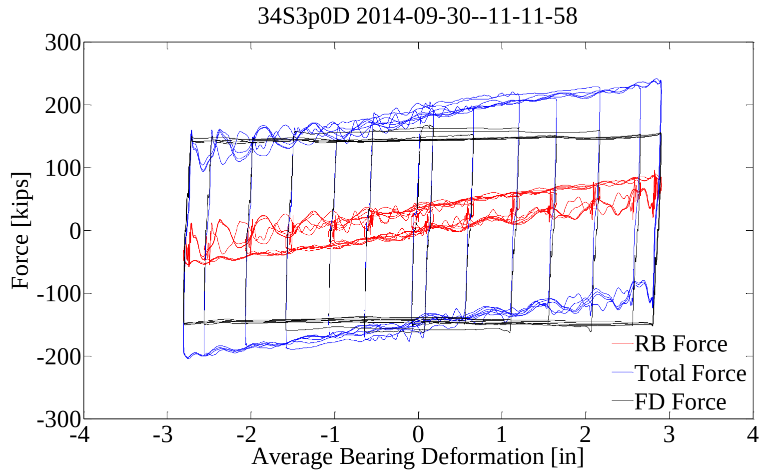

Figure 4.141: Test 34, Force – deformation plots for the deformable connection and its individual components in phase II [pg. 121; pg. 114]

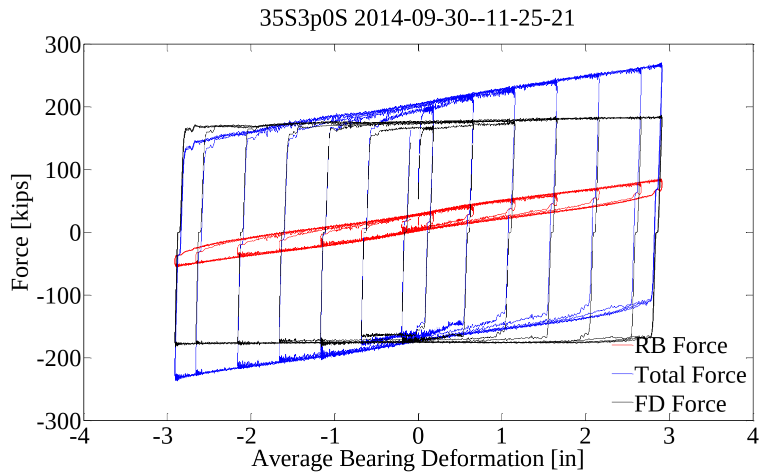

Figure 4.142: Test 35, Force – deformation plots for the deformable connection and its individual components in phase II [pg. 120; pg. 114]

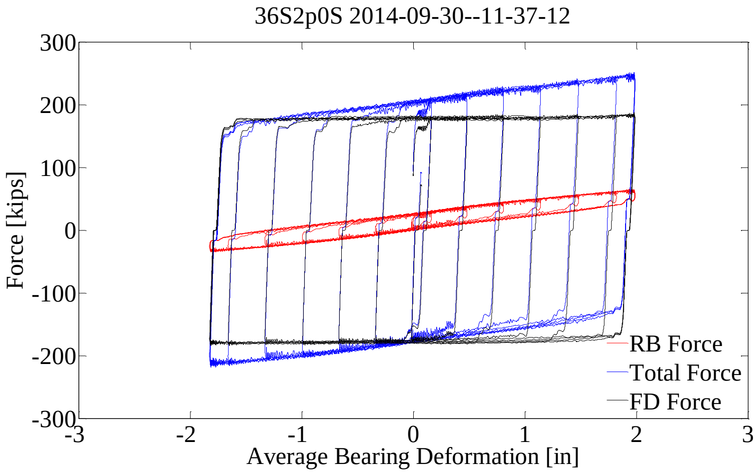

Figure 4.143: Test 36, Force – deformation plots for the deformable connection and its individual components in phase II [pg. 121; pg. 115]

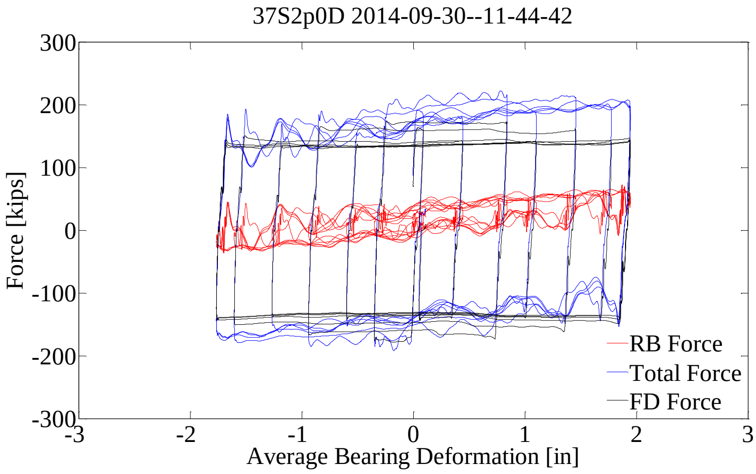

Figure 4.144: Test 37, Force – deformation plots for the deformable connection and its individual components in phase II [pg. 121; pg. 115]

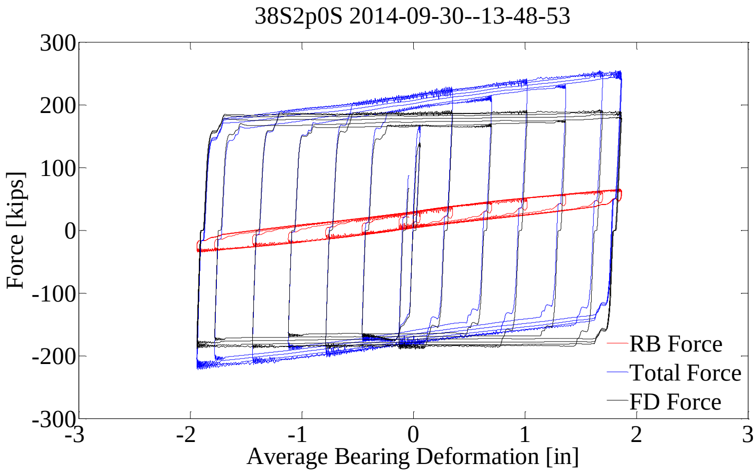

Figure 4.145: Test 38, Force – deformation plots for the deformable connection and its individual components in phase II [pg. 121; pg. 116]

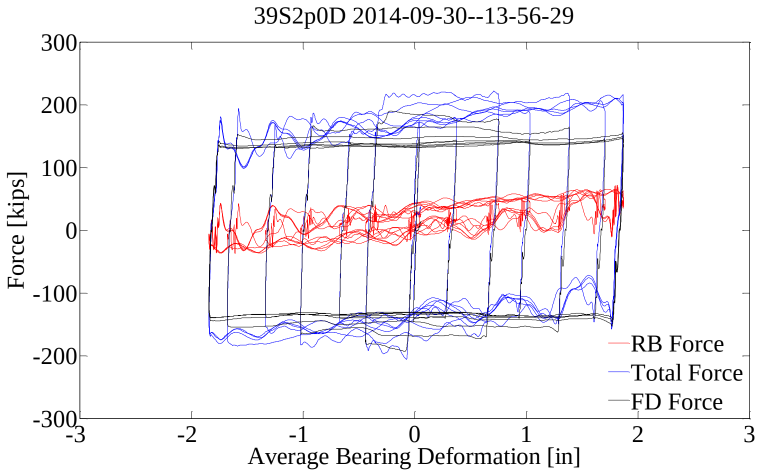

Figure 4.146: Test 39, Force – deformation plots for the deformable connection and its individual components in phase II [pg. 121; pg. 116]

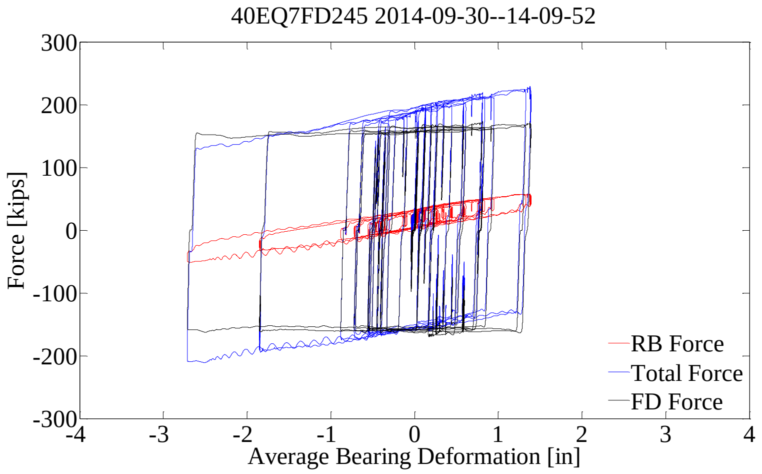

Figure 4.147: Test 40, Force – deformation plots for the deformable connection and its individual components in phase II [pg. 120]

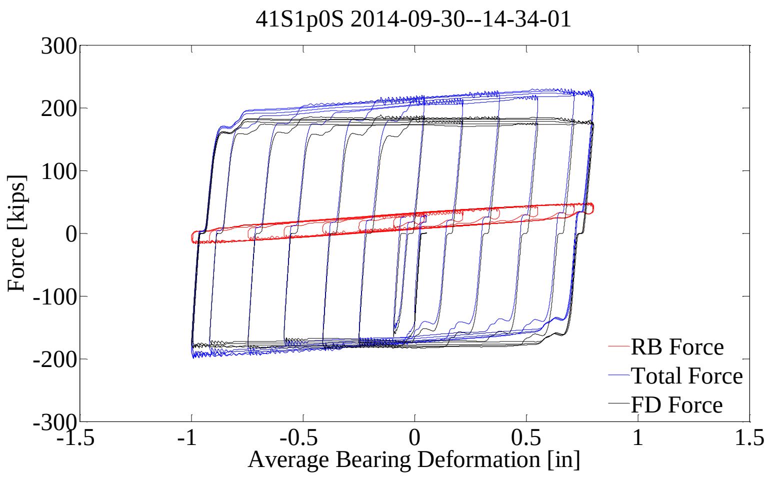

Figure 4.148: Test 41, Force – deformation plots for the deformable connection and its individual components in phase II [pg. 122; pg. 117]

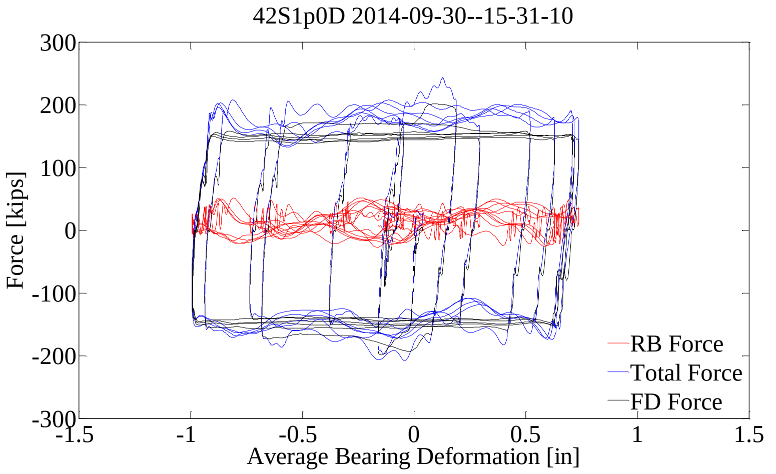

Figure 4.149: Test 42, Force – deformation plots for the deformable connection and its individual components in phase II [pg. 122; pg. 117]

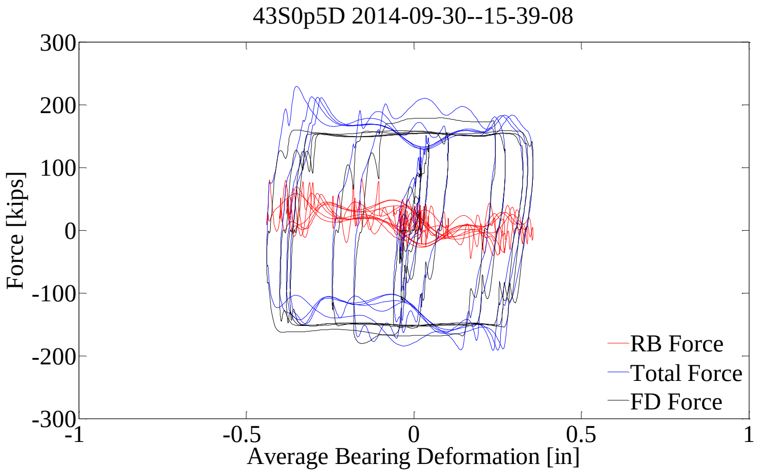

Figure 4.150: Test 43, Force – deformation plots for the deformable connection and its individual components in phase II [pg. 122; pg. 118]

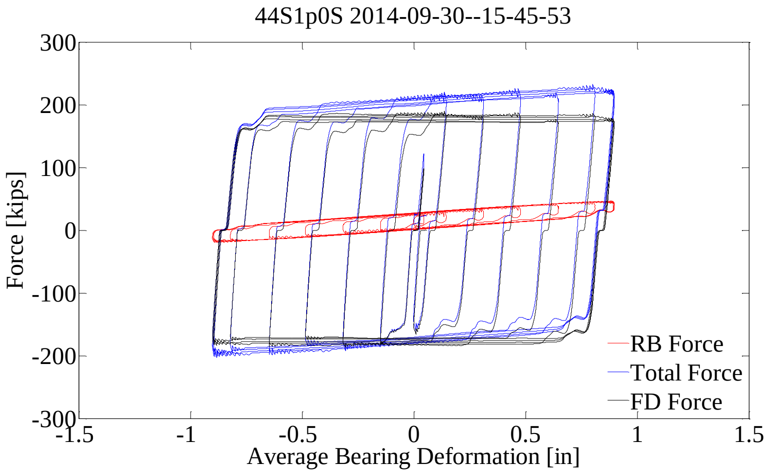

Figure 4.151: Test 44, Force – deformation plots for the deformable connection and its individual components in phase II [pg. 122; pg. 118]

Figure 4.152: Condition of the FD at the end of phase II-4

PICTURE TO BE TAKEN

Figure 4.153: Gatke 398 friction plates at the end of phase II-4

4.5 Conclusions

The nonlinear hysteretic response of the deformable connection was stable and reliable. It can be concluded that a robust and reliable deformable connection has been developed utilizing either a BRB or a FD as a limited-strength load-carrying hysteretic component, with steel or carbon fiber reinforced RB provide and out-of-plane stability of the LFRS and partial re-centering.

Both configurations of the deformable connection were successfully subjected to earthquake and sinusoidal displacement histories at different amplitudes and frequencies. The force-deformation responses were stable under large and repetitive deformation demands.

Structural details that are easy to implement in practice have been used to attach the components of the deformable connection to the shear wall and the floor system. The connection details performed well during numerous tests. Proper detailing of the shear wall and slab reinforcement is required at the locations where the limited-strength load-carrying hysteretic device and the bearings are attached to transfer the combined axial force, shear force and bending moment that is expected.

REFERENCES

[1] R. Fleischman and K. Farrow, "Dynamic behavior of perimeter lateral-system structures with flexible diaphragms," *Earthquake Engineerign and Structural Dynamics,* vol. 30, no. 5, pp. 745-763, 2001.

[2] M. Rodriguez, J. Restrepo and A. Carr, "Earthquake - induced floor horizontal accelerations in buildings," *Earthquake Engineering and Structural Dynamics,* pp. 693-718, 2002.

[3] M. Rodriguez, J. Restrepo and J. Blandon, "Seismic design forces for rigid floor diaphragms in precast concrete building structures," *Journal of structural engineering,* pp. 1604-1615, 2007.

[4] T. Kelly, "Floor response of yielding structures," *Bulletin of New Zealand National Society for Earthquake Engineering,* pp. 255-272, 1978.

[5] S. Ray-Chaudhuri and T. Hutchinson, "Effect of nonlinearity of frame buildings on peak horizontal floor acceleration," *Journal of earthquake engineering,* pp. 124-142, 2011.

[6] R. Sewell, A. Cornell, G. Toro and R. McGuire, A study of factors influencing floor response spectra in nonlinear multi-degree-of-freedom structures, 1986.

[7] A. K. Chopra, Dynamics of Structures, Berkeley,CA, California: Pearson Prentice Hall, 2007.

[8] D. Roke, "Damage-Free Seismic-Resistant Self-Centering Concentrically-Braced Frames, Ph.D. Dissertation," Lehigh University, Bethlehem,PA, 2010.

[9] A. D. Amaris Mesa, "Dynamic amplification of seismic moments and shear forces in cantilever walls, M.Sc. Thesis," University of Pavia, Pavia, 2002.

[10] L. Wiebe and C. Christopoulos, "Mitigation of Higher Mode effects in Base-Rocking Systems by Using Multiple Rocking Sections," *Journal of Earthquake Engineering,* pp. 83-108, 2009.

[11] L. Wiebe, C. Christopoulos, R. Trembley and M. Leclere, "Mechanisms to limit higher mode effects in a controlled rocking steel frame. 1: Concept, modelling, and low-amplitude shake table testing," *Earthquake Engineering and Structural Dynamics,* pp. 1053-1068, 2013.

[12] R. Skinner, J. Kelly and A. Heine, "Hysteretic dampers for earthquake resistent structures," *Earthquake Engineering and Structural Dynamics,* pp. 287-296, 1975.

[13] C. Key, "The seismic performance of energy absorbing dampers in building structures," *Bulletin of the New Zealand Society for Earthquake Engineering,* vol. 17, pp. 38-46, 1984.

[14] J. E. Luco and F. C. P. De Barros, "Control of the seismic response of a composite tall building modelled by two interconnected shear beams," *Earthquake Engineering and Structural Dynamics,* vol. 27, no. 3, pp. 205-223, 1998.

[15] D. Mar and S. Tipping, "Smart Frame Story Isolation System: A New High-Performance Seismic Technology," Tipping Mar and Associates, Berkeley, CA, 2000.

[16] S. T. Crane, "Influence of Energy Dissipation Connections between Floors and the Lateral Force Resisting System," University of California, San Diego, San Diego, CA, 2004.

[17] Y. -. N. Huang, A. S. Whittaker and N. Luco, "Seismic performance assessment of base-isolated safety-related nuclear structures," *EARTHQUAKE ENGINEERING AND STRUCTURAL DYNAMICS,* vol. 39, pp. 1421-1442, 2010.

[18] R. Fleischman, J. Restrepo, A. Nema, D. Zhang, U. Shakya, Z. Zhang, R. Sause, G. Tsampras and G. Monti, "Inertial Force-Limiting Anchorage System for Seismic Resistant Building Structures," in *2015 Structures Congress*, Portland, OR., 2015.

[19] Real-Time Multi-Directional (RTMD) earthquake simulation facility, "RTMD User's Guide," 2014. [Online]. Available: http://www.nees.lehigh.edu/wordpress/uploads/usermanual/RTMD%20Users%20Guide.pdf.

[20] AISC, ANSI/AISC 341 Seismic Provisions for Structural Steel Buildings, Chicago, Illinois: American Institute of Steel Construction, 2010.

[21] BSSC and FEMA, "Recommended provisions for seismic regulations for new buildings and other structures (FEMA 450) Part 2: Commentary," BUILDING SEISMIC SAFETY COUNCIL NATIONAL INSTITUTE OF BUILDING SCIENCES, Washington, DC, 2003.

[22] AASHTO, LRFD Bridge Design Specification, Washington, DC, 2010.

[23] AASHTO, "Guide Specifications for Seismic Isolation Design," 2010.

[24] J. Kelly and D. Konstantinidis, Mechanics of rubber bearings for seismic and vibration isolation, John Wiley and Sons Ltd, 2011.

[25] P. Lindley, "Engineering Design with Natural Rubber, NR Technical Bulletins," The Malaysian Rubber Producers' Research Association, 1978.

[26] Y. Chae, K. Kazemibidokhti and J. M. Ricles, "Adaptive time series compensator for delay compensation of servo-hydraulic actuator systems for real-time hybrid simulation," *Earthquake Engineering and Structural Dynamics,* vol. 42, p. 1697–1715, 2013.

[27] Champion Technologies, "AFT200 Description and Application," [Online]. Available: http://www.stillchampion.com/docs/PDS/PDS_200.pdf. [Accessed 2014].

[28] ScanPac, "Product Data Sheet: RF42," [Online]. Available: http://scanpac.com/cm/pdfs/tds-RF42.pdf.

[29] ScanPac, "Gatke material selection guide," [Online]. Available: http://www.scanpac.com/cm/pdfs/gatke_material_selection_sheet2010.pdf.

[30] AISC, Steel Construction Manual, 2014.

[31] A. Nilson, Design of Prestressed Concrete, John Wiley & Sons, 1987.

[32] S. Merrit, C.-M. Uang and G. Benzoni, "Subassemblage testing of Corebrace Buckling Restrained Braces," University of California, San Diego, San Diego, 2003.

[33] L. A. Fahnestock, R. Sause, J. M. Ricles and L.-W. Lu, "Ductility demands on buckling-restrained braced frames under earthquake loading," *Earthquake Engineering and Engineering Vibration,* vol. 2, no. 2, pp. 255 - 268, 2003.

[34] BSSC and FEMA, "NEHRP Reccommended provisions for seismic regulations for new building and other structures (FEMA 450) Part 1: Provisions," BUILDING SEISMIC SAFETY COUNCIL NATIONAL INSTITUTE OF BUILDING SCIENCES, Washington, DC, 2003.

[35] C. G. Lee, K.-C. Chang and K. Sigiura, "The experimental basis of material constitutive laws of structural steel under cyclic and nonproportional loading," in *Stability and ductility of steel structures under cyclic loading*, CRC Press, 1992, pp. 3-14.

[36] C. J. Black, N. Makris and I. D. Aiken, "Component Testing, Seismic Evaluation and Characterization of Buckling-Restrained Braces," *Journal of Structural Engineering,* vol. 130, no. 6, pp. 880 - 894, 2004.

[37] ASCE, ASCE Standard ASCE/SEI7 - 10: Minimum Design Loads for Buildings and Other Structures, Reston, Virginia: American Society of Civil Engineers, 2010.